DEVELOPMENT OF WEARABLE SYSTEMS FOR THE DETECTION AND CLASSIFICATION OF KNEE OSTEOARTHRITIS AND ITS VALIDATION THROUGH RADIOGRAPHIC IMAGES

A Thesis Submitted in

Partial Fulfillment of the Requirements

for the Degree of

DOCTOR OF PHILOSOPHY

By

DHIRENDRA KUMAR VERMA

(Roll No.176103116)

DEPARTMENT OF MECHANICAL ENGINEERING

INDIAN INSTITUTE OF TECHNOLOGY GUWAHATI

NORTH GUWAHATI-781039, ASSAM-INDIA

SEPTEMBER-2024

Dedicated to my parents and siblings for their endless love, support, and encouragement throughout my pursuit of this academic endeavor.

I hope this achievement will fulfill the dream they envisioned for me.

Certificate

This is to certify that the thesis entitled "**Development of Wearable Systems for the Detection and Classification of Knee Osteoarthritis and Its Validation Through Radiographic Images**" being submitted by **Mr. Dhirendra Kumar Verma** to the Indian Institute of Technology Guwahati, for the award of the degree of Doctor of Philosophy in Mechanical Engineering is a record of original bonafide research work carried out by him under our supervision and guidance. The thesis work, in our opinion, has reached the requisite standard fulfilling the requirements for the degree of Doctor of Philosophy.

The results contained in this thesis have not been submitted in part or full to any other University or Institute for the award of any degree or diploma.

Dr. Poonam Kumari
(Thesis Supervisor),
Department of Mechanical Engineering,
IIT Guwahati-781039, Assam India.

Dr. Subramani Kanagaraj
(Thesis Co-Supervisor),
Department of Mechanical Engineering,
IIT Guwahati-781039, Assam India.

Declaration

I, Dhirendra Kumar Verma (Roll no: 176103116) declare that the present written submission is my thoughts in my own words. I have adequately cited and referenced the original sources, where other's ideas have been involved. I also declare that I have adhered to all principles of academic honesty and integrity and have neither fabricated nor falsified any idea/data/fact/source in my submission. I understand that any violation of the above will be cause for disciplinary action by the Institute and can also evoke penal action from the sources which have thus not been properly cited or from whom proper permission has not been taken when needed.

Date: Dhirendra Kumar Verma

Place: IIT Guwahati Roll No. 176103116

Acknowledgements

First and foremost, I want to express my sincere gratitude toward my Ph.D. supervisors, Dr. Poonam Kumari and Dr. Subramani Kanagaraj, for providing me with an opportunity to work under their supervision. I am grateful to them for their consistent guidance, motivation, patience, kindness, and family support as well, over these years. They have always made themselves available for discussion despite their busy schedules. Their enthusiasm, sublime work ethics, analytical abilities, and never-say-die attitude toward research and life as well, has nurtured my scientific skills and also inspired me immensely to work hard. I am proud to have them as my Ph.D. supervisors. Thank you, Ma'am, and Thank you, Sir, for all your help, advice, and support.

I gratefully acknowledge the New Generation Innovation and Entrepreneurship Development Centre (NewGen IEDC), Department of Science and Technology (DST), Government of India for providing the IEDC grant (Project Number: xxMESP-NEDII00635xRGN005 & Project Code: IEDC/2019-20/SK2_PK1) for the project "Sensing Acoustical Emissions from the Knee for Wearable Joint Health Assessment." to support this research work.

I am grateful and acknowledge the Department of Science and Technology (DST), Ministry of Science and Technology, Government of India for the financial support during my doctoral studies at IIT Guwahati under the project "Development and testing of a wearable device for the early detection of cartilage damage in a knee stepping towards an osteoarthritis condition using acoustic emission" (grant number TDP/BDTD/03/2021(G)." I am also thankful to the Ministry of Education, Government of India for providing me the financial support during my Ph.D. at IIT Guwahati.

I sincerely appreciate the North East Centre for Biological Sciences and Healthcare

Engineering (NECBH), Grant Number BT/COE/34/SP28408/2018, sponsored by the Department of Biotechnology (DBT), Government of India and all clinical staff of the Gait and Motion Analysis Laboratory at IIT Guwahati for facilitating a platform to conduct the experiments. I am also thankful to the industrial research partner "Olatus System Pvt. Ltd." at IIT Guwahati for contributing to the electronic circuit development and PCB fabrication for the final product development.

I am very much thankful to the administrative and medical team of the Guwahati Neurological Research Centre (GNRC) Hospital Guwahati, and North Guwahati Block Physical Health Center in Mariapatty Kamrup Guwahati, for giving permission and a platform to conduct the data collection camps of osteoarthritic subjects.

I am thankful to Dr. Agyapal Singh Brar, Dr. Sathish K. Ramakrishnan, and Dr. M.S. Deva Malika for their kind guidance, timely suggestions, and kind help to keep forward my research journey. I want to thank my labmates, Akshay Daydar, Vaibhav Jaiswal, Arnab Sarmah, Anirban Basumatary, Subhojit Jash, Raagdeep Raj, Lipika Boruah and, Vaibhav Raman Pratap, for their timely help, suggestions, and encouragement. I am indebted to my close friends, labmates, and colleagues, Mridusmita Bora, Rishabh Saluja and, Ambrish Singh with whom I had a very good time and they always motivated me in my critical time.

I would like to gratefully acknowledge the unwavering support and encouragement provided by my parents and siblings throughout my Ph.D. journey. Their boundless faith in my abilities and their continuous moral and emotional support have been the cornerstone of my success. To my parents, whose sacrifices, dedication, and unending love have been my constant motivation, I owe an immeasurable debt of gratitude. Their belief in my dreams has fueled my determination and made this achievement possible. I

am thankfut to my siblings, for being my pillars of strength and my closest confidants. Their unwavering support, late-night discussion, and words of wisdom have carried me through the challenges of this academic endeavor.

Finally, I thank God for always being with me.

Dhirendra Kumar Verma

Abstract

Knee osteoarthritis (OA) is a prevalent degenerative joint disorder characterized by a gradual degeneration of articular cartilage, leading to joint stiffness, discomfort, and restricted joint movements. The conventional diagnostic methods of knee OA include clinical assessments and radiographic imaging, often limited to early diagnosis, treatment cost, and sensitivity. The chronic condition of osteoarthritis may lead to total knee replacement surgeries. Early intervention in knee OA can prevent such painful surgeries and also saves on the cost of treatments. In recent decades, sensor-based disorder detection has received focused attention in OA identification. These procedures are non-invasive and very helpful in the early detection of OA. The primary objective of this research is to develop wearable systems for the detection of knee osteoarthritis and classification of it using acoustic emission technology and validate through radiographic images. In the present work, a total of two hundred ten human subjects from various places in the North-Eastern region of India have participated, and the acoustic waves generated from their knees during 0°-90° sit-stand-sit (S-T-S) activity are captured using AE sensors to diagnose different stages of OA. All subjects are examined through the digital goniometer and acoustic sensors placed at their medial tibiofemoral knee joint locations. Joint angle-based signal features are recorded for biomarker identification under the S-T-S data collection protocol. Joint space narrowing (JSN) of the knee for OA subjects is calculated through image processing of the knee X-ray, and the AE findings are validated from the obtained JSN and Kellgren-Lawrence (KL) grades. Results obtained from the study demonstrate distinct AE signal patterns in participants with knee osteoarthritis

compared to healthy individuals. Moreover, a significant difference is observed among AE parameters in all OA grade participants, and the KL grades are classified through JSN obtained from radiographic findings. All signal parameters are acquired in increasing order with decreased JSN among the KL grades. The highest values of signal features like the number of acoustic hits 167±11, amplitude 76±1 (dB), signal duration 10±3 (ms), absolute energy 401±151 (fJ), and signal frequency 103±3 (kHz) are identified as per their dominance and suitability as a biomarker in the KL-4 grade group. The outcomes from two-dimensional Principal Component Analysis (PCA) analysis are evaluated for primary biomarker identification for OA detection, and it is revealed that sound amplitude (dB) is the most dominating feature in the first principal component. In summary, the AE technology is successfully validated in a quantitative assessment of OA detection. The KL grade groups are distinguished successfully based on the obtained signal parameters and their validation through JSN confirmed the classification of grades among the groups. The study findings concluded that the AE is found to be a promising tool for the quantitative evaluation of knee OA using acoustic sensors and has proven efficacy in signal feature identification and differentiation among the KL grades. Further, sensor-based wearable systems are successfully developed for knee joint OA detection. AE can be used as a non-invasive and non-radiographic tool for the progressive monitoring of knee osteoarthritis, which could be explored for the continual monitoring of cartilage degradation.

Contents

List of Figures

List of Tables

List of Abbreviations

AE = Acoustic Emission

AS = Ankylosing Spondylitis

ACL = Anterior Cruciate Ligament

ADCs = Analog to Digital Converters

AA = Ascending-Acceleration

AD = Ascending-Deacceleration

BA Plots = Bland-Altman Plots

CT =Computed Tomography

CDF = Cumulative Density Function

DOF = Degrees of Freedom

DA = Descending-Acceleration

DD = Descending-Deacceleration

ECM = Extracellular Matrix

EA = Extension-Acceleration

ED = Extension-Deacceleration

FA = Flexion-Acceleration

FD = Flexion-Deacceleration

F-E = Flexion-Extension

FFT = Fast Fourier Transform

GA = Gouty Arthritis

GAG = Glycosaminoglycans

ICRS = International Cartilage Repair Society

IMU = Inertial Measurement Unit

IHEC = Institute Human Ethical Committee

IoT = Internet on Things

JSN = Joint Space Narrowing

KGN = Kartogenin

KL = Kellgren and Lawrence

LCL = Lateral Collateral Ligament

LCD = Liquid crystal display

LoA = Limits of Agreements

MRI = Magnetic Resource Imaging

MSCs = Mesenchymal Stem Cells

MCL = Medial Collateral Ligament

MEMS = Micro-Electro-Mechanical Systems

OA = Osteoarthritis

OCT = Optical Coherence Tomography

PCL = Posterior Cruciate Ligament

PLA = Polylactide

PCB = Printed Circuit Board

PSD = Power Spectral Density

PCA = Principal Component Analysis

RA = Rheumatoid Arthritis

RMSE = Root Mean Squared Error

S-T-S = Sit-Stand-Sit

SEM = Standard Error of Measurement

SDC = Smallest Detectable Change

STFT = Short-term Fourier Transform

TKR = Total Knee Replacement

US = Ultrasonography

VAG = Vibroarthrography

WHO = World Health Organization

WOMAC = Western Ontario and McMaster Osteoarthritis Index

Chapter 1

Introduction

1.1 Preface

Osteoarthritis (OA), is a degenerative joint disorder and an important global health concern, especially in weight-bearing joints like the knee. Severe osteoarthritis in the knee may substantially impact a person's quality of life (Felson *et al.*) [1]. It may happen due to various reasons like aging degeneration of soft tissues, obesity, the inadequacy of synovial fluid in the joint capsule, severe accidents, etc (Nguyen *et al.*) [2]. As the population ages and habits become more sedentary, the prevalence of knee osteoarthritis increases and imposes an enormous burden on healthcare systems globally (Zhang *et al.*) [3]. Once people fall into severe OA knee condition, very costly medicines are required regularly, and sometimes it leads to total knee replacements (Losina *et al.*) [4]. Early identification of knee osteoarthritis is essential for immediate medical treatments that may reduce symptoms, decrease disorder progression, and improve overall knee health conditions (Nagai *et al.*) [5]. Furthermore, the traditional diagnostic methods for knee osteoarthritis frequently involve non-invasive clinical examinations and imaging modalities such as X-ray imaging, computed tomography (CT), ultrasonography, and magnetic resource imaging (MRI), while optical coherence tomography (OCT) and arthroscopy are semi-invasive methods. These examination procedures include substantial cost as well as time dependency (Nippolainen *et al.*) [6]. However, in the early stages of the disorder, these approaches may be less informative, and by the time symptoms become apparent and as an outcome, per-

manent joint damage might have taken place. Sometimes, it is very late to diagnose the actual stage of osteoarthritis, and the patient is forced to undergo total knee replacement surgeries. These surgeries cost a higher monetary value, pain, and patient's precious time with uncertainty of the success of the operation (Wylde *et al.*) [7].

Emerging technologies such as vibroarthrography (VAG) and acoustic emission (AE) procedures are gaining importance in this discipline as non-invasive and sensitive tools for the early detection of knee osteoarthritis. VAG is a technique that captures and interprets vibrational signals generated during joint motion and provides vital information about biomechanical changes in the knee joint (Blodgett) [8]. These vibrations, which are frequently unnoticeable to the human ear, can be captured using specialized sensors placed on the skin of the joint. The slight structural changes associated with osteoarthritis in the knee joint appear as different vibrational patterns that can be analyzed for diagnostic objectives. VAG has a distinct benefit as it can detect early pathological alterations in joint tissues, allowing for proactive treatments before severe clinical symptoms develop (Peylan) [9]. In addition to VAG, acoustic emission methodology introduces another dimension to the diagnostic evaluation of knee osteoarthritis. This method includes detecting and analyzing high-frequency sound waves generated within the joint during movement. Acoustic emissions can indicate underlying disorder processes as the joint experiences friction, wear, and other degenerative changes (Chu *et al.*) [10]. Clinicians may acquire essential details about the health of the joint by capturing and interpreting these small sound signals, and allowing them to recognize early indicators of osteoarthritis with higher accuracy than standard diagnostic techniques. The integration of VAG and acoustic emission technology has the potential to provide a comprehensive and sophisticated understanding of knee joint health (Mollan *et al.*) [11]. Furthermore,

these approaches are non-invasive, cost-effective, and easily deployable in clinical settings which makes them a suitable method of diagnosis for routine screening and monitoring of knee joints. In recent years, a significant advancement is observed in the development of standardized methodologies and improved signal-processing techniques to extract the relevant information from the complicated signals generated from VAG and acoustic emission measurements (Befrui *et al.*) [12]. These continuous improvements provide ease of clinical assessment in the early diagnosis and management of knee osteoarthritis. Ultimately, detecting and classifying knee osteoarthritis using vibroarthrography and acoustic emission technology is an innovative approach that deals with overcoming the limitations of traditional diagnostic methodologies. The use of these technologies holds enormous promise for revolutionizing the early detection and management of knee osteoarthritis, improving patient outcomes and reducing the socioeconomic burden associated with this knee joint disorder. Implementation of VAG and AE techniques in clinical practice may become an important tool against the rising global health burden posed by knee osteoarthritis (Karpinski *et al.*)[13].

1.2 Knee Joint Anatomy

In the human body, the skeletal system combines various typical bones with a systematic arrangement that provides structural stability and protection against the organs. The knee joint acts as a load bearer that gives stability to the upper limb and helps to do various daily activities like walking, running, jumping, playing, etc. (Verma *et al.*) [14],(Abulhasan *et al.*) [15]. It is also known as a tibiofemoral joint, and it is the largest articulation in the human body as shown in Fig. 1.1. The translation mode is in the axes of anterior-posterior, medial-lateral, and proximal-distal, and further details can

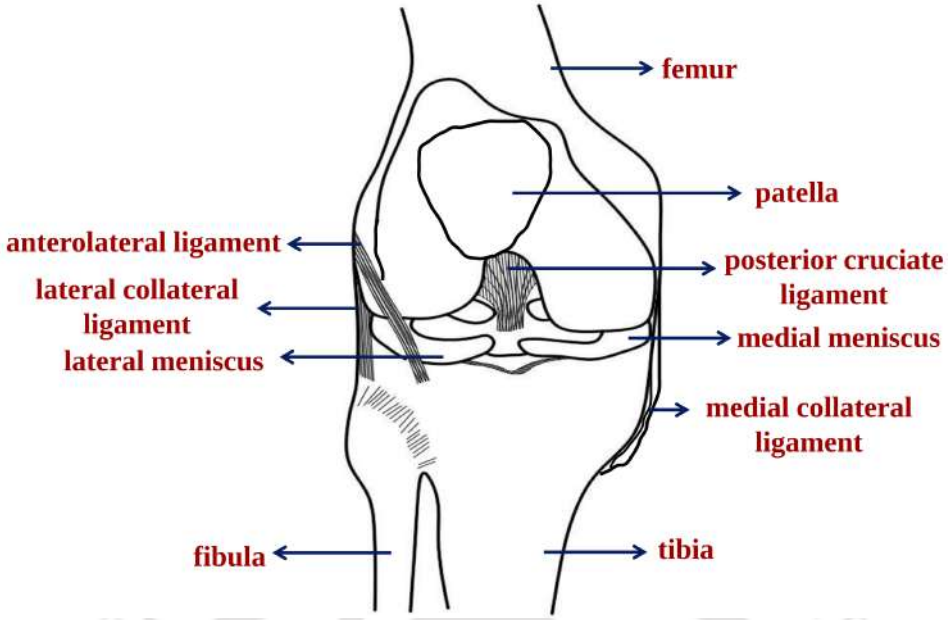

Figure 1.1: Knee Joint Anatomy (Verma *et al.*) [1].

be found in the referred literature (Gerard *et al.*) [16]. On the other hand, the knee joint allows flexion-extension, varus-valgus, and internal-external rotations (Daniel *et al.*) [17]. The rotation motion is also associated with some degree of translation and vice-versa as shown in Fig. 1.2. It happens because, during rotation, the femur and menisci move over the tibia while the femur rolls and glides over the menisci in flexion-extension (Wu *et al.*) [18]. It can effectively move from 0° extension to 135° flexion, together with 20° to 30° rotation of the flexed leg on the femoral condyles. Knee joint permits a total of six degrees of freedom system, including three translations and three rotations. The joint has four important features like a joint cavity, articular cartilage, a synovial membrane, and a fibrous capsule. The knee joint is known as a synovial joint, as it contains a lubricating substance called the synovial fluid. It comprises three main articulating bones, i.e., femur, tibia, and patella. The strongest and longest bone is the femur, also said as thighbone, tibia as the shinbone, and the patella, as the knee cap. There is another bone fibula, i.e., next to the tibia which is not involved in the joint capsule but helps to support the joint stability. There are two round shaped protuberances at the end of the

femur and called femoral condyles. From the geometry of a knee joint, the inner side of the knee is said as the medial side, and the outer side is said as lateral side (Gerard *et al.*) [16]. So the femoral condyles are also classified as lateral and medial condyles of the femur. Similarly, the tibial lateral and tibial medial condyles are identified. Inside the joint, these femoral condyles form a grooved shape over which the patella glides. The gliding direction of the patella is along the bottom front surface of the femur between the femoral condyles. Patella protects the knee during the flexion-extension motion by relieving the friction between cartilages and muscles. Tibia, also said as shinbone or shank bone helps to stabilize the joint. At the top of the tibia, there is the attachment of two sickle-shaped menisci, and as per the joint geometry, they are named as lateral and medial menisci respectively. The primary function of these two shock-absorbing menisci cartilages is to provide structural integrity to the knee when it undergoes tension and torsion. They also help to disperse the load and reduce friction over the articular surfaces of the tibia, and femur in the knee joint (Hamblen *et al.*) [19].

Two types of cartilage are present in the knee joint: the articular cartilage, which covers the ends of bones, and the wedge-shaped fibrocartilaginous structure called the menisci, located between the femur and the tibia. The shock-absorbing menisci are composed of the medial meniscus and the lateral meniscus, which are two crescent-shaped plates of fibrocartilage that lie on the articular surface of the tibia. The articular surfaces of the knee joint are the large curved condyles of the femur, the flattened condyles (medial and lateral plateaus) of the tibia, and the facets of the patella as shown in Fig. 1.1. There are three types of articulation: an intermediate articulation between the patella and the femur and lateral and medial articulation between the femur and the tibia. The articular surfaces are covered by cartilage, like all the major joints of the body. Cartilage

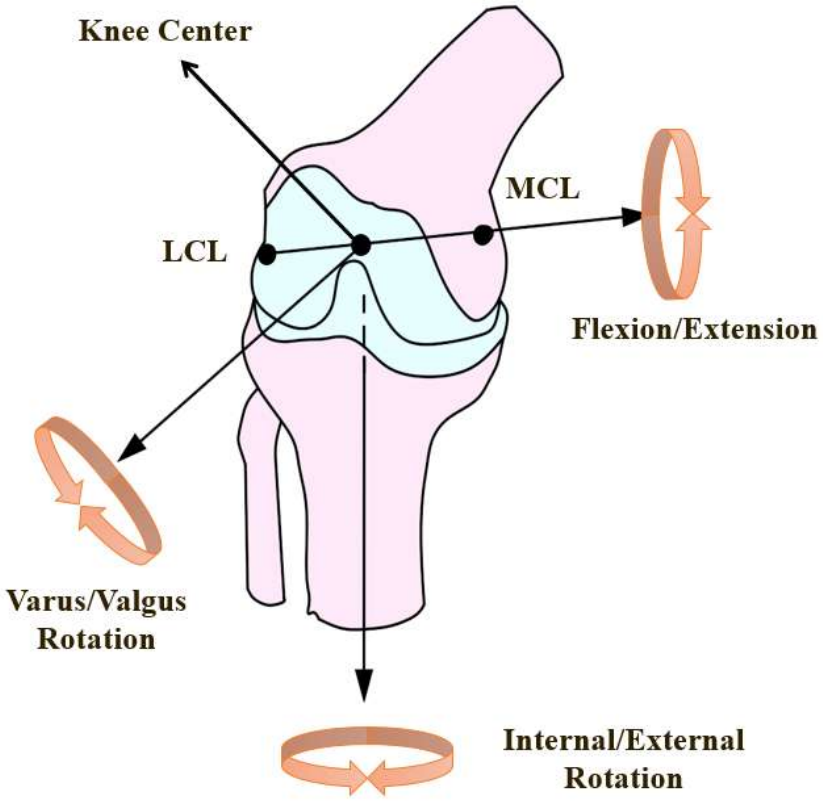

Figure 1.2: Knee Joint Movements (Verma *et al.*) [1].

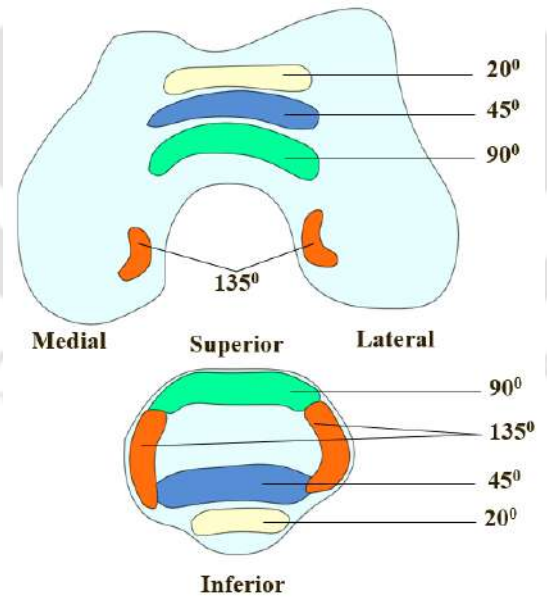

Figure 1.3: Patellar Contact Areas during Patellofemoral Articulation (Verma *et al.*) [1].

is vital to joint function because it protects the underlying bone during movement. Loss of cartilage function leads to pain, decreased mobility, and in some instances, deformity

and instability. The movable joint, which ensures the presence of fibrocartilage or hyaline cartilage layer opposite to the bone surface along with the synovial fluid in the cavity, is known as a diarthrodial joint. Articular cartilage provides the smooth and lubricated function of articulation during load-bearing actions and also has a low coefficient of friction. In the human body where the stiffness of bone is improper, soft white tissue is found and said as Cartilage.

Under the full extension of the joint, the tibia and femur are locked in place, and they become unlocked until the flexion is not initiated. Once the knee flexed, the area under contact with the patellofemoral surface starts moving upward. In this process, both medial and lateral facets are involved up to 20° flexions as shown in Fig. 1.3. When the knee flexed up to 90°, the contact areas of the patellofemoral engage the upper pole of the patella, and about 120° to 135° of flexion, the odd patellar facet articulates with the lateral margin of the medial femoral condyle (Freeman *et al.*) [20].

Another very important joint part is the articular cartilage, which has a thickness between 2 to 4 *mm*, and its deterioration results in severe knee osteoarthritis. It mainly consists of a highly organized extracellular matrix (ECM) with a thin dispersion of the only resident cell called chondrocyte. The extracellular matrix (ECM) naturally exists in two phases; fluid phase of water and a solid organic phase. The water phase contains synovial fluid (65-85% of total wet weight), and the solid phase contains organic ECM proteins (15-35% of total wet weight) (Chen *et al.*) [21], (Sophia *et al.*) [22]. Knee anatomy plays an important role in the designing of a wearable device. A further detailed investigation related to knee joint biomechanics and its structural features can be found in the reported literature (Zhang *et al.*) [23].

1.3 Mechanical Properties of the Articular Cartilage

Akizuki *et al.* [24] investigated the tensile properties of the human knee cartilage. They examined the influence of ionic conditions, weight-bearing, and fibrillation on the tensile modulus. Viscoelastic and biphasic responses were observed under the tension, compression, and shear. They also reported that even under uniaxial tensile loading, the mechanical behavior of cartilage depends on the various parameters like strain rate, ionic condition of fluid, biochemical composition, and the arrangement of collagen fibers and proteoglycans, i.e., structural organization of the cartilage tissue. For determining the equilibrium tensile properties, the authors used isometric tensile apparatus (ITA) and concluded that the ECM shows a linear variation (up to 15% strain) in the equilibrium tensile stress-strain behavior. Also, the tensile modulus value in the range from 1.0 *MPa* to 30 *MPa*. It was observed that the variation in the tensile modulus as in superficial zone, and it is 10.1 *MPa* while in the middle zone the value is 5.4 *MPa*. The higher value in the superficial zone was observed because the collagen fibers are highly organized here. In the knee joint capsule, the cartilage volume is small in comparison to other ligaments, muscles, and tendons, so it is capable of sustaining a lesser amount of shock and energy in human locomotion (Hu and Jerry) [25]. Apart from the cartilage structure, it is also essential to analyze the biomechanical properties of cartilage-like tensile, compressive and shear. As stated above that the tensile properties are mainly contributed by the collagen fibers, and in the total volume of the cartilage, their diameters are varying. Due to the diameter variation and varied orientations of collagen fibers in different zones, the tensile property also varies.

1.4 Knee Joint Disorders

The knee joint plays a significant role in the human gait cycle and supports almost the entire weight of the body. The joint disorders can be broadly classified, such as joint injuries, degenerative cartilage disorder like arthritis, mechanical problems in the joint, and other like patellofemoral pain syndrome, etc. A knee injury causes severe pain in the joint and some times, and it may lead to total knee replacement (TKR). The knee disorders are explained here in detail.

1.4.1 Ligament Injuries

Knee joint ligaments are of four types. From the joint anatomy, these are anterior cruciate ligament(ACL), posterior cruciate ligament(PCL), lateral collateral ligament (LCL), and medial collateral ligament (MCL), respectively. Majewski *et al.* [26] reviewed the epidemiology of athletic knee injuries, including ten years of study. During the survey in 10 years, the authors listed 17,397 patients with 19,530 sports injuries. Out of the total sample data, 6,434 patients (37%) had 7,769 injuries (39.8%) related to the knee joint. The percentage damage was recorded as 20.3% in ACL, 7.9% in MCL, 1.1% in LCL, and 0.65% in PCL. Yu *et al.* [27] studied the mechanisms of non-contact anterior cruciate ligament (ACL) injuries in soccer. They concluded that the significant ACL loading mechanisms include the sagittal plane biomechanical factors like small knee flexion angle, great posterior ground reaction force and great quadriceps muscle force. If the posterior ground reaction force is high, then it will increase the quadriceps muscle force, and as a result, it will cause a high anterior draw force at the knee. They also reported that, if the knee flexion is small, then it is associated with a high patella tendon-tibia shaft angle

and ACL elevation angle, and as a result, the load on ACL is high. ACL is not playing a significant role to bear the knee valgus-varus moment and internal-external rotation loadings so due to these movements ACL injuries are less. Chandrasekaran *et al.* [28] reviewed the posterior cruciate ligament (PCL) injuries and focused on its anatomical, biomechanical, and kinematic findings. During hyperflexion or hyperextension of the knee joint, if tibia is displaced posterior to the femur, then PCL injuries are more prone to occur.

1.4.2 Meniscus Injuries

Meniscus injuries can be classified as acute tears and chronic tears. An acute meniscus tear is generally observed during sports injuries or trauma, whereas chronic damages occur due to severe overload. Surgical repair is recommended for acute tears, and physical therapy or anti-inflammatory medications are prescribed for chronic tears. The meniscus is associated with several functions together in the knee joint like stability, shock absorption, lubrication and articular cartilage nutrition, load transmission, and proprioception (Pyne and Scott) [29]. Lateral meniscus provides support in weight-bearing activity, and medial meniscus provides joint stability. The meniscus is divided into three vascular zones, and it has different tear orientations as shown in Fig. 1.4 The dark shed shows the most vascular zone and has higher self-healing capability in comparison to middle and central light shaded zones. Mesiha *et al.* [30] studied the pathologic characteristics of the torn human meniscus and reported that meniscus repair significantly depends on the age of the patients.

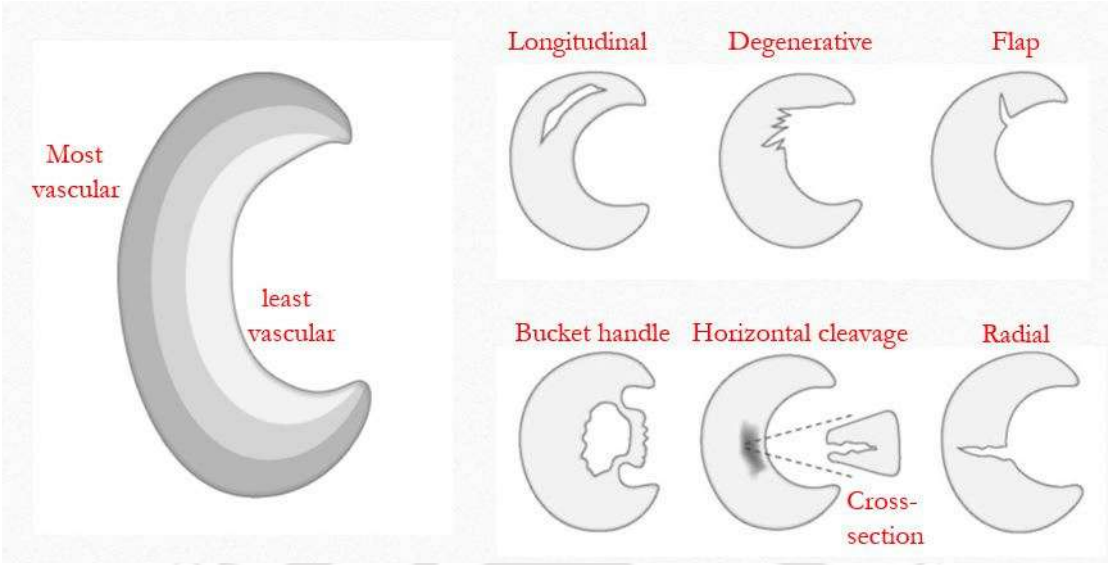

Figure 1.4: Meniscus Vascularity System and Different Tear Orientations (Pyne and Scott) [16].

1.4.3 Osteoporosis

Osteoporosis is a bone disorder and usually occurs due to low bone mass density. It is a skeletal disorder in which the bones become fragile and leads to fracture. Osteoporosis related fractures are more severe in the cancellous bone, which includes the proximal femur, vertebrae, and distal radius. The disorder is more prone to occur in the female gender and usually due to the low calcium intake with the extensive prevalence of vitamin-D deficiency (Khadilkar *et al.*) [31]. The authors estimated that 46 million women (i.e., 20% of 230 million Indians over the age of 50 years) have osteoporosis.

1.4.4 Cartilage Disorders

Arthritis is a cartilage disorder that includes inflammatory and degenerative deficiencies in bone joints like the hip, knee, spine, foot, and fingers, etc. The exact cause of arthritis in the human body is still not well known. Arthritis symptoms may include chronic pain

and swelling in the body joints. It is often referred to as a single disorder, but in reality, it is an umbrella term for more than 100 medical conditions that affect the musculoskeletal system in people from various countries and continents (Murray *et al.*) [32]. The most common types of arthritis are Rheumatoid Arthritis (RA), Ankylosing spondylitis (AS), Gouty Arthritis (GA), and Osteoarthritis (OA). Among all the above types of arthritis, Osteoarthritis is one of the most prominent and common chronic disorders in adults, mainly due to cartilage degradation or change in ECM structure. It causes severe pain during joint articulation, mechanical instability, and sometimes inferior knee health condition, which leads to total knee replacement (TKR) surgeries. Other joint level factors like muscle strength and mass (musculoskeletal factors), joints load and alignment (human gait patterns) and leg length inequality, etc., may also be responsible for this chronic disorder (Allen *et al.*) [33], (Buckwalter *et al.*) [34]. Inside the joint tissue, the chondrocyte binds the calcium pyrophosphate and sodium urate crystals and confirms the cause of osteoarthritis (Kim *et al.*) [35], (Liu *et al.*) [36]. The most common types of arthritis are as follows:

(i) Rheumatoid Arthritis (RA):- Sweeney *et al.* [37] studied that rheumatoid arthritis is a disorder which causes swelling and pain in the joints. It is an autoimmune inflammatory disorder that presents as a symmetric polyarthritis. RA occurs with synovial inflammation and observed between the ages of 30 to 55 years in 1% of the total population. Rheumatoid arthritis can occur at any age, but it has been noted in the later life of the people. In the US, around 2.1 million adults are affected by RA, and it results in irreversible joint disorder (Bird and Anthony) [38]. Mostly, it affects the small wrists and ankle joints in the human body as shown in Fig. 1.5, (Andrea *et al.*) [39].

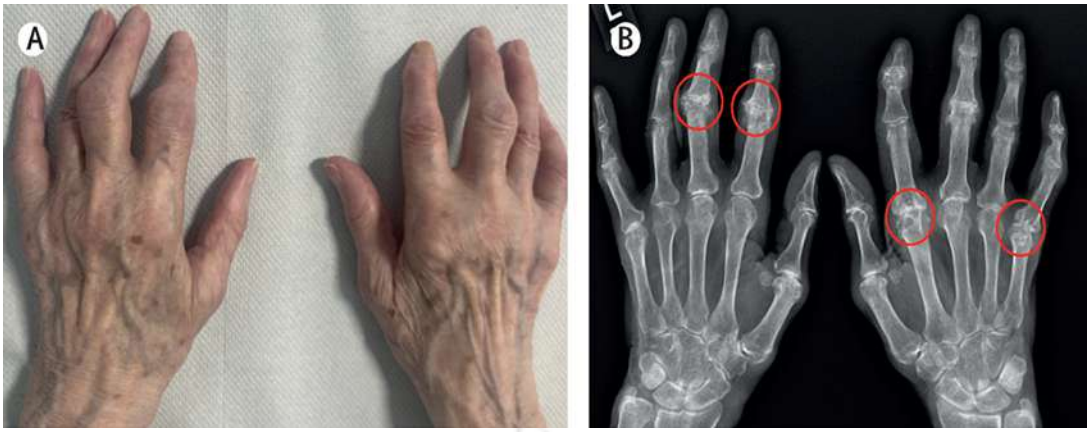

Figure 1.5: Hand Changes of Rheumatoid Arthritis (Andrea *et al.*) [26].

(ii) Ankylosing spondylitis (AS):- It is an inflammatory rheumatic disorder that usually affects the young people and the axial skeleton in the human body as shown in 1.6. It results in inflammatory back pain, structural and functional loss in the body, and reduced life quality. Ankylosing spondylitis (AS) is linked with major histocompatibility complex (MHC) class I molecule HLA B27. Nonsteroidal anti-inflammatory drugs (NSAIDs) and structured exercises are recommended for patients with ankylosing spondylitis (Braun *et al.*) [40].

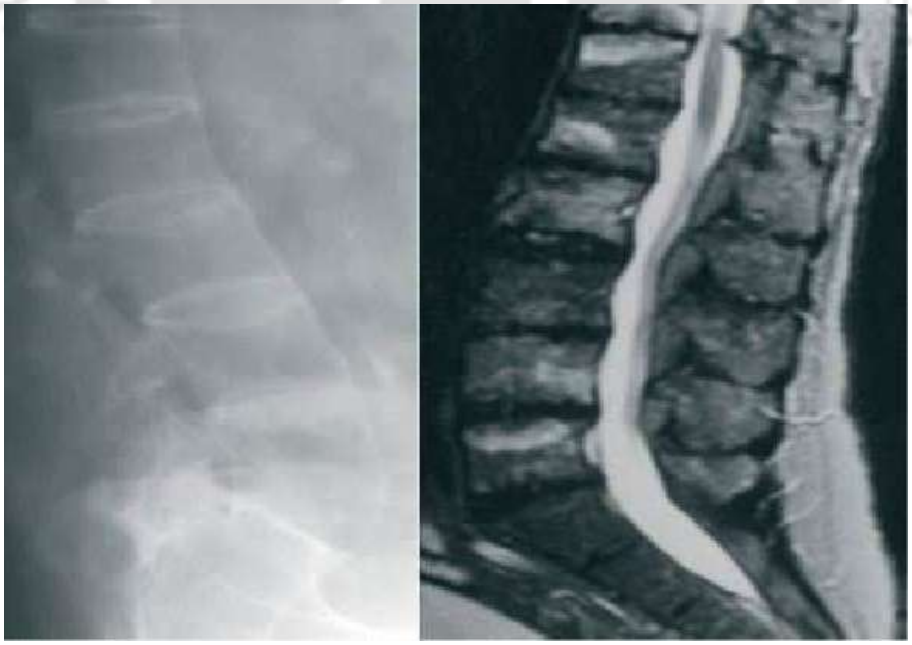

Figure 1.6: MRI Radiograph of Chronic and Active Changes in the Lumbar Spine of a Patient with Ankylosing Spondylitis (Braun *et al.*) [27].

Figure 1.7: Clinical Image of the Right Foot showing Gouty Arthritis with Extreme Swelling, Erythema, and Tophi (Keyser *et al.*) [28].

(iii) Gouty Arthritis (GA):- Gout is also a disorder under the inflammatory arthritis category, which mainly occurs with the increasing age of the people (Keyser *et al.*) [41]. It happens due to the deposition of uric acid crystals in the joint and results in poor health issues as shown in Fig. 1.7. Mikuls *et al.* [42] reported the prevalence of gout as 1.5% (2.8% in men and 0.4% in women) by using the Framingham data. The observation was found to be similar as the available data from UK General Practice Research Database which shows the 2% among men and 1% among men and women combined which is an approximately similar prevalence of gout. Gout seems to be more prevalent in an urban population with high-purine diet intake, excessive alcohol consumption and physical inactivity (Smith *et al.*) [43].

(iv) Osteoarthritis (OA):- Osteoarthritis is one of the most prominent and common chronic disorders among adults, which mainly occurs due to cartilage degradation. It causes severe pain during joint articulation, mechanical instability, and sometimes inferior knee health condition, which leads to total knee replacement

(TKR) or knee arthroplasty (KA). In the human body, osteoarthritis may severely affect various joints like hip, knee, foot or ankle, etc. The occurrence of the disorder may involve various person-level risk factors like demographic characteristics and family history (genetic), obesity and metabolic syndrome, lack of nutrition and vitamins in the body, bone density and bone mass and smoking habits, etc. Other factors, which involve joint levels are like bone/joint shape, injury, muscle strength and mass (musculoskeletal disorders), joints loads and alignment (human gait patterns), occupation and physical activity, leg length inequality, etc. (Allen *et al.*) [33].

1.5 Assessment of Cartilage Degradation

This section refers to the recent developments related to dominant causes of cartilage degradation and its assessment methods. The first time tissue-level FE modeling and indentation testing were performed on human tibial cartilage. OA severity has been verified by using modern fibril-reinforced poroelastic (FRPE) computational models (Ebrahimini *et al.*) [44]. Further, they characterized the human tibial cartilage and investigated a depth-wise structure-function relation in a statistical analysis model. Properties like contents of proteoglycans and collagens along with collagen orientation angle were compared in a derived model with traditional elastic and viscoelastic biomechanical cartilage properties. Human tibial cartilage at different stages of osteoarthritis was reported as a first study to establish structure-function relationships (Ebrahimini *et al.*) [45]. Recently, Ebrahimi and his coworkers extended the research for the study of human femoral condyle cartilage, and its constituent material properties were also analyzed. A significant degradation in mechanical properties was observed in severe OA samples (Ebrahimini *et*

al.) [46]. An article has been published on the study of chondrocyte deformation under mild dynamic compression of cartilage. During dynamic compression in ECM, the metabolic behavior of chondrocyte changes and leads to its volume loss and mass transfer from cell to ECM. It is observed at minimal strain (0–10)% (Komeili *et al.*) [47]. A new electromechanical grading system is developed for the qualitative assessment of human cartilage and its reliability test. The generated data set was compared with the arthroscopic International Cartilage Repair Society (ICRS) grading system. This development can assist surgeons in human cartilage examination (Sim *et al.*) [48]. The effect of joint relative surface velocity is more prominent for OA progression, as observed in an ovine model study. In their work, a significant oscillations were observed in the relative velocity in the tibiofemoral joint after injury (Vakiel *et al.*) [49]. Cartilage regeneration methods have opened a broader scope for regenerative cell therapies. It is known that hyaline articular cartilage and meniscal fibrocartilage lesions do not heal immediately. Researchers generated 3D microtissues and self-assembled spheroids as a future therapy for cartilage and meniscal lesions (De *et al.*) [50]. In a recent investigation, chondrogenesis of human mesenchymal stem cells (MSCs) has been performed on scaffolds. These gelatin-based scaffolds contained partially sulfated cellulose and a sulfated glycosaminoglycans (GAG) mimetic derived from cellulose and compared with native GAGs. The authors concluded that cartilage repair could be supported by using partially sulfated cellulose sulfate, and it may be a feasible way for supporting chondrogenesis (Menezes *et al.*) [51].

Almeida *et al.* [52] explored Kartogenin (KGN) in human MSC chondrogenesis. It is a small synthetic molecule used as an encapsulated nanoparticle that is helpful to decrease the heterogeneity of MSCs and improve the potential to treat osteoarthritis. Authors investigated the effects of KGN-loaded-PLGA-poly (lactic acid-co-glycolic acid) nanopar-

ticles, PLGA–poly (ethylene glycol) (PEG) nanoparticles, and PLGA–PEG–hyaluronic acid (HA) nanoparticles. It is observed that human MSC chondrogenesis has been improved by using all KGN-loaded nanoparticles compared with non-KGN-loaded. Neidlin *et al.* [53] introduced a novel drug evaluation method for healthy and OA subjects. They evaluated the change in protein release in the ECM patterns and concluded that the macroscopic behaviour changes by changing the structural properties in the cartilage.

1.6 Organization of the Thesis

The complete research work presented in the thesis has been organized into eight chapters. The following is a brief outline of the each chapter's content.

- Chapter One presents an introduction to the knee joint anatomy, various types of cartilage diseases, mechanical properties of the articular cartilage and, different types of knee joint disorders with their methods of assessment.

- In chapter Two, a thorough review of the literature in the domain of vibroarthrography and, acoustic emission based knee OA detection is presented. On the basis of in depth literature survey, research gaps are identified and, research objectives are proposed.

- The development of an IMU sensor-based digital goniometer and its performance validation for studying the knee joint kinematics is presented in Chapter Three.

- In Chapter Four, the development, performance validation, and outcomes of the testing of a contact microphone-based wearable device on healthy and pathological subjects are presented.

- In Chapter Five, the study is performed using a commercial acoustic sensor system on healthy and OA subjects of different age groups, and the outcomes are investigated quantitatively in the form of various signal features.

- Chapter Six shows the validation of acoustic signal features with the obtained Joint Space Narrowing (JSN) from the radiographic findings of OA subjects having different KL grades and the features are identified as a suitable biomarker for OA detection and classification.

- Chapter Seven shows the fabrication and validation of an indigenously developed acoustic microphone and Raspberry Pi 4-based knee joint health monitoring device.

- Finally, in Chapter Eight, the research summary and significant conclusions are presented with suggestions for future research.

Chapter 2

Literature Survey

2.1 Introduction

This chapter provides a comprehensive review of pertinent literature surrounding OA prevalence and the necessity for advanced detection methods. The sections provide an overview of the prevalence rates of osteoarthritis in India and other countries, emphasizing the urgent need for effective monitoring strategies. Subsequently, various methodologies are explored employed in osteoarthritis detection, assessing their respective strengths and limitations. Special attention is given to sensor-based joint monitoring systems, with a focus on vibroarthrography as a potential diagnostic tool. However, the discussion ultimately transitions to acoustic emission-based joint monitoring, highlighting its real-time assessment capabilities and enhanced sensitivity in detecting pathological changes. Based on the thorough literature survey, technical gaps are identified and research objectives are framed with a proposed methodology.

2.2 Prevalence of Osteoarthritis

As discussed in the previous chapter 1, knee OA is the most common degenerative joint disorder and mainly occurs due to the degradation of articular cartilage (Pal *et al.*) [54]. It is a global burden, and it affects around 18% of females and 9.6% of males over the age of 60 years worldwide (Alkady *et al.*) [55], (Glyn *et al.*) [56]. Its prevalence

increases dramatically with aging and is considered as the 10^{th} leading cause of nonfatal burden worldwide (Rahaman *et al.*) [57]. Pathological alterations become apparent in the advanced stage of OA. These transformations result in the softening of articular cartilage that leads to chronic ulceration and localized erosion on the femoral and tibial condyle surfaces. As a result, it becomes an irreversible disorder in humans, especially in females and older people, allowing severe joint pain and stiffness (Akinpelu *et al.*) [58]. Brennan *et al.* [59] studied arthritis in six low-middle-income countries. The survey was done in China, Ghana, India, Mexico, Russia, and South Africa. They analyzed the data of 44,747 samples from the World Health Organization (WHO) on global aging and adult health. The highest standardized arthritis rate was observed as 38% for men and 17% for women in Russia. Kellgren and Lawrence [60] established a radiological assessment method that identifies the prevalence of knee osteoarthritis, classifying the condition into five grades.

As shown in Fig. 2.1, Grade-0 confirms that there are no OA symptoms. Grade-I signifies a doubtful narrowing of joint space and possible osteophytic lipping. Grade-II assures the osteophyte certainty and possible narrowing of joint space. Grade-III confirms the moderate multiple osteophytes, inevitable joint space narrowing, presence of few sclerosis, and some possibility for the damage of bone contour. Grade-IV falls under the severe stage of OA and confirms the large osteophytes, marked narrowing of joint space, severe sclerosis, and deformity of bone contour (Chen *et al.*) [61]. Another method was reported by Ackerman for the Western Ontario and McMaster Osteoarthritis Index (WOMAC), which is widely used for the measure of the knee and hip osteoarthritis and was developed in the early 1980s (Ackerman and Ilana) [62], (Gandek *et al.*) [63]. The analysis of a pain management system WOMAC consists of three different dimensions

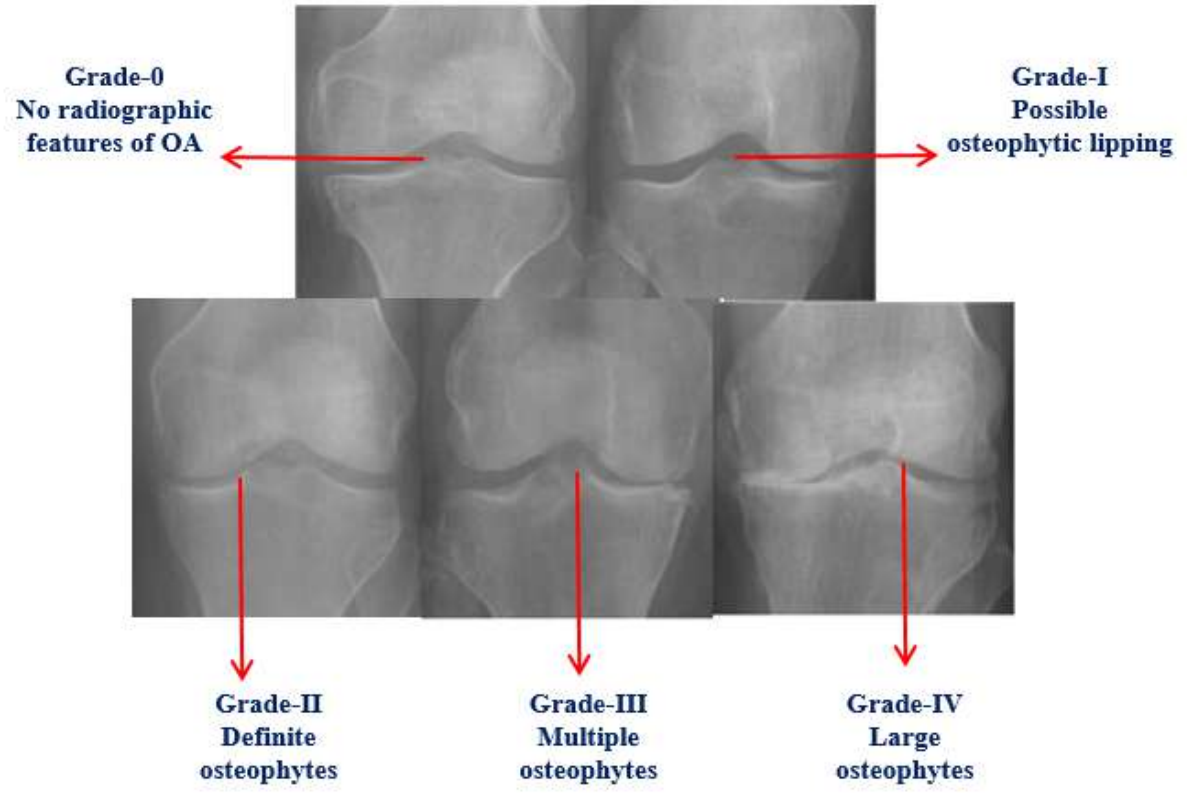

Figure 2.1: X-ray Radiographs of KL Grades in Knee Osteoarthritis (Chen *et al.*) [48].

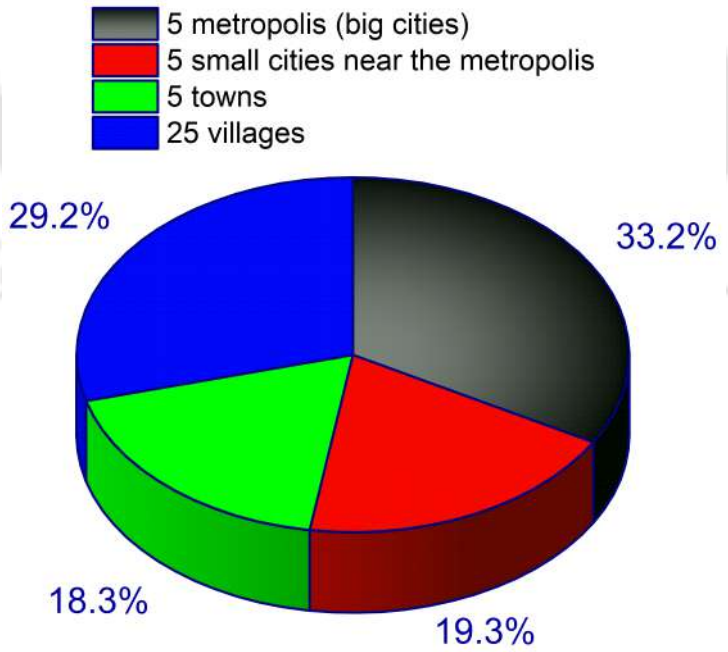

Figure 2.2: Cross-sectional Study Reported OA Prevalence in India (Yadav *et al.*) [52].

of diagnosis like pain, stiffness, and physical function in the ordinal scale index between 0-4. The lower index indicates a lower level of symptoms (McConnell *et al.*) [64].

In a recent study, five major sites in India are reported with the prevalence of OA knee over the sample size of 1000 people per site as shown in Fig. 2.2. The overall prevalence of primary OA knee in different sites of India is reported to be 33.2% in large cities, 19.3% in small cities, 18.3% in towns, and 29.2% in villages (Yadav *et al.*) [65]. Very limited research data from the North-Eastern region of India on the prevalence of knee OA is published so far. Some studies are reported based on work culture, habitats, and other health aspects. The prevalence of knee OA is found to be 29.4% among 320 subjects working in the tea garden in the Jorhat District of Assam (Buragohain *et al.*) [66], 7.6% over the target population of 539 in the Keinou Village of Manipur (Ghodke *et al.*) [67], and 85% in the sample size of 200 people residing high-altitude areas of Tripura (Haque *et al.*) [68].

2.3 Methods of Osteoarthritis Detection

Knee osteoarthritis is an epidemiology in India and other countries, which challenges to find the best possible solutions in knee health care and advance medical treatments for the same. Various diagnostic methods are already available, and they have their importance as a diagnostic tool with certain limitations. Multiple sensors are also used to develop advanced wearable systems for knee joint health assessment in different aspects. However, selecting sensors to build an accurate and reliable joint monitoring system is a critical criterion. For the development of a wearable device, essential features include high efficiency and accuracy, excellent reliability, high sensitivity, small size, lightweight, low energy consumption, and minimal processing resources. This section covers a detailed literature survey on osteoarthritic diagnostic methods, advanced sensor systems, and their use in OA detection with limitations.

2.3.1 X-Ray Imaging

The X-ray examination of an osteoarthritic knee mainly shows the presence of joint space narrowing, osteophytes, and subchondral bone sclerosis (Nagaosa *et al.*) [69]. It is a non-invasive method in which joint space narrowing reflects the cartilage thickness on X-ray images. Osteophytes indicate marginal bone reaction proportional to the cartilage loss, and subchondral bone reactions or condensation is associated with the overlying fibro cartilaginous damage (Fife *et al.*) [70], (Felson *et al.*) [1]. These X-ray examinations can be performed in three different joint views (frontal view, lateral view, and tangential view), but only in two dimensions. It is understood that these radio graphical X-ray examinations must be performed very carefully with proper alignment of the X-ray beam and orientation of the patellofemoral compartment (Bedson *et al.*) [71].

Limitations: Chaisson *et al.* [72] revealed that there is a limitation in radiographic X-ray imaging. It was found that the skyline or lateral view of the patellofemoral joint gives an unsatisfactory image from an osteoarthritis point of view. Joint space narrowing and osteophytes are the OA identification criteria, but Teichtahl *et al.* [73], in their study, revealed that in X-ray images, the longitudinal reduction in the joint space is not necessarily an accurate measurement of the articular cartilage volume. The authors also stated that osteophytes might be the outcome of musculoskeletal traction forces. Thus, the conventional radiography technique is not ideally suitable for the detection of osteoarthritis.

2.3.2 Ultrasonography

Ultrasound imaging is a susceptible detection method for soft tissue changes like joint space narrowing and subchondral bone density in the musculoskeletal structures (Doria *et al.*) [74]. It is a non-invasive and cost-effective method in which high-frequency transducers are used. For hip joint assessment, the ultrasonic frequency should be less than 10 *MHz*, while for optimal cartilage visualization, it should exceed 13 *MHz* (Moller *et al.*) [75]. The ultrasonography method is well suited for OA detection. Moreover, low-intensity pulsed ultrasound (LIPUS) has remarkable benefits in bone fracture healing. It is reported that LIPUS is highly effective in cell metabolism and the resurrection of soft tissues like mandibular condylar cartilage (Tanaka *et al.*) [76]. It can record positional and dimensional changes of soft tissues, tendons, ligaments, synovial recesses, bursae, cartilage, and peripheral conditions of the meniscus (Hossian *et al.*) [77]. This method has diagnostic potential in knee OA and reveals long term predictability for disease progression as an imaging biomarker (Oo and Bo) [78].

Limitations: The application of the ultrasound method in OA detection has a challenging restriction (Iagnocco *et al.*) [79]. The ultrasonic visualization of the articular cartilage is limited by the acoustic window, whose width is determined by the anatomy of the joint tested because the ultrasound beam is not able to penetrate the bony cortex (Ostergaard *et al.*) [80]. Assessments of the cartilage of the weight-bearing areas are difficult in patients with advanced OA due to limited active flexion. The cartilages of the patella and the tibia are always challenging to examine, and also the depth of subchondral bone erosion cannot be predicted by using the ultrasound method. Furthermore, the examination of multiple scanning planes in the clinical setting can be time consuming (Guermazi *et al.*) [81].

2.3.3 Magnetic Resonance Imaging (MRI)

Magnetic resonance imaging is the non-invasive assessment of the articular cartilage and sensitive to identify the defects of articular cartilage surfaces (Bredella *et al.*) [82]. MR imaging can be used for repeatable determination of articular cartilage thickness, and topographical maps obtained from MR images may assist in the characterization of in-vivo orthopedic conditions (Eckstein *et al.*) [83]. 3-D reconstructions of the cartilage thickness and the joint are a beneficial assessment for detecting the knee OA (Leersum *et al.*) [84]. MRI examinations of the knee are also useful to detect chondromalacia, which is not possible with conventional X-ray images. A chondromalacia patella is a disorder in the knee in which the cartilage under the patella surface deteriorates and softens (Cashman *et al.*) [85]. MRI data is helpful to predict the development of OA. It is reported that, template-based finite element (FE) modeling is an appropriate solution for knee joint analysis and OA detection (Mononen *et al.*) [86]. Further, the authors extended their work applied computed tomography (CT) to model the knee joint. They concluded that the CT method could produce similar results as MRI data sets [86] at high resolution and low cost (Mohammadi *et al.*) [87]. In a recent study, the characteristic recovery time is proposed as a non invasive marker with its potential to measure cartilage mechanical properties through quantitative MRI (Cutcliffe *et al.*) [88].

Limitations: The MR imaging technique is still under development, and routine imaging of human joints is not fully established in clinical practice. It is a costly diagnosis method. Additionally, an excellent histological and macroscopic correlation can only be observed in severe grades of chondromalacia, and MR does not meet this requirement.

2.3.4 Optical Coherence Tomography (OCT)

It is an infrared-based imaging technique that gives a supportive environment to the in-vivo cartilage images at a micrometers resolution. When the infrared beam is scanned across the tissue surface, three-dimensional images can be produced to interpret the tissue's microstructure. Li *et al.* [89] revealed osteoarthritic knee cartilage imaging using high-resolution optical coherence tomography during open knee surgery. The author achieved the first non-invasive, real-time in-vivo imaging of human cartilage in healthy and osteoarthritic knee joints, with a resolution measured in micrometers. Rashidifard *et al.* [90] studied that OCT is beneficial for the microstructural interpretation of the cartilage tissue. Over the current imaging methods like MRI, and X-ray, OCT reflects various advantages. It can surface at a resolution 25x higher than the clinical subsurface at a speed of 120 high-resolution images per second. Chu *et al.* [91] reported that optical coherence tomography could provide quantitative information about the disease state of articular cartilage. The authors also stated that the simultaneous evaluation of arthroscopy and T2 MRI measurements in OCT makes it a powerful potential tool for the detection of early chondral changes.

Limitations: The combination of arthroscopy and T2 MRI makes this method more invasive, which is highly dependent on the operator use and image post processing for the direct assessment of the articular surface. In a study by Mokbul and Mobin [92], the author explained the limitations of OCT in the measurement of smaller vessels less than 20 micrometers. The various OCT setups are under development, which can reach up to the 1 μm imaging depth.

2.3.5 Arthroscopy

It is a semi-invasive surgical procedure in which quantitative mechanical evaluation is performed using a hand-held indentation of a probe. Arthroscopy is a valuable technique for inspecting the interior of a knee using an arthroscope, which is inserted into the joint through a small incision during the procedure. It is an excellent tool for the assessment of cartilage losses and the classification of chondromalacia lesions. In a patellofemoral study, it is reported that arthroscopy is an adequate tool for the diagnosis and classification of degenerative changes of the patellofemoral joint (Fleming *et al.*) [93]. A custom fiber-optic arthroscopic probe having near-infrared (NIR) spectroscopy detection was used to measure the damage in cartilage associated with post-traumatic OA and idiopathic OA knee. This will be a useful technique for cartilage repair in arthroscopy (Nippolainen *et al.*) [6].

Limitations: The influence of the indenter geometry has been observed in the arthroscopic evaluation of cartilage degeneration. The porosity and the indenter geometry may produce distinct deformation properties in cartilage, which may affect the precise evaluation (Li and Herzog) [94]. A limitation of the procedure is that it cannot be used for patients with highly degenerated knees due to OA, ligamentous instability, meniscectomy, or patellectomy. The arthroscopic treatment cannot be used as a repeated assessment of patients over time due to its semi-invasive nature and anesthesia requirements. Knee arthroscopy is not efficient for patients who suffered severe degenerative changes in both femoral condyles like chondrocalcinosis (Ogilvie *et al.*) [95].

2.4 Sensor-Based Joint Monitoring System

Various sensors have been used for the knee joint health assessment in different aspects. Mukhopadhyay [96] reviewed the selection of sensors to develop an accurate and reliable joint monitoring system. High efficiency and accuracy, excellent reliability, high sensitivity, small size, lightweight, lower energy consumption, and limited processing resources are the critical features for developing a sensor-based wearable device. The different sensor technologies for the monitoring of human body joints are discussed below.

2.4.1 Optical Sensors

Donno *et al.* [97] reported that the Optical sensor-based joint monitoring systems are mostly used with intensity modulation or visual navigation methods. A prototype of a flexible optical fiber goniometer has been developed for the measurement of relative angle in a rotating joint. The sensor prototype has a range of a relative angle of 90°, and it was lightweight, flexible, and highly accurate. Quantitative human gait analysis was performed by (Bilro *et al.*) [98], and the authors introduced a low-cost wireless and wearable gait monitoring system based on a plastic optical fiber sensor. Lim *et al.* [99] proposed a reliable and non-intrusive design of an optical-based goniometer for human joint measurement. The device was compact, lightweight, and confirmed the adherence to human skin even during the stretch. Stupar *et al.* [100] developed a low-cost and straightforward intensity modulated fiber optic curvature sensor to measure joint movements. Plastic optical fiber was used for sensor fabrication, and the sensor was optimized for small curvature measurements. It was a wearable, non-invasive, non-intrusive, and completely harmless device. By measuring the attenuation of the optical

signal, the bending angle of the fiber is determined, and due to this simple sensing principle and structure, the optical fiber sensors can be integrated into a monitoring system for measuring human joint angles (Rantala *et al.*) [101]. Li *et al.* [102] developed a mathematical model and prototypes for monitoring the motion of human elbow and wrist joints. The designed wearable device can examine the upper limb gestures and convert the joint motion angle into a displacement. Vakiel *et al.* [103] fabricated a small Fiber Bragg Grating (FBG) sensor (diameter of 125-300 μm and sensing length of 1 mm) which can be inserted in the joint space. The possibility of degenerative conditions was observed by measuring cartilage stresses in both healthy and injured knee joints.

2.4.2 Imaging and Video-Based Tracking System

For the monitoring of human joints, imaging and video-based human skeletal tracking is widely recognized and accepted. In November 2010, Microsoft released an inexpensive accessory device known as Kinect. The device was able to measure joints and their positions without any markers. Kinect is a peripheral device for the Microsoft Xbox 360 console, allowing users to control games with their bodies instead of conventional controllers (Mobini *et al.*) [104]. In a study, MATLAB Kinect Skeletal Tracking (MKSTS) system was designed using MATLAB programming software. An economic system as an alternate gait analysis method is developed and suggested that MKSTS is valid for use as an alternative method in determining the gait parameters (Abiddin *et al.*) [105]. Islam *et al.* [106] reported that musculoskeletal disorder is increasing in humans due to accidents and aging. It is a significant concern for future orthopedics, and they proposed a system to monitor the movement of human body parts in different yoga poses. Microsoft Kinect was used for real-time detection of joint points, and they determined the various

angles to measure a particular yoga pose's accuracy. Wang *et al.* [107] observed that a single depth camera could only estimate the human joint position in its field of view. Imaging and video-based joint tracking systems are a popular and reliable monitoring technique, but they require complex, expensive infrastructure and sophisticated analyses. This system is only useful with a pre-equipped environment and setup, restricting users and their usual movements, making it unsuitable for continuous and long term joint monitoring (Patsadu *et al.*) [108].

2.4.3 Textile Based Sensors

Textile based sensors are highly suitable to measure joint angles. Flexible conductive sensors, flex sensors, strain sensors, etc., are the significant types. They work on the principle of resistance changes, which is directly related to the corresponding joint angles (Bergmann *et al.*) [109]. These sensors can be easily integrated into stretchable skin-tight fabrics around the joints. Gibbs *et al.* [110] developed a new method using conductive fibers incorporated into comfortable, flexible structures to monitor and measure human movement by measuring single or multi-axis joint angles. Bakshi and Mahoor [111] reported a wearable sensor system for the measurement of joint body flexion. The authors used multiple flex sensors and mounted them on a supportive cloth to measure a joint's flexion angle, and error was estimated. Gioberto [112] developed a garment-integrated wearable sensor for knee joint monitoring by stitching sensors into the fabric to detect stretch and, compiling the error estimation in the measured joint angles. Totaro *et al.* [113] studied the lower limb joint position by developing soft smart garments. A capacitive strain sensor was used in the process with a combination of conductive and dielectric layers, and a knee brace embedded with three capacitive strain sensors is devel-

oped. Jeong *et al.* [114] developed a microfiber-based wearable health-care sensing device that can monitor the human body's health status even without affecting the sweat of the body and water. The device was made of Polyurethane (PU)–Tin oxide (SnO2)–carbon nanotube (CNT) composite microfiber. Park *et al.* [115] used conductive yarns and different textile substrates like braided elastic fabric, knit fabric, and woven fabric to produce a wearable sensor for the human body. These sensors give output signals corresponding to the folding motion of the spinal joint over a predetermined angle of movement and the gait pattern of the wearer of the sensor. A sensor is fabricated based on flexible and stretchable CCF (chopped carbon fiber)/PDMS (polydimethylsiloxane) conductive yarns in recent development. These sensors are designed on the piezoresistive (resistance strain) principle for detecting human joint motion (Montazerian *et al.*) [116].

2.4.4 Inertial Measurement Unit (IMU) Sensors

IMU sensors are widely used to measure three-dimensional accelerations, angular velocity, and the magnetic field vector. As a unit, three sensors (accelerometer, gyroscope, and magnetometer) are assembled in one device and are usually termed as micro-electro-mechanical systems (MEMS) having 9 degrees of freedom (DOF). These IMUs are the most promising and compact units for clinical applications and play an important role in designing wearable devices. IMUs can be used to measure joint motion, its angular position, and joint orientation with precision and accuracy. The authors suggested using two IMUs for the compensation of joint alignment and accurate measurement of joint angle (Bakhshi *et al.*) [117], (Favre *et al.*) [118]. Favre *et al.* [119] developed a new calibration method for the joint coordination system. They validated the measured data from IMU against the Liberty magnetic motion capture and tracking device (Polhemus, Vermont,

USA). A functional calibration procedure was added to assess the error by comparing the results obtained from the combined method to the reference system. In another study by Seel *et al.* [120], the use of a magnetometer was excluded from the IMU unit, and the device used only accelerometer and gyroscope data. They identified through indoor measurements that nine degrees of freedom IMUs could suffer from magnetic disturbances due to other magnetic devices present in the experimental environment. Two IMUs and six DOF systems were suggested to improve the accuracy of joint angle measurements by doing precise calibration and alignment.

Here, the recent developments in IMUs positioning on the joint, their frequency ranges, and method of analysis are reviewed. Optical tracking systems for hip and knee joints have been reported with RMS error less than 3.0° using three IMUs with 9 DOF unit at a sampling rate of 10-100 *Hz* (Salehi *et al.*) [121]. A similar study was conducted with a stereophotogram metric system to measure hip and knee joint angles using three IMUs with a 9 DOF system and reported RMS error less than 3.2° with a sampling rate of 100 *Hz* (Bonnet *et al.*) [122]. Four IMUs and 9 DOF systems were introduced for the hip and knee joint tracking in consecutive years using a computer mathematical simulation at 50 *Hz* sampling frequency. The maximum RMS error was reported as 1.7° (Vargas *et al.*) [123]. Goniometer based two IMU system has also been reported to estimate knee joint angle with 100 *Hz* sampling frequency, where 5.15° mean RMS error was reported (Tognetti *et al.*) [124]. A vision-based motion capture system became most popular in the last few years and widely used for human gait analysis (Crews *et al.*) [125]. The authors introduced two IMUs with 9 and 6 DOF systems for angle measurement, heel-strike and toe-off event in gait analysis. They reported a very high correlation (less than 0.947) with this system and estimated the RMS error of 8° during the joint

angle measurement. During the data collection, the sampling frequency of 30 *Hz* and 128 *Hz* was followed. A similar study by Ong *et al.* [126] was reported with an improved and economic human motion analysis device for quantitative assessment in human gait experiments. Authors reported with two IMUs and 6 DOF, a commercial video motion analysis system. The RMS error was estimated to be 5% in angular velocity and 7% in average bending angle with sampling frequency in the range of 20-50 *Hz*.

2.5 Vibroarthrography

Vibroarthrography (VAG) is recognized as an emerging tool for the detection of knee osteoarthritis. In this technique, the sound or vibrations originated from the infected knee are mainly targeted to capture. After analyzing the vibration and sound frequency pattern, the Kellgren and Lawrence grades of osteoarthritis are determined. This disease detection method is advantageous because it integrates real-time examination in dynamic mode, is radiation-free and inexpensive, and effectively assesses knee cartilage damage during various movements such as flexion-extension, sit-to-stand, and stand-to-sit. This method is entirely non-invasive, cost-efficient, and perfectly suitable for the dynamic detection of knee joint disorders. Blodgett [8] was the pioneer author in vibroarthrography, who suggested that auscultation may be an innovative method for detecting joint diseases. In his experimental procedures, he used the full-sized bowles stethoscope with a soft rubber cap that sprung over the diaphragm and suggested that in comparison to other joints, the knee is the most suited for the analysis of sounds.

Steindler [127] used a cardiophone (a diaphragm connected to a crystal) to exclude the skin's friction noises and recorded the output on an oscillograph. Steindler found the two major problems in his experiment; (i) the difficulty in eliminating the outside and

extra-articular noises and (ii) the difficulty in locating the sound center from where the sound originates. Steindler's report was the first communication on the appreciation of sound phenomena in the locomotor system for diagnostic purposes. He also introduced the nomenclature of knee sounds like crunching, grating, cracking, and isolated sounds. Crunching sounds were observed as very fine, low, weak, and sustained. Grating sounds were higher, coarser, and louder while cracking was a harsh, continuous, and high pitched sound. Peylan [9] studied around 214 patients with several arthritis types using a regular and an electronic stethoscope. The aim of the experiment was to distinguish between osteoarthritis and rheumatoid arthritis but could not get positive outcomes. Hunter and Brooks [128] detected the articular joint noises by using the crystal type microphone applied on the medial and lateral knees and recommended that the technique can be used as a diagnostic tool. Chu *et al.* [10] reported that a unique acoustic signature could be obtained from rheumatoid and degenerated knee joints. It was observed that cartilage deterioration has a significant correlation with the degree of acoustic power. The authors verified the observations by using bovine joints and in-vitro simulations. For knee joint sound pick up, the authors used two microphones and a differential amplifier. Mollan *et al.* [11] followed the previous pilot studies and conducted various experiments to capture the knee joint sounds using a condenser microphone. Attempts were made to exclude skin friction and ambient noise. Mollan and his coworkers further studied and revealed that using a piezoelectric based accelerometer is the more suitable method for detecting vibrations from human joints (McCoy *et al.*) [129].

Kernohan *et al.* [130] developed the concept of vibration arthrometry and applied the technique to examine hip dislocation in an infant group. In this method, an accelerometer was used with a piezoelectric crystal with a mass resting on it and covered in a metal

case. In another study by Kernohan *et al.* [131], joint angular velocity was analyzed during the vibration arthrometry measurement. The authors strongly recommended the standardization of the joint speed to correct the signal level and accurate measurement of the degree of the joint damage. Tavathia *et al.* [132] introduced a method of linear prediction (LP) modeling for the segmental and quantitative analysis of the knee joint. They revealed that the past studies did not consider the nonstationary nature of the obtained signal in their investigation. Zhang and Rangayyan [133] focused on the importance of muscular interference during the vibroarthrography (VAG). They concluded that along with the skin friction and ambient noise, the muscle contraction interference (MCI) is also significant to rectify because this artifact contaminates the low-frequency VAG signals produced by the knee joint. Reddy *et al.* [134] focused on the fast leading technology in health care engineering and characterized knee arthritis and chondromalacia by using a non-invasive acceleration method. Shen *et al.* [135] introduced the localization of knee joint cartilage pathology by multichannel vibroarthrography. They revealed the limitations that the number of transducers is not enough to locate the source of VAG signals originating from the joint. Maussavi *et al.* [136] reported a screening method of vibroarthrographic signals using adaptive segmentation and linear prediction modeling. Rangayyan *et al.* [137] worked on the parametric representation of the VAG signals and reported the study between three parameters; Autoregressive (AR) coefficients, dominant poles, and cepstral coefficients. The authors reported that cepstral techniques were well suited for analyzing signals that contain echoes (wavelets) of a fundamental wavelet or a signature. The other related articles in this field are summarized in Table 2.1.

Table 2.1: Summary of the knee joint vibroarthrography

References	Methodology	Conclusions
Rangayyan and Wu [138]	Analyzed the variability of the VAG signals and their radial basis functions were carried out on the database of 89 VAG signals.	The screening efficiency was achieved by up to 85%.
Wu and Krishnan [139]	Again the same previous database of 89 VAG signals was analyzed using the least squares support vector machine (SVM) method.	Classification accuracy was improved up to 80.9% by using multiple classifier systems (MCS) based on a recurrent neural network (RNN).
Tanaka and Hoshiyama [140]	Analyzed VAG signals and angular changes of the knee in a total of 145 patients, and joints were recorded by using three axes accelerometer with an amplifier.	Maximum VAG signals were observed in the OA knees at $50-99$ Hz and $100-149$ Hz during standing up and sitting down movements, respectively.

Table 2.1: Continued on next page

Table 2.1: continued from previous page

References	Methodology	Conclusions
Wu *et al.* [141]	Performed the signal classification using Fisher's linear discriminant analysis, SVM with polynomial kernels, and the maximal posterior probability decision criterion to model the distributions of the VAG signals recorded from healthy and unhealthy subjects.	The signal classification accuracy was recorded as 86.67 % in the maximal posterior probability criterion compared to other methods.
Wu *et al.* [142]	Introduced the ensemble empirical mode decomposition (EEMD) and detrended fluctuation analysis (DFA) approach for removing the artifacts in the VAG signals.	Recorded signal to noise ratio (SNR) as 20.52 *dB* in EEMD and 20.87 *dB* in DFA. The authors concluded the possibility of improving the SNR by combining two algorithms.
Andersen *et al.* [143]	The authors used an accelerometer as a sensor in the majority, and signals were recorded in a frequency range below 1000 *Hz*.	The authors suggested the use of multichannel VAG recordings for better differentiation in knee joint disorders.

Table 2.1: Continued on next page

Table 2.1: continued from previous page

References	Methodology	Conclusions
Befrui *et al.* [12]	A machine learning approach with a linear SVM was used for the signal characterization and placed a miniature accelerometer and one piezoelectric disk on each subject's knee.	Using machine learning with a linear support vector machine, a classification specificity of approximately 0.8 at a sensitivity of 0.75 could be achieved.
Karpinski *et al.* [13]	The knee's open and closed kinematic chain movements have been differentiated by doing FFT, recurrence plots, and recurrence quantification analysis (RQA).	Cartilage degradation was validated, and a method was suggested for bioacoustics signal analysis.
Safaei *et al.* [144]	Used an external vibration simulation by considering the knee as a linear system between 50 Hz and 10 kHz frequency under a compression force of less than 5 N and characterized the vibration signals in audible frequencies.	Substantial attenuation of the transmitted vibration energy is observed in the frequency for a few kHz and, above 1 kHz. A gradually increasing trend of the frequency response was reported for frequencies above 3–4 kHz.

Table 2.1: It ends from the previous page.

Various researchers recommended using the accelerometer, IMUs, goniometers, amplifiers, bandpass filters, analog to digital converter, and a software package to receive complete information from the knee. The correct positioning of the vibration or acous-

tic sensor on the knee is also very important to detect acoustic emissions. Background noise is always a matter of concern while recording the signals. Choi *et al.* [145] developed an advanced piezoelectric sensor by considering design modifications. The authors used a pin-type probe at the center of a unimorph device in which a disk-shaped piezoelectric ceramic and a metal plate were bonded. They concluded that the probe would make direct contact with the skin site, and there will be no need to eliminate the background noise in such a system. The study was conducted using a piezoelectric sensor on twenty healthy subjects (11 males and 9 females, age: 25.4±1.9 *years*; body mass: 64.0±10.0 *kg*; height: 169.5±6.0 *cm*). The subjects have no previous injuries, symptoms of swelling, and pain. The experimental protocol was followed by informing each participant, and written consent was approved by the Yonsei University Research Ethics Committee, South Korea. Fourteen more OA patients were diagnosed with Kellgren Lawrence grades I and II (3 males and 11 females, age: 63.0±8.9 *years*; body mass: 63.3±9.7 *kg*; height: 162.4±8.4 *cm*). The authors constructed a sensor verification system using four piezoelectric sensors to measure the time delay and sensitivity characteristics of output signals between sensors. During the test, the subject was asked to cross their arms across the chest and performed flexion-extension (non-weight-bearing) and four-phase sit-stand-sit exercise (weight-bearing). The acoustic sensors were placed at the medial epicondyle of the tibia, the tibia's lateral epicondyle, and the front of the patella. Two inertia sensor units were also attached to the thigh and tibia, and the knee joint angles were calculated using relative angles during the tasks. The sampling rate was 50 *kHz* for acoustic sensors and 100 *Hz* for inertia sensors. A 30 *bpm* metronome was used to maintain the speed of exercise. The maximum flexion angle was 90° during the test exercise and repeated in 2 minutes break for both methods. Short-time Fourier transform (STFT) was used

for the spectral analysis of the AE signal, and each signal was divided into small data frames. Then Fast Fourier Transform (FFT) was applied to each data frame. The authors verified their findings from previous study (Toreyin *et al.*) [146]. They suggested that a pin-type probe in the piezoelectric sensor can detect the knee joint sounds, and there is no need to remove the artificial background noise by using this sensor. Studies also reported that the bending velocity of the hip joint varied during sit-stand-sit exercise. The height of the chair also affects the lower extremity muscles and knee joint. In this research, the speed influence was eliminated using a metronome, and the chair's height was adjusted such that the knee joint angle was 90° when the subject was seated. The VAG signals are also associated with the age of the subjects, yet this method appears to be a promising non-invasive and low-cost tool for OA detection (Bkaczkowicz *et al.*) [147], where the range of frequency of VAG signals in healthy and OA patients. The healthy group exhibits a frequency less than 1 *kHz*, while in the OA groups, it lies above and up to 10 *kHz*.

2.6 Acoustic Emission-Based Joint Monitoring

Various researchers from different groups have focused on the piezoelectric film-based or MEMS-based microphones for capturing the knee joint sounds during the last few years. The sound originated from the knee is termed acoustic emission (AE) and produces vibroarthographic (VAG) signals. Ali *et al.* [148] introduced the role and importance of piezoelectric energy harvesters in biomedical applications. The authors investigated the influence of new piezoelectric materials to design biomedical devices like cardiac pacemaker and active pressure sensors. Prior *et al.* [149] used piezoelectric transducers to detect the sound waves up to 400 *kHz* in a joint acoustic analysis system. They preferred

to use a laptop controlled data acquisition system connected with two AE sensors and an electrogoniometer. Electrogoniometer recorded the point of each movement where angular velocity crossed the threshold of 0.1°. Burst signal waveforms were defined above a threshold of 32 *dB* in the joint acoustic events. Shark *et al.* [150] reported the importance and use of piezoelectric sensors as a biomarker in a knee joint acoustic analysis. Two electrogoniometers and an amplification unit were also attached to the AE sensors on the medial compartment of the knee joint. Signal analysis was conducted on 53 healthy and OA knees, focusing on the four-phase sit-stand-sit movements and considering joint movement angle and angular velocity. The number of AE hits in statistical analysis has increased with the growing age group and a change of knee condition from healthy to OA in each movement phase. The maximum increase was found to occur in the ascending-acceleration movement phase. Paul *et al.* [151] used the piezoelectric transducers to develop a novel Wireless Health Orthopedics system. Mohd Noor Anas [152] developed a non-invasive bioacoustics measurement system to assess articular cartilage diseases in the human knee joint. The dynamic cycle of flexion-extension and sit-stand-sit movements were observed by using a high sensitive piezopolymer transducer. The author noted a lower frequency component (<120 *Hz*) in the healthy knee and a higher frequency component (>200 *Hz*) in the abnormal knees. He also suggested improving the measurement by using extra weight on the subjects and using multi-sensors. Impulse response method is used to give continuous impulse to the knee. A custom made load cell is used to record the sound and vibration from the knee. The authors used it as a non-invasive screening tool on the healthy and OA subjects, and they obtained a 21 *Hz* to 30 *Hz* power spectrum from the tibia as output and noted a higher spectrum in OA subjects (Aimoto *et al.*) [153].

Teague *et al.*[154] quantified and characterized joint sound changes during recovery from musculoskeletal injury. The authors used three different microphones along with the IMU. Unloaded flexion-extension and sit-to-stand movements were observed during the experiments. An important conclusion was that the joint sound's morphology and timing were repeatable during several repetitions of the same activity. The primary acoustic emissions were observed at consistent joint angles. In the successive study by Teague and their coworkers using the same set of sensors, the authors compared each sensor's signal quality. They recommended the air microphones for the wearable joint sound sensing system. The use of contact microphones was suggested to reduce interface noise, but the piezoelectric film was not extensively analyzed in their work due to low signal output and interface noise (Teague *et al.*) [155]. In their further development of wearable knee health rehabilitation system, Teague *et al.* [156] used two miniature piezoelectric contact microphones and two IMUs. The system was designed for patients to assess knee joint health. In a recent study, Rajalakshmi *et al.* [157] detected the vibroarthographic signals from the crepitus knees using Arduino and piezoelectric sensors. The correct position of the sensor placement was suggested at the medial compartment of the knee and slightly below the midline of the patella. However, the use of the AE technique opened a broader scope of its application in wearable implementation. It can be used as a biomarker for knee joint health assessment. It is recently reported that apart from the joint sounds, joint loads can also be assessed using the AE method and can give better predictions rather than a model-based approach (Scherpereele *et al.*) [158], (Whittingslow *et al.*) [159].

2.7 Technical Gaps

After a detailed literature survey, the following research gaps are identified:

- **Limited Capability of Existing Radiological Methods for Dynamic Knee Joint Assessment:** Existing radiological methods are not suitable for knee joints during dynamic weight-bearing activities. It is challenging to accurately detect knee osteoarthritis (OA) in such conditions to improve diagnosis accuracy.

- **Limitations of X-ray in Assessing Cartilage Volume and Degradation:** X-ray imaging can provide longitudinal assessments of joint space reduction, but it can not accurately measure cartilage volume or assess its degradation. This limitation poses a significant gap in obtaining comprehensive information about the structural changes associated with osteoarthritis (OA) progression.

- **Inadequate Visualization of Patellofemoral Joint in X-ray Examinations:** The skyline or lateral view of the patellofemoral joint in X-ray examinations offers inadequate visualization for assessing osteoarthritis (OA), creating a gap in accurate diagnosis and treatment planning.

- **Investigation into Joint Angle-Based Acoustic Emission for Classifying Osteoarthritis Severity According to KL Grades:** The joint angle-based acoustic emission for classifying osteoarthritis severity based on Kellgren-Lawrence (KL) grades has not yet been explored. This highlights the need for further research to explore the feasibility and efficacy of this approach in accurately categorizing the severity of osteoarthritis.

- **Inadequate Accessibility and Suitability of Radiological Tools for Take-home Healthcare System:** Existing radiological methods like X-ray does not fall under early diagnostic tools. MRI as a diagnostic method for routine imaging of human joints in clinical practice is limited by its high cost. It creates a gap in cost-effective and accessible diagnostic options for subjects requiring routine joint assessments.

2.8 Objectives of the Present Work

The primary objective of this research is to develop wearable systems for the detection of knee osteoarthritis and classification of it using acoustic emission technology and validate through radiographic images.

To accomplish the proposed significant objective, the following sub-objectives are framed for the present research work:

- To develop a digital goniometer for the kinematic analysis of a knee joint.
- To develop a wearable device to capture the acoustic waves generated during the knee motion to differentiate between healthy and pathological subjects.
- To collect the knee joint acoustic data from healthy and osteoarthritic subjects for their quantitative evaluation and feature characterization.
- To collect the knee joint acoustic data from osteoarthritic subjects to identify a biomarker for its classification and validation.

Chapter 3

In-house Development of an Inertial Measurement Unit-Based Digital Goniometer

3.1 Introduction

This chapter presents the in-house development of an inertial measurement unit (IMU)-based digital goniometer, focusing on various aspects from conventional methods of joint monitoring to the final device fabrication and performance validation. Conventional methods of joint monitoring are initially reviewed, highlighting the limitations that necessitate the development of novel solutions. The subsequent sections are reported with a step-by-step process of developing the digital goniometer, including the integration of IMUs, Arduino Nano microcontroller, data storage module, and LCD module. Details regarding the final device fabrication and methods of calibration are discussed, followed by a thorough examination of the statistical analysis techniques employed. The chapter culminates in the presentation of results and a comprehensive discussion, evaluating the performance and implications of the developed digital goniometer for joint monitoring applications.

3.2 Conventional Methods of Joint Monitoring

The word goniometer is derived from the Greek words "gonia" and "metron," which mean angle and measure, respectively. In physical therapy, the physicians assess the joint range of motion using a Universal goniometer, as shown in Fig. 3.1. It is the most conventional method for joint monitoring in the physical rehabilitation system. This device is commercially available in two forms, short arms and long arms; out of that, one is stationary, and another is movable (Rome *et al.*) [160]. The use of such goniometers in physical therapy imposes some restrictions on the physician as both hands are involved during the examination, leading to instability and error.

Figure 3.1: Universal Goniometer.

Other advancements for correcting such problems evolve different goniometers like fluid goniometers, flexible electrogoniometers, and optical fiber goniometers. They have different working principles and can be used for a range of motion analysis (Tesiol *et al.*) [161]. Recent research trends towards inertial measurement systems as they have a broad scope of integration with various health joint monitoring wearable systems.

3.3 Development of Digital Goniometer

In this work, a compact wearable device in the form of a digital goniometer using IMU (MPU-6050) is developed. This IMU has six degrees of freedom sensor system containing an accelerometer and a gyroscope. A magnetometer is avoided in this design as an error estimation in biomedical applications is expected if the device is not calibrated correctly or placed near ferromagnetic materials, like prosthetic implants or tools (Kendell *et al.*) [162]. The selected inertial sensors are integrated with Arduino Nano V3.1 as an ATmega 328 microcontrollers, SD card modules for data storage, data display units, and a power supply by designing a primary circuit using a breadboard, jumper wires, resistors, potentiometers, LED, SPDT switches, and DC jack. The developed circuit is then transferred into a through-hole type printed circuit board (PCB) and all related accessories are mounted on it. After successfully placing the mountings, a device casing is printed using 3D printing technology and PLA polylactic acid (or polylactide) material. The separate casing has been printed to integrate the IMU into the human subjects, and velcro tapes are used to fix the sensors on the required positions on human lower limbs. The data is sampled at 110 Hz from the IMU sensor.

3.3.1 Inertial Measurement Units

Inertial measurement unit (IMU) is widely used in biomedical applications like the clinical assessment of patients, an ambulatory measurement for monitoring patient's daily activities, and upper and lower limb joint kinematics analysis (Liu *et al.*) [163]. These IMU can be distinguished according to the number of perceived state variables (DOF), among which the 6-DOF IMU is the most common. The 9-DOF IMU will have an additional

three-axis magnetometer. A 10-DOF IMU may also exist, and that will have a different pressure sensor or temperature sensor as per the specific need. The major application areas are robotics, virtual and augmented reality, platform stabilization, human-machine interfacing, biomedical devices, etc. These IMU are also categorized based on their different measurement principles. These are mainly divided into two categories, i.e., MEMS and fiber optic gyroscopes. The application area of fiber optic gyroscopes is aerospace and military, while most civil applications are based on MEMS sensors (Passaro *et al.*) [164]. A Complete hardware solution can be obtained for various applications by using one small MEMS device (Abbate *et al.*) [165]. For the current study, an MPU 6050 inertial measurement unit is selected with a 3-axis accelerometer and 3-axis gyroscope as a total of 6 degrees of freedom system as shown in Fig. 3.2 .

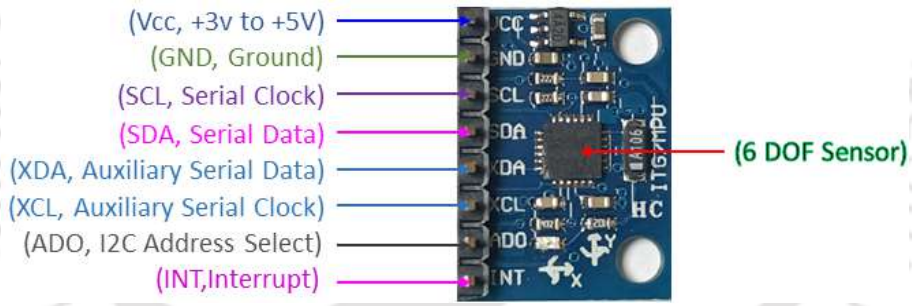

Figure 3.2: MPU 6050 Sensor Module.

A magnetometer is avoided here as it may create an error estimation in biomedical applications if the device is not calibrated correctly or placed near ferromagnetic materials, like prosthetic implants or tools (Kendell *et al.*) [162]. MPU 6050 sensor supports data fusion in biomedical posture calculation and can be easily integrated with Arduino microcontroller (Mendes *et al.*) [166]. It has a user-friendly attribute for writing code in Arduino IDE software for the MPU 6050 module and also supports the inverse kinematics analysis for biomechanical analysis in OpenSim software. This device is readily

commercially available in small size and consumes low power during operation. There are three major components of an IMU as follows:

(i) Accelerometer:- The accelerometer measures acceleration by measuring the change in capacitance, and it is based on Newton's second law. It has a mass attached to a spring, which is confined to move along one direction and fixed with outer planes. When the acceleration in a particular direction is applied, the mass moves, and the capacitance between the plate and the mass changes. This change in capacitance is measured, processed, and recorded for a corresponding linear acceleration value (m/s^2 or g). The triple-axis MEMS accelerometer in MPU-6050 includes a wide range of features like its triple-axis digital-output is the full-scale programmable with the range of $\pm 2g$, $\pm 4g$, $\pm 8g$, and $\pm 16g$. It integrates with 16-bit Analog to digital converters (ADC's) that enable simultaneous sampling of accelerometers while requiring no external multiplexer. The normal operating current is 500 μA. It also facilitates low power accelerometer mode current as 10 μA at 1.25 Hz, 20 μA at 5Hz, 60 μA at 20 Hz, 110 μA at 40 Hz (Shkel and Wang) [167].

(ii) Gyroscope :- It measures angular rate using the Coriolis effect. When a mass moves in a particular direction with a specific velocity and an external angular rate is applied, a force will occur perpendicularly. As a result, the vertical displacement of the mass comes into the picture. So similar to the accelerometers, this displacement will cause a change in capacitance which will be measured, processed, and correspond to the particular angular rate (rad/s or deg/s). The triple-axis MEMS Gyroscope in MPU 6050 includes a wide range of features like its triple-axis digital-output is the user-programmable with a full-scale range of ± 250, ± 500, ± 1000, and $\pm 2000^{\circ}/s$. This also facilitates the image, video, and GPS synchronization and is

integrated with 16-bit ADC's (John and James) [168].

(iii) Magnetometer:- It measures the magnetic field of the earth using the Hall or magnetoresistive effect. It works on similar principle like a conductive plate and the current is set to flow in it. Then, the electron will start flowing from one side to the other side of the plate. Now, if some magnetic field is exposed near the plate, the electrons flow will be disturbed, and the electrons will be deflected at the one side of the plate and the positive poles to the other side of the plate. As a result, if a multimeter is attcahed at the edges of the plate, it will give some voltage which depends on the magnetic field strength and its direction (micro-Tesla or Gauss).

3.3.2 Arduino Nano

In this work, an Arduino Nano microcontroller board is used. As the name indicates, it is small, compact, and highly compatible with breadboard and other electronic components. It is a readily commercially available board that weighs around 7 gm, 4.5 cm in length, and 1.8 cm in width as shown in Fig. 3.3. Nano is almost similar to the Arduino UNO, except it does not facilitate a DC power jack. It works with a Mini-B type USB cable and is smaller in size than UNO. The USB port is used for both serial monitoring and programming. It is available with two different versions of the microcontroller, i.e., Atmel ATmega168 and ATmega 328. It consists of a total of 30 pins configuration, and each has its specific functionality. Mini-B USB connection gives power to the board in the range of 6-20 V unregulated external power supply at pin 30. The regulated 5 V power can be supplied at pin 27.

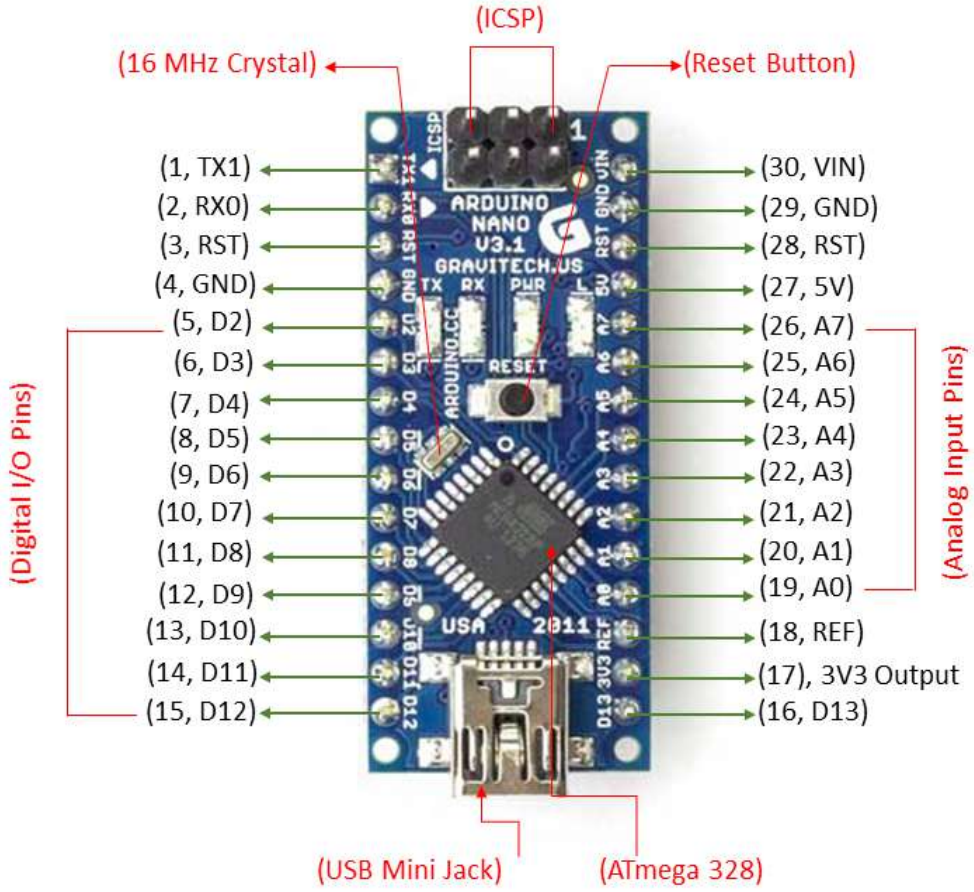

Figure 3.3: Arduino Nano.

3.3.3 Data Storage Module

The MicroSD Card Adapter is a module or SD card reader used to read and write data through the file system FAT 32 (File Allocation Table 32) and SPI (Serial Peripheral Interface) driver. It also supports Micro SDHC (Secure Digital High Capacity) high-speed cards. It has an inbuilt level conversion circuit board that can interface with 5 V or 3.3 V as shown in Fig. 3.4. It works on a 4.5 V-5.5 V power supply through a 3.3 V voltage regulator circuit board, and the current requirement is 0.2-200 mA. The most important part of this module is the control interface. It has six pins like GND (Ground), VCC, MISO (Master in slave out), MOSI (Master out slave in), SCK (Serial clock), and CS (Chip select).

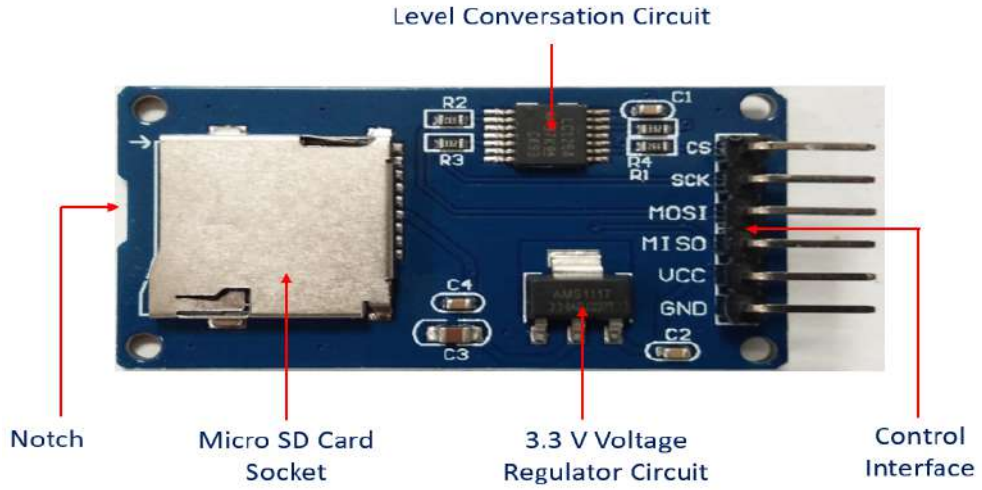

Figure 3.4: SD Card Module.

3.3.4 LCD Display Module

The LCD (Liquid Crystal Display) is an electronic display module commercially available in various combinations like 8×1, 8×2, 10×2, 16×1, etc. The most common 16×2 LCD is used in this work, in which a total of 16 pins are present on the module with two rows of character display, and each character is displayed in a 5×7 pixel matrix. Among the 16 pins configuration, Ground and V_{cc} care the source pins and connected to the ground and supply voltage of the power source, respectively. As shown in Fig. 3.5, VE, RS, RW, and E are the control pins used for specific purposes.

VE is the supply voltage pin and connects to the supply pin of the power source, while RS toggles between command/ data register. RW stands for read/write pin and interfaces between reading and writing the data. Pin E enables the read /write operation. Pin no 7 to 14 are the 8-bit data pins that allow sending commands or data to the LCD. Pin 15 and 16 are the LED pins to illuminate the LCD module and provide a ground connection.

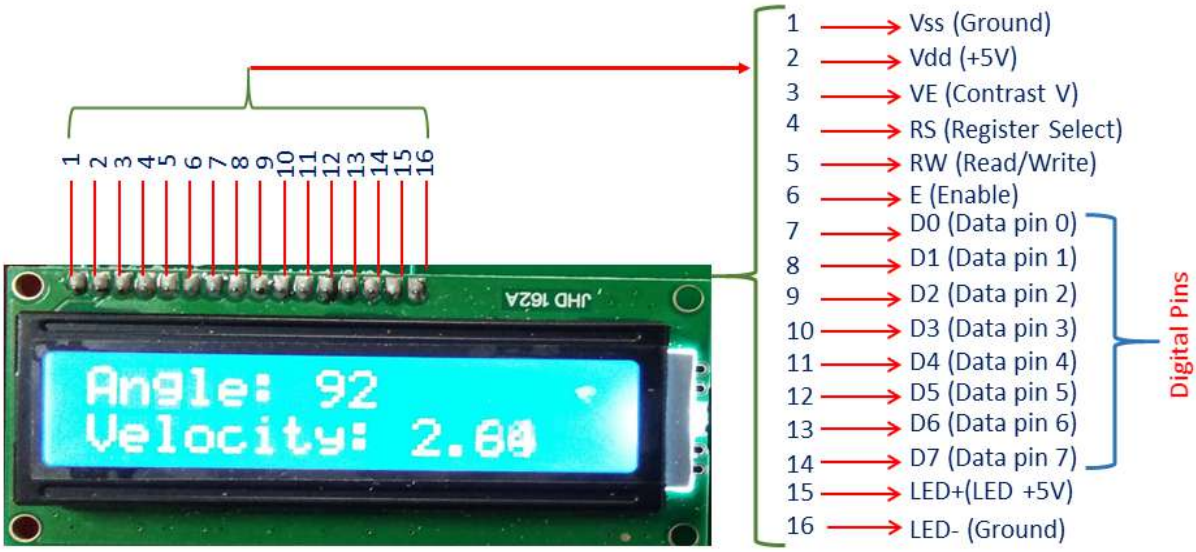

Figure 3.5: LCD Module (16×2).

3.4 Final Device Fabrication

A primary circuit is developed with the integration of different modules, as discussed in the previous sections. Using a breadboard, jumper wires, resistors, potentiometers, LED, SPDT switches, and DC jack along with the Arduino nano and data storage module is integrated into the circuit, and MPU 6050 sensors are connected as shown in Fig. 3.6.

The developed circuit is then successfully tested and calibrated by writing the programs in Arduino IDE software. The performance is tested through the mechanical goniometer at the initial stage. This circuit development is modified to reduce the wiring connections by printing them on a circuit board. A through-hole type PCB (printed circuit board) is used for the fabrication, and all related accessories are mounted on one board. A device casing is printed using 3D printing technology and PLA polylactic acid (or polylactide) material. The separate casing is printed to integrate the IMU to the human subjects, and velcro tapes are used to fix the sensors on the required positions on human lower limbs. The final development of the digital goniometer is shown Fig. 3.7.

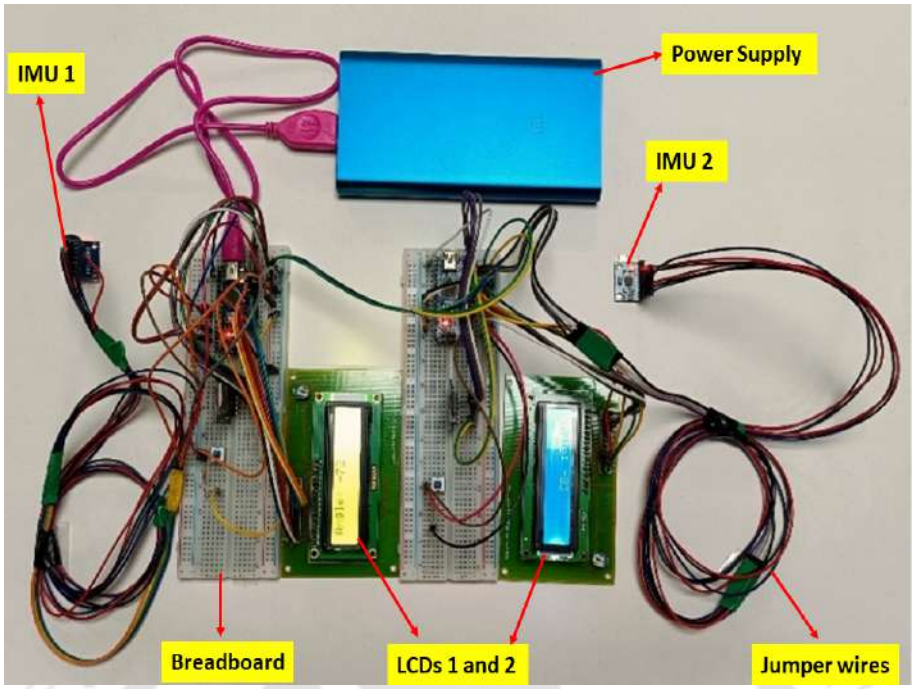

Figure 3.6: Primary Circuit Development.

Figure 3.7: Fabricated Digital Goniometer.

3.5 Performance Validation of Digital Goniometer

This section refers to the complete pathway in this research work on the device testing, calibration, positioning of IMU on the human subjects, its performance validation, and

necessary protocols.

3.5.1 Study Design

In this study, ten healthy subjects including five males (30.80±3.96 *years*, 77.24±8.72 *kg*, 168.60±6.58 *cm*) and five females (28.00±1.58 *years*, 60.60±9.61 *kg*, 156.28±6.88 *cm*) are recruited for their participation and confirmed with no lower extremity injury. ICMR (Indian Council of Medical Research) guidelines are strictly followed for the research and experimentation (Ananthakrishnan *et al.*) [169]. Here, the validation of the fabricated device with 10 subjects can be justified from previous works of literature (Rezende *et al.*) [170], (Bakhshi *et al.*) [111], (Ajdaroski *et al.*) [171], where 10 participants or lesser were considered for the statistical analysis. Ethical consent is taken from all the subjects, and inclusion and exclusion criteria is followed, and the same has been approved by the Institute Human Ethical Committee (IHEC), IIT Guwahati. Subjects are instrumented with an indigenously developed inertial measurement based digital goniometer and motion capture markers located on their right lower extremity. The tests are carried out in two different postures: sit-stand-sit (S-T-S) and open cycle flexion-extension (F-E). Here, F-E is a non-weight-bearing exercise, whereas S-T-S is a weight-bearing exercise. In both the postures, the reference is taken to be a sitting position while the femur and tibia are at a right angle. The subjects are asked to do five S-T-S cycles in one trial for the data collection. Similarly, the subjects are asked to do five F-E cycles in another trial. All subjects have performed the following modes of exercises, initially sitting on the chair. Each mode consists of the following four-phase motion:

1. In F-E mode:
    - Extension-Acceleration (EA)

- Extension-Deacceleration (ED)
- Flexion-Acceleration (FA)
- Flexion-Deacceleration (FD)

2. In S-T-S mode:

- Ascending-Acceleration (AA)
- Ascending-Deacceleration (AD)
- Descending-Acceleration (DA)
- Descending-Deacceleration (DD)

Two F-E and S-T-S joint motion cycles are considered individually for analyzing the results, including repeating all four phases. Moreover, each joint motion cycle is completed within a range of 4.5-6.5 seconds. As per the protocol to complete each cycle within the time, the subjects are suggested to synchronize their motion with the metronome. The data received from this dynamic action are stored in the goniometer using micro SD cards attached to the device.

3.5.2 Position for Fixing the Device

For accurate estimation of knee kinematic parameters using a wearable device, sensor placement plays an essential role. It is observed that appropriate sensor fixation reduces the error caused by artifices of skin movement and improper alignment to anatomical axes (Yang *et al.*) [172]. Previous studies reported the use of Velcro straps, double-side adhesive tape, elastic straps, and neoprene straps for fixing motion sensors on the body of subjects as they are convenient to use and flexible. A semi-rigid belt and exoskeleton are also reported for better sensor fixation, but they are not suitable for long-term ambulatory

use (Chinmilli *et al.*) [173], (Noort *et al.*) [174]. In the present work, the Velcro strap is used for fixing the sensors on the sagittal anatomical axis of the knee joint of the subjects. Along with the two IMU, three surgical tape pieces are placed on the right leg of each subject as markers for the video motion analysis in the sagittal plane. The first tape is placed at the thigh, the second is at the joint of the lateral femoral condyle and the lateral tibial condyle, and the third is placed at the tibia axes, as shown in Fig. 3.8. Similarly, the IMU position for femur assessment is assigned from the midpoint of the greater trochanter to lateral femoral condyle and lateral tibial condyle to lateral malleolus for tibia axes (Laudanski *et al.*) [175].

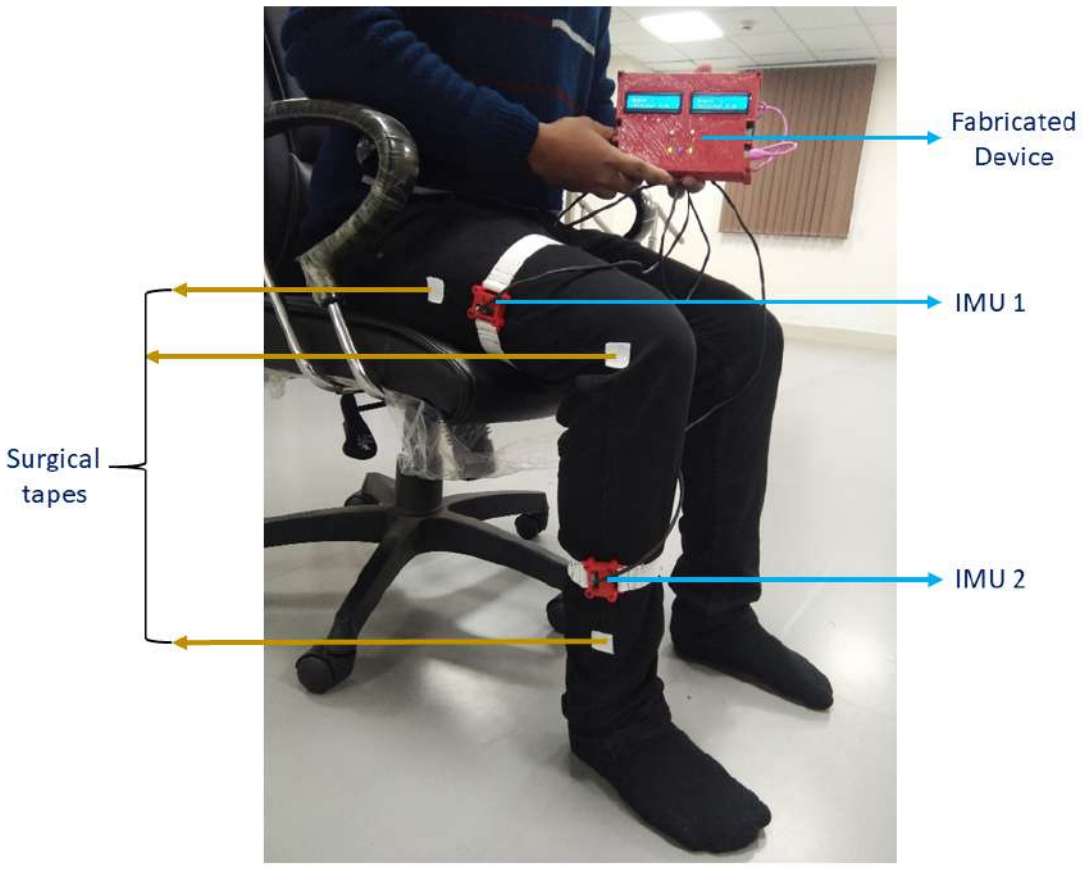

Figure 3.8: Test Procedure and IMU Positioning.

3.5.3 Methods of Calibration

The primary automatic calibration method for the fabricated device on the human subject with the metronome and video camera system is the subject-dependent on-body control approach followed by a minimal-to-null physical and cognitive effort by the subjects themselves. The steady-state of each subject is carefully observed in both the modes of leg exercises before data sampling. The individual subject is asked to maintain the holding posture for 15 seconds in each trial while wearing the fabricated device. Proper care has been taken while positioning the IMU in the sagittal plane and placing the surgical tape on the lower limb for video motion analysis. Static postures are repeatedly observed before the data collection in all individual trials. However, the dynamic motion involves inaccuracy in the data recording due to sensor movement, which has been identified during the post-processing of the data. A reset button is provided to initialize the boot process by the subject before starting each trial for repeating initial calibration. A moving average filter algorithm is applied during the data processing to obtain the sensor output. This algorithm can minimize the noise in the initial signal values without compromising large amounts of data (Ghio *et al.*) [176]. It takes input samples at a time and the average data is produced in a single output point by following the characterization equation below:

$$y[i] = \frac{1}{N} \sum_{k=0}^{N-1} x[i+k] \tag{3.1}$$

Where $x[i]$ is the input, N is the number of readings that will be averaged, and $y[i]$ is the output of the recorded signal.

3.5.4 Video Motion Analysis

The results obtained from a fabricated device can be validated with an OMC system in the gait lab but it is time-consuming and a specific protocol is needed for validation. However, the validation can also be done with video motion analysis software. An open-source software 'Kinovea' is used for video motion analysis. It allows linear and angular kinematic calculations both in real-time and normalized time. The analysis can be performed manually or using a semi-automated tracking function in Kinovea. The reliability of this software for the study of a range of motion has been reported as high in both intra-rater and inter-rater assessments (Elrahim *et al.*) [177].

3.5.5 Statistical Analysis

The data from all ten subjects are obtained from the digital goniometer and Kinovea. A descriptive mean and standard deviation analysis are carried out. Then, the two-sample t-test is performed to compare the sample mean values from the recorded data. A linear regression analysis is performed to analyze the strength of a relation between two variables, and a correlation coefficient (r) is estimated for all modes of evaluation by the following mathematical relation:

$$r = \frac{\Sigma(g_i - \bar{g})(k_i - \bar{k})}{\sqrt{\Sigma(g_i - \bar{g})^2 \Sigma(k_i - \bar{k})^2}} \tag{3.2}$$

Where g_i and k_i are the variables corresponding to data obtained from the digital goniometer and Kinovea and their respective means are $\bar{g}$ and $\bar{k}$. Then Bland-Altman (BA) plots are generated to understand the degree of agreement between two measurement systems of the same variable and their concurrent validity. The inter-rater reliability is

estimated to calculate intraclass correlation coefficient (ICC) values for 95% confidence interval (CI) and interpreted them as moderate (0.50 to 0.69), high (0.70 to 0.89), and excellent (0.90 and above) (Koo *et al.*) [178]. To indicate a good reliability, standard error of measurement (SEM), root mean squared error (RMSE), and intraclass correlation coefficient (ICC) are calculated between the two measurement systems.

3.6 Results and Discussion

3.6.1 Validation of Joint Angle and Joint Angular Velocity

In this study, the IMU is placed in the sagittal plane during the experiments on the leg of the human subject and the velocity of the yaw rotation of the IMU is considered for angle identification from each sensor. Thus, for each IMU, the angle is calculated in the Arduino code through the integration of angular velocity obtained from the gyroscope, and the final angle and velocity are displayed on the screen of the fabricated device. The primary purpose of finding an angle and angular velocity is to identify the four-phase motion of a subject in each cycle. A similar trend of the data points is obtained from the two measurement systems in the plots. The average knee joint angle from the data of all subjects is observed approximately in the range of 0° to 90° in F-E and S-T-S modes as shown in Fig. 3.9(a) and, Fig. 3.10(a), respectively, where the shaded region shows the range of all healthy subjects with ±SD. The mean and standard deviation of the data points are calculated for all ten subjects. The maximum standard deviation was found to be approximately ±18.8° (at 9.6 s) and, ±21.3° (at 6.8 s) for both Goniometer and Kinovea in F-E and S-T-S modes, respectively. Similarly, Fig. 3.9(b) and, Fig. 3.10(b) illustrate the average rate of change of angle for all subjects in F-E and S-T-S mode and

found to be approximately in the range of $0°/s$ to $100°/s$ for both cases with their maximum standard deviations of $\pm 52.6°/s$ (at 6.5 s) and, $\pm 40.01°/s$ (at 6.5 s), respectively.

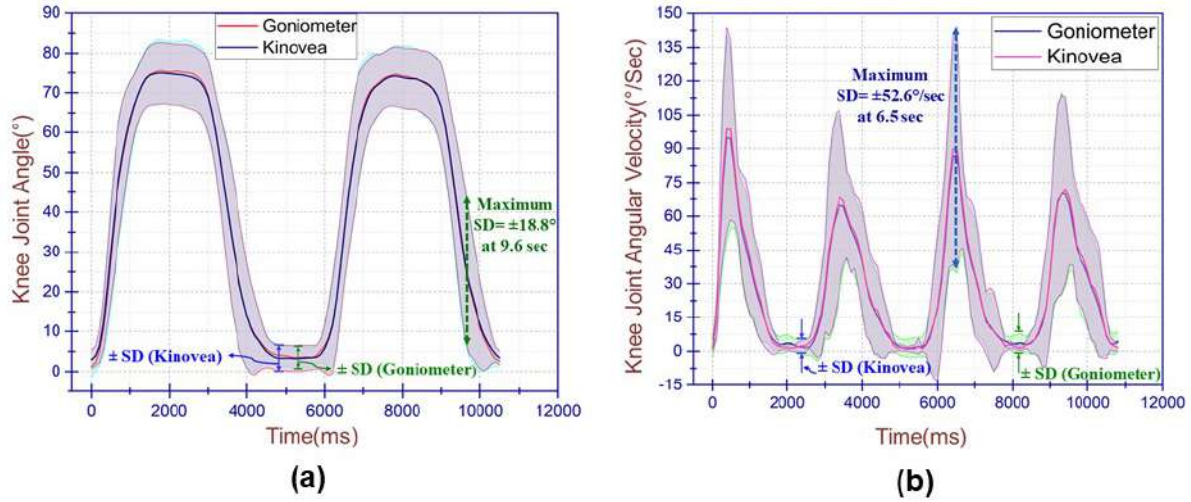

Figure 3.9: F-E Mode Validation (a): Knee Joint Angle (b): Knee Joint Angular Velocity.

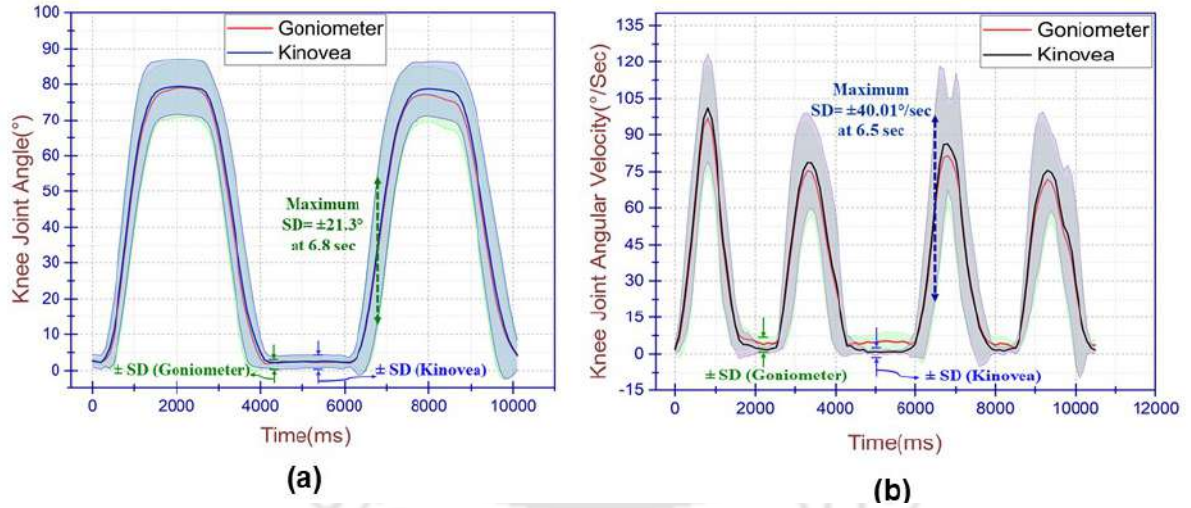

Figure 3.10: S-T-S Mode Validation (a): Knee Joint Angle (b): Knee Joint Angular Velocity.

3.6.2 Hypothesis Testing and Linear Regression Analysis

It is noted that only the validation through the superimposition of data points is not a sufficient judgment for the accuracy of a fabricated device. For further investigation of the performance of the digital goniometer, parametric hypothesis testing is always needed

to be carried out. The device responses are studied by analyzing a descriptive mean and standard deviation for the joint movement phases and measurement methods. To compare the means of the sample data outputs from two different measurement systems, a two-sample t-test is performed.

The p-value in the case of F-E and S-T-S modes is observed to be 0.99 and 0.77 for knee joint angle, respectively and the corresponding values are 0.80 and 0.84 for the joint angular velocity at a significance level (α=0.05). The results obtained from the t-test indicate that the difference in the sample mean values from the two measurement systems is not significantly different from 0°. As shown in Fig. 3.11 and 3.12, a high correlation coefficient value is observed (r=0.99) for both F-E and S-T-S, in the case of joint angle and joint angular velocity, where a robust finding of the data point distribution along the regression line is found and validated from the previous study (Bakhshi *et al.*) [111]. The statistical analyses have been performed in Origin-2021 and IBM SPSS Statistics 20.0 data analysis software.

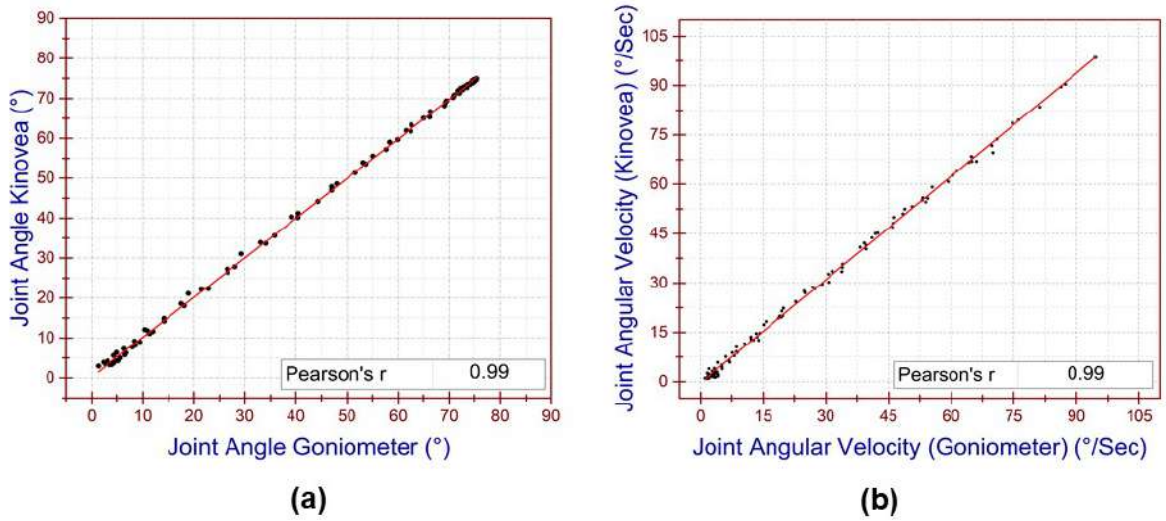

Figure 3.11: Linear Regression Analysis (F-E Mode) (a): Knee Joint Angle (b): Knee Joint Angular Velocity.

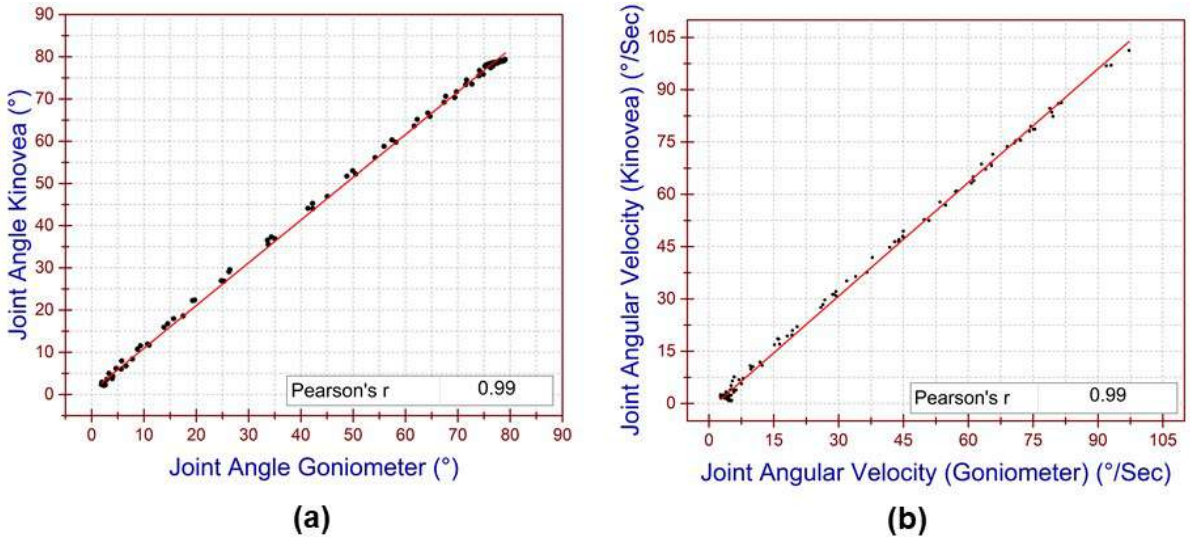

Figure 3.12: Linear Regression Analysis (S-T-S Mode) (a): Knee Joint Angle (b): Knee Joint Angular Velocity.

3.6.3 Comparision of Means (BA Plots) and Error Estimation

Detecting a constant error in the reliability validation is impossible only with finding the correlation coefficient. Furthermore, a descriptive statistical analysis is performed to describe the agreement between two measurement systems quantitatively. To perform this analysis, it is essential to conduct a non-parametric hypothesis test initially. Thus, data normality is checked by performing the Kolmogorov-Smirnov test (Giavarina and Davide) [179] and the p-value is obtained to be greater than 0.2 for both angle and velocity in each mode. Since the p-value is greater than the significant level =0.05, the null hypothesis is accepted which denotes that the data points are normally distributed. After confirming the data normality, the Bland-Altman (BA) analysis is performed under 2 σ limits of 95% CI to provide an agreement between two measurement methods. These plots estimate the scattering of data points in a standard normal distribution for any measurement system, where underestimation and overestimation of data point dispersion are analyzed, and agreement is verified (Bland *et al.*) [180]. In BA plots, if one of the

methods always gives high values, all points will lie either above or below the zero line. If the data points are found to be scattered above and below the zero line on the Bland-Altman plot, then it can be said that there is no consistency bias between one method versus the other (Kalra *et al.*) [181], (Santos *et al.*) [182]. In Fig. 3.13(a), since the mean line is observed to deviate from the zero line by 0.02° (approximately 0°), thus the agreement can be said to be closed to an unbiased agreement in the case of F-E joint angle validation. However, in the Fig. 3.13(b), 3.14(a), and 3.14(b), the magnitude of the bias are found to be 0.88, 1.30, and 0.82 respectively. From the above analysis, the maximum bias is found to be 1.3, which can be justified by earlier literature (Ajdaroski *et al.*) [171], (Svensson *et al.*) [183] where the validation is done with a similar range of observed bias.

The F-E mode for knee joint angle indicates scattering of data points above and below the zero line, as shown in Fig. 3.13(a). It is also observed that there is no overestimation of data points (N=0), whereas few data points are underestimated (N=6). In the case of joint angular velocity, as shown in Fig. 3.13(b), there is no underestimation (N=0), while only two data points (N=2) are found to be overestimated. In the two measurement systems, the highest absolute differences are observed to be in the range of 0° to 30° for the F-E joint angle and nearer to 0° in the case of F-E angular velocity.

Similarly, the data points are also scattered between the 2 σ limits of standard normal distribution for the S-T-S mode. It is also significantly observed that no underestimation and overestimation of data points are found in the case of joint angle as shown in Fig. 3.14(a), and joint angular velocity as shown in Fig. 3.14(b) in S-T-S mode, respectively. In this study, considering the "n" number of data points (for F-E Angle, n=106; S-T-S angle, n=102; for F-E angular velocity n=109; and S-T-S angular velocity n=106)

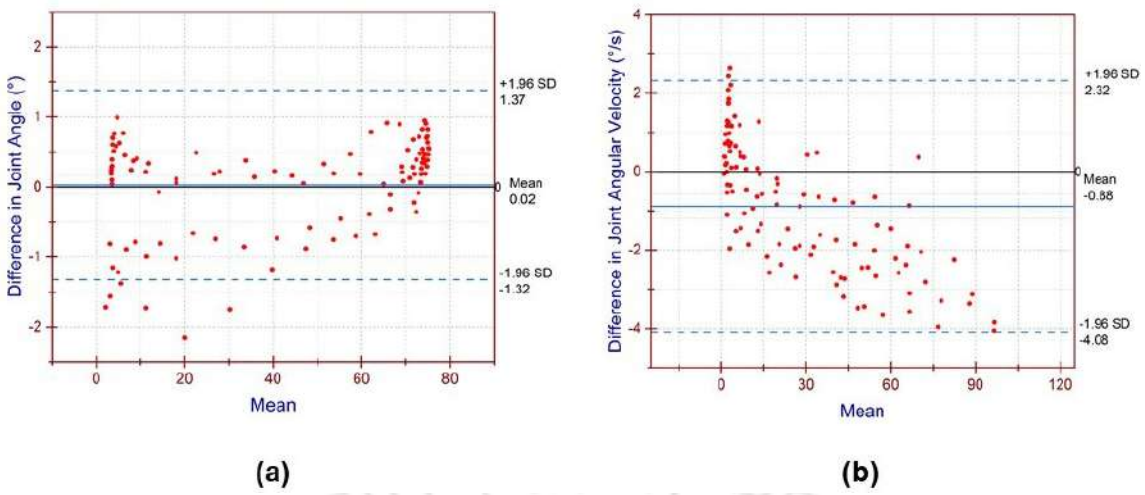

Figure 3.13: Mean Difference Analysis (F-E mode) (a): Knee Joint Angle (b): Knee Joint Angular Velocity.

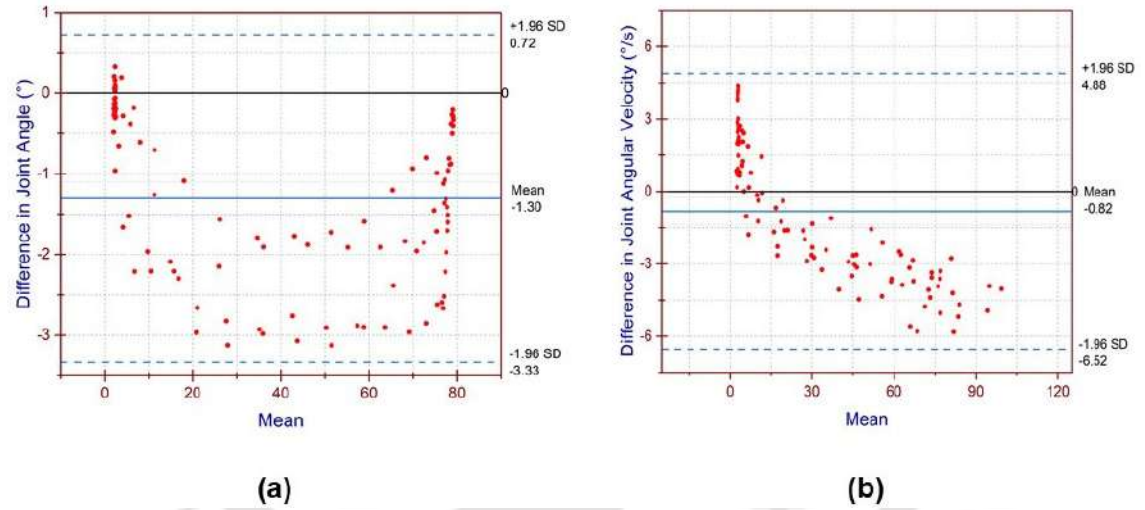

Figure 3.14: Mean Difference Analysis (S-T-S mode) (a): Knee Joint Angle (b): Knee Joint Angular Velocity.

for two cycles in a particular mode of exercise, the mean difference values are calculated with their corresponding upper and lower limits of agreements (LoA). The limits within which the proportions of the differences between the two systems lie are estimated by the limits of agreement for 95% CI on the BA plot. In all the modes of exercise, the magnitude of the observed mean difference in joint angle and angular velocity between the two systems is found closer to zero. It signifies that the mean value of the output obtained from the two measurement systems is quite comparable. Further, the standard

error of measurement (SEM) and root mean squared error (RMSE) analyses are included as they indicate the correct clinical interpretations in test observations. The SEM is a measure of the average amount of error expected in the measurements and RMSE is the measure of the average magnitude of prediction errors.

Table 3.1: Statistical Analysis

Knee joint assessment parameter (Unit)	Different Postures	Mean of Difference (SD)	LoA(95% CI)	RMSE	SEM	ICC (95% CI)	SDC(1.96*$\sqrt{2}$*SEM)
Joint angle (°)	F-E	0.02(0.69)	-1.32 to 1.37	0.68	0.04	1	0.11
Joint angle (°)	S-T-S	-1.30(1.03)	-3.33 to 0.72	1.66	0.09	0.99	0.25
joint angular velocity ($^\circ/s$)	F-E	-0.88(1.63)	-4.08 to 2.32	1.85	0.10	0.99	0.28
joint angular velocity ($^\circ/s$)	S-T-S	-0.82(2.91)	-6.52 to 4.88	3.01	0.13	0.99	0.36

From Table 3.1, the magnitude of SEM for all the cases is found to be low and this lower value of SEM indicates the higher absolute reliability in the two measurement systems (Huber *et al.*) [184]. The root mean squared error is calculated from the squared root value of the average of the square of the differences between the two measuring systems. It is a measurement residual or anticipated error that indicates the distance from regression line data points or the scatter pattern of data points around the best-fit regression line. The observed values are less than 2° in the case of joint angles and a maximum of approximately $3^\circ/s$ in the case of joint angular velocities. The inter-rater reliability test is performed to calculate intraclass correlation coefficient (ICC) values for 95% CI. It showed an excellent reliability measure (>0.99) in all the measurement modes for both the measuring systems. The results from the experimental observations from the

current study are compared with the previously published literature, and it is assessed that the obtained results are in line with them (Lim *et al.*) [185], (Nicolas *et al.*) [186]. Thereafter, the smallest detectable change (SDC) is calculated, and the magnitude of SDC is found to be less than 1 for all cases that reflect the minimal detected change in joint angle and angular velocity values during the performed exercise, as well as the difference between the two measurement systems.

3.7 Limitations

While finding the kinematic parameters accurately, precaution should be taken such that the position of the sensor must be in the sagittal plane. The camera position should also be in the parallel plane as the sensor is placed for video motion analysis. While validating the data from the digital goniometer with Kinovea for many subjects, the exercises should be performed within the same cycle time for data averaging. Thus, to achieve the same cycle time, the mode of exercises like F-E and S-T-S should be synchronized with the metronome properly.

3.8 Novelty

The fabricated digital goniometer also displays and records the joint angular velocity along with the joint angle, simultaneously w.r.t. real-time. Thus, this development is helpful in joint kinematic analysis within a particular range of velocity in each phase after post-traumatic treatments or total knee arthroplasty. It is also useful for the rehabilitation exercise where controlled joint motion is required to monitor the joint rehabilitation as well as to monitor the joint mobility function for strength interpretation.

3.9 Summary

The current findings infer that the fabricated digital goniometer is a reliable and valid device to measure the knee joint angle and angular velocity. It is a portable and wearable system proposed for segmental joint kinematic analysis. The results from the statistical analysis reveal the precise and accurate device output while monitoring of dynamic activities, which are successfully validated in different postures. The satisfactory validation of knee joint angle and angular velocity observed in the present research is helpful for further implementation of joint range of motion analysis and obtaining precise information about the motion phases, respectively. Based on the current observations, it is concluded that the fabricated device showed good reliability, which can be proposed to monitor the rehabilitation progress of a human subject. Further, the inertial measurement units can be an alternative to traditional goniometry for analyzing the knee joint kinematics.

Chapter 4

In-house Development of a Knee Health Monitoring Device Using Contact Microphone

4.1 Introduction

The aim of this work is to design, fabricate, and validate a small and compact wearable system for knee joint sound detection, utilizing a contact microphone (CM-01B) and Arduino Nano microcontroller. Vibroarthrography, a non-invasive diagnostic tool, has long been utilized in knee joint health assessment, typically requiring costly data acquisition systems for sensor data analysis. In this work, the initial stages involve circuit design and signal amplification, followed by data filtering. Subsequently, electronic components are assembled onto a self-designed printed circuit board to fabricate the device. Validation of the signal output is conducted using a digital oscilloscope, assessing the sensor voltage at frequencies generated by an online tone generator. The instantaneous signal records a maximum sensor voltage of up to 3 V at a sinusoidal wave frequency of 200 Hz. The results are successfully validated through MATLAB (R2021a), and further, the device is tested on healthy human subjects. Fast Fourier transform and short-time Fourier transform analyses are also performed, with the output frequency observed to be less than 100 Hz in healthy subjects. The short-term Fourier transformation is applied to the obtained decibel value range. Spectral density analysis of a pathological knee re-

veals continuous emission of joint sound, with signal power distribution observed across the frequency range of 0 *Hz*-500 *Hz*. The complete procedure from signal acquisition to feature extraction is depicted in Fig. 4.1.

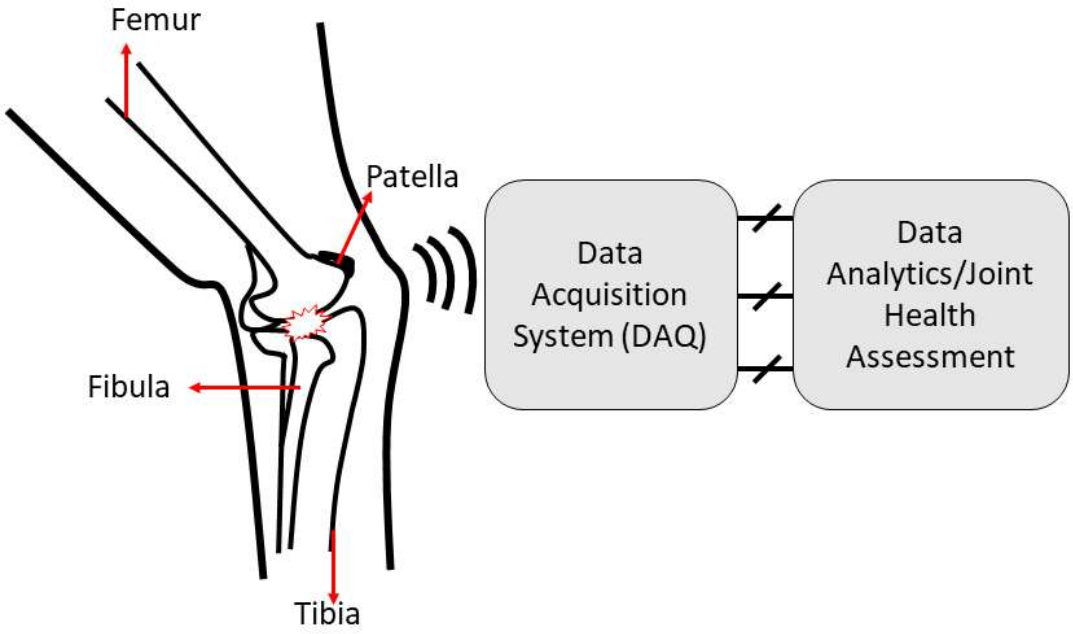

Figure 4.1: Knee Joint Vibroarthrography Schematic.

4.2 Materials and Methods

4.2.1 Device Fabrication

In this work, the initial circuit is fabricated on the breadboard by using primary components like jumper wires, resistors, a push-button DPDT (double-pole, double-throw) switch, a light-emitting diode (LED), power supply, Arduino Nano, SD card module, and a contact microphone (CM01-B). The selected microphone used for this study is consist of a piezoelectric sensor that can sense the acoustic emission in the range of limiting frequency from 8 *Hz* to 2.2 *kHz*. Arduino Nano is a microcontroller board, and as the name indicates, it is small, compact, and highly compatible with breadboard and other elec-

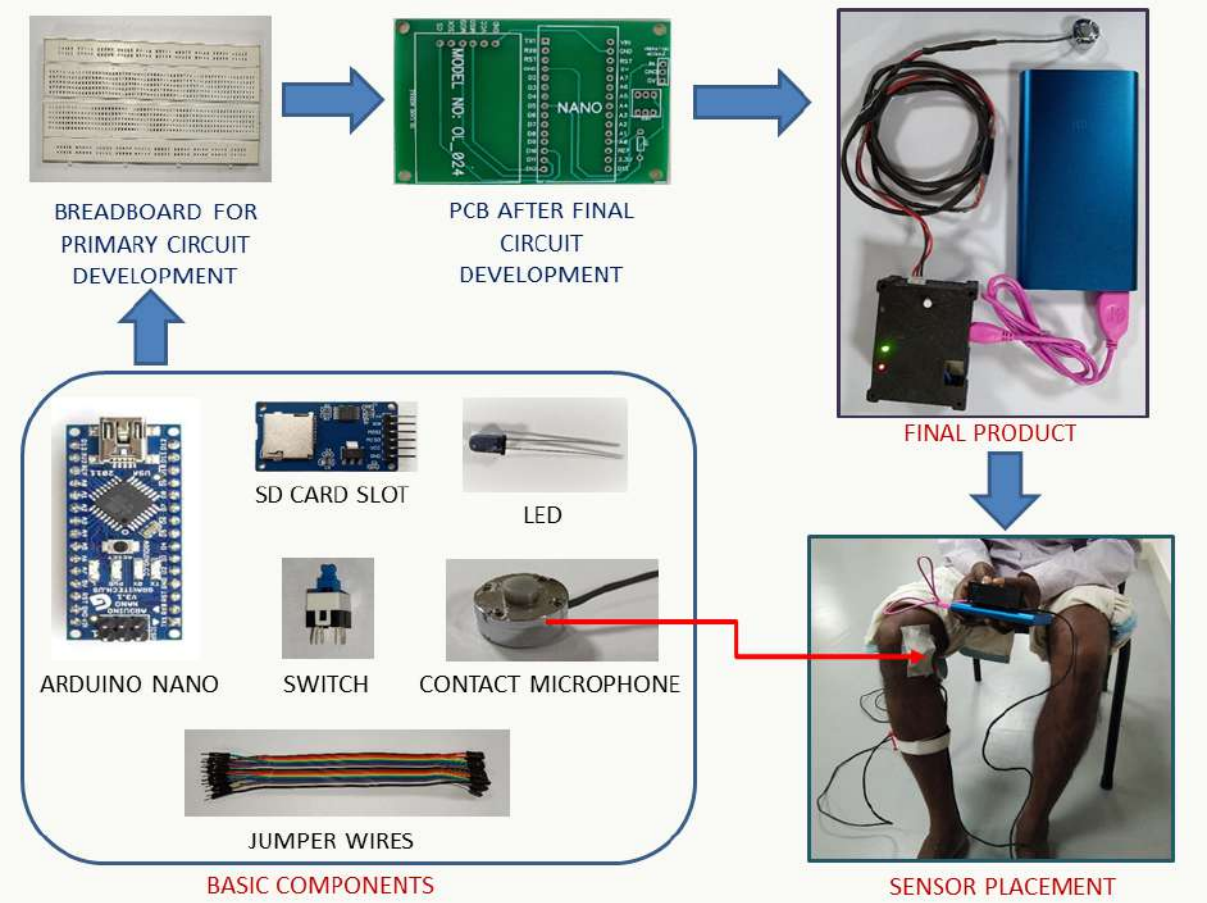

Figure 4.2: Schematic of Basic Components to a Final Wearable Device and Sensor Placement.

tronic components. A primary circuit is successfully fabricated and the signal is amplified for knee joint sound detection. The fabricated circuit is then converted into a printed circuit board (PCB) and a final version of the wearable device has been fabricated using 3D printing of the casing and assembly of components which is shown in Fig. 4.2.

4.2.2 Device Performance Validation

As shown in Fig. 4.3, the fabricated wearable device is tested through a digital oscilloscope. For this goal, an online tone generator is used using a laptop and a speaker on which the contact microphone is attached. The sensor surface is kept exactly stuck to the diaphragm of the speaker and tested on different generated sinusoidal sound waves of

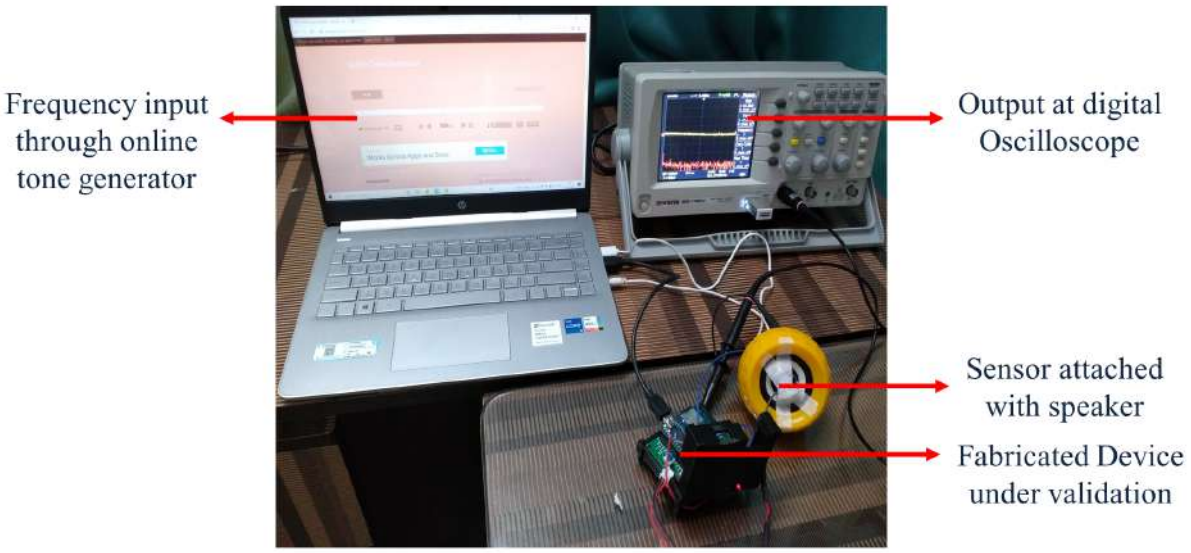

Figure 4.3: Device Validation through Digital Oscilloscope.

different frequencies. The aim of this experiment is to validate the input frequency from the tone generator with the output of the contact microphone and the results are verified on the screen of a digital oscilloscope. Here the objective is to verify the performance of the device through the arbitrarily generated sound waves at different frequencies. An instantaneous click of the signal is recorded from the oscilloscope and simultaneously the sensor output is stored in the SD card attached to the device.

Fig. 4.4 shows the output of the fabricated device at 200 Hz sinewave generated from an online tone generator. The data sampling duration is 2.8 s and the instantaneous signal is recorded on the oscilloscope simultaneously the generated voltage of approximately 3 V is also recorded in the device. The first observation is seen on the oscilloscope as the output frequency is obtained to be 199.8 Hz. Further, the recorded data in the device is post-processed in MATLAB (R2021a) and it is observed in the fast Fourier transform analysis the output frequency is 201.93 Hz at a decibel value of 74.95 dB. This observation indicates the approximately same frequency output validation from two different methods at the same time in the experiment.

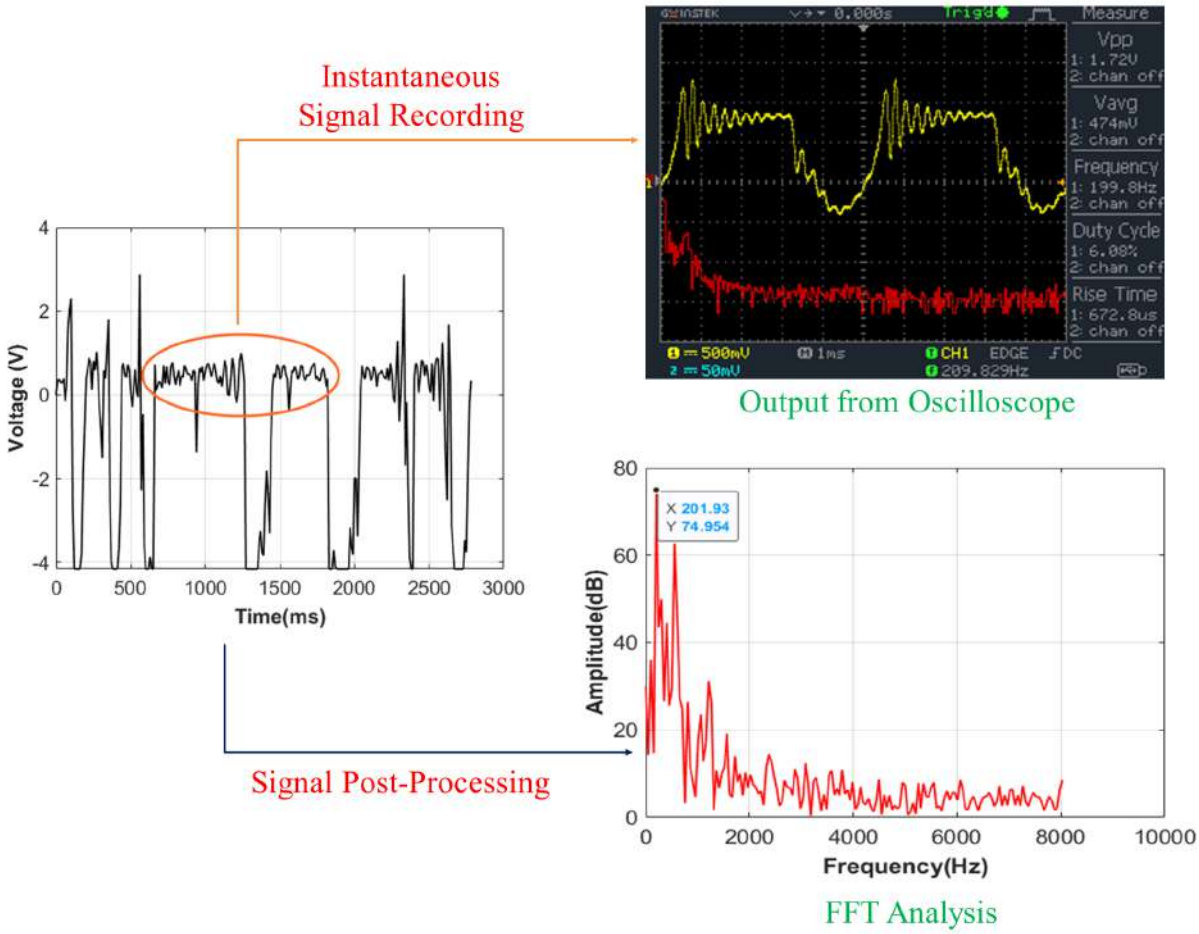

Figure 4.4: Sensor Output Validation at 200 *Hz* Sinusoidal Sound Wave.

4.2.3 Study on the Participants

A total of twenty-four healthy subjects including sixteen males (30.31±12.15 *years*, 66.73±10.10 *kg*, 170.19±8.26 *cm*) and, eight females (28.00±4.96 *years*, 62.21±9.78 *kg*, 154.68±5.95 *cm*) are recruited for their participation and confirmed with no lower extremity injury. Simultaneously, two pathological male subjects (50.00±18.34 *years*, 72.85±3.47 *kg*, 163.75±10.25 *cm*) are also recruited for identification of the OA suspicion and confirmed with a prior medical history of knee joint pain. Each participation is confirmed with standard inclusion and exclusion criteria followed by their written ethical consent. The study is approved by the Institute Human Ethical Committee (IHEC), IIT Guwahati.

4.2.4 Sensor Positioning

It is always critical to fix the sensor on the skin surface in a correct manner and to record acoustic signals accurately. Previous studies reported the optimized placement location at the medial condyle of the patella, i.e., slightly below the midline of the patella. This point is identified as the closest one nearby to the contact area during joint articulation. It is a stable position during joint movement and does not affect by actual joint motion (Song *et al.*) [187], (Befrui *et al.*) [12]. Along with the contact microphone, a self-fabricated inertial measurement unit (IMU) based digital goniometer is also placed on the mid of the thigh and the shank bone on each subject in the sagittal plane.

4.2.5 Data Collection

During the data collection individual subject is trained to perform an active knee joint weight-bearing sit-stand-sit (S-T-S) activity for recording the vibroarthrographic signals. The subjects are asked to do three S-T-S cycles in one trial for the data collection and synchronized with the metronome. Each cycle consists of the following four phases of motion as shown in figure 4.5:

- Ascending-Acceleration (AA)
- Ascending-Deacceleration (AD)
- Descending-Acceleration (DA)
- Descending-Deacceleration (DD)

This device gives the output in terms of voltage which is produced due to the knee joint auscultation during S-T-S activity and the real-time data is stored in the attached SD

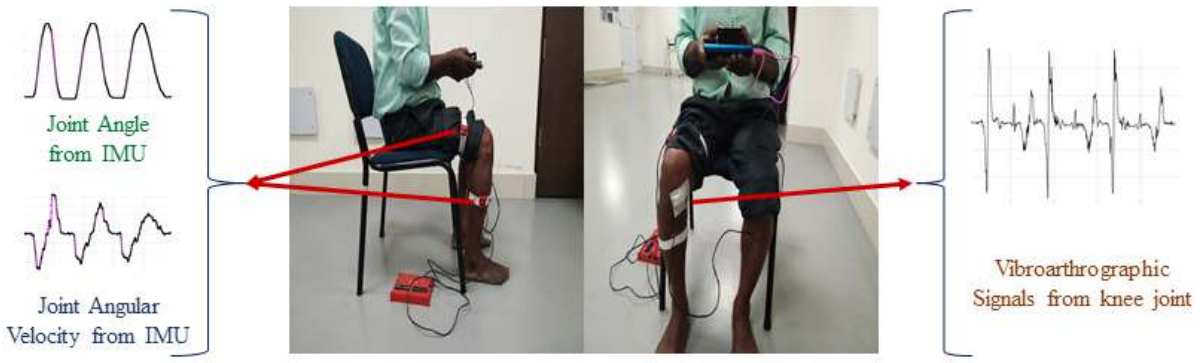

Figure 4.5: Sensor Positioning and Test Procedure.

card with the device. The knee kinematic parameters are obtained from the developed digital goniometer. The primary function to attach the goniometer in this work is to identify the variation of voltage w.r.t. the four different joint motion phase. Fig. 4.5 shows the results from a subject who performed a sit-stand-sit motion for five continuous cycles for the duration of 28 s approximately. The position of the contact microphone and the IMU sensors is also clearly shown in Fig. 4.2 and Fig 4.5. Here the three different outputs are shown in one figure with the same time frame. Knee joint angle and its angular velocity were also measured using a digital goniometer in the same time duration for five cycles. The sensor output was measured in terms of millivolts and recorded at its maximum value up to 8 mV. In Fig. 4.5, it can be seen that the velocity and angle output is clearly distinguished by the output of sensor voltage and motion phases in five cycles individually. The output velocity can distinguish the four motion phases in each cycle. Comparing the variation of the output voltage with respect to the different motion phases, it has been observed that the value of output voltage becomes higher while the subject starts moving from the sitting position to the standing position from a chair.

4.3 Results and Discussion

4.3.1 Sensor Output and Motion Phase Identification

Fig. 4.6(a),and 4.6(b) show the output of the contact microphone-based wearable device and the digital goniometer from an active knee joint S-T-S activity of a healthy subject in terms of voltage, knee joint angle, and angular velocity and are plotted in the same time series to distinguish the voltage in different phases. Here the output voltage obtained is found to be in the range of 0 mV to 6 mV, for the joint angular movement between 0° to 90° and the simultaneous joint angular velocity in the range of $0°/s$ to $80°/s$. This same time series distinguishes the voltage in different phases w.r.t. joint movement during the exercise performed. From Fig. 4.6(c), it can be seen that during the activity, there are differences among the vibroarthrographic signals in four phases, the output voltage becomes higher while the subject proceeds towards the standing position from the sitting position.

4.3.2 Fourier Transform Analysis

The obtained data from the microphone in terms of voltage *vs* time series is post-processed by using MATLAB. Signal processing features are obtained and the frequency spectrum is analyzed. During data processing the 'N' point, time-domain signals are decomposed into 'N' time-domain single point signals, and then corresponding 'N' frequency spectrums are calculated. This results in the contained frequency of the input signal on the fast Fourier transform (FFT) plot. Further, the Short-term Fourier transform (STFT) is obtained for all segments of the frequency spectra on a single plot. This STFT is a very powerful way to represent all contained frequencies in the scale of time, frequency, and

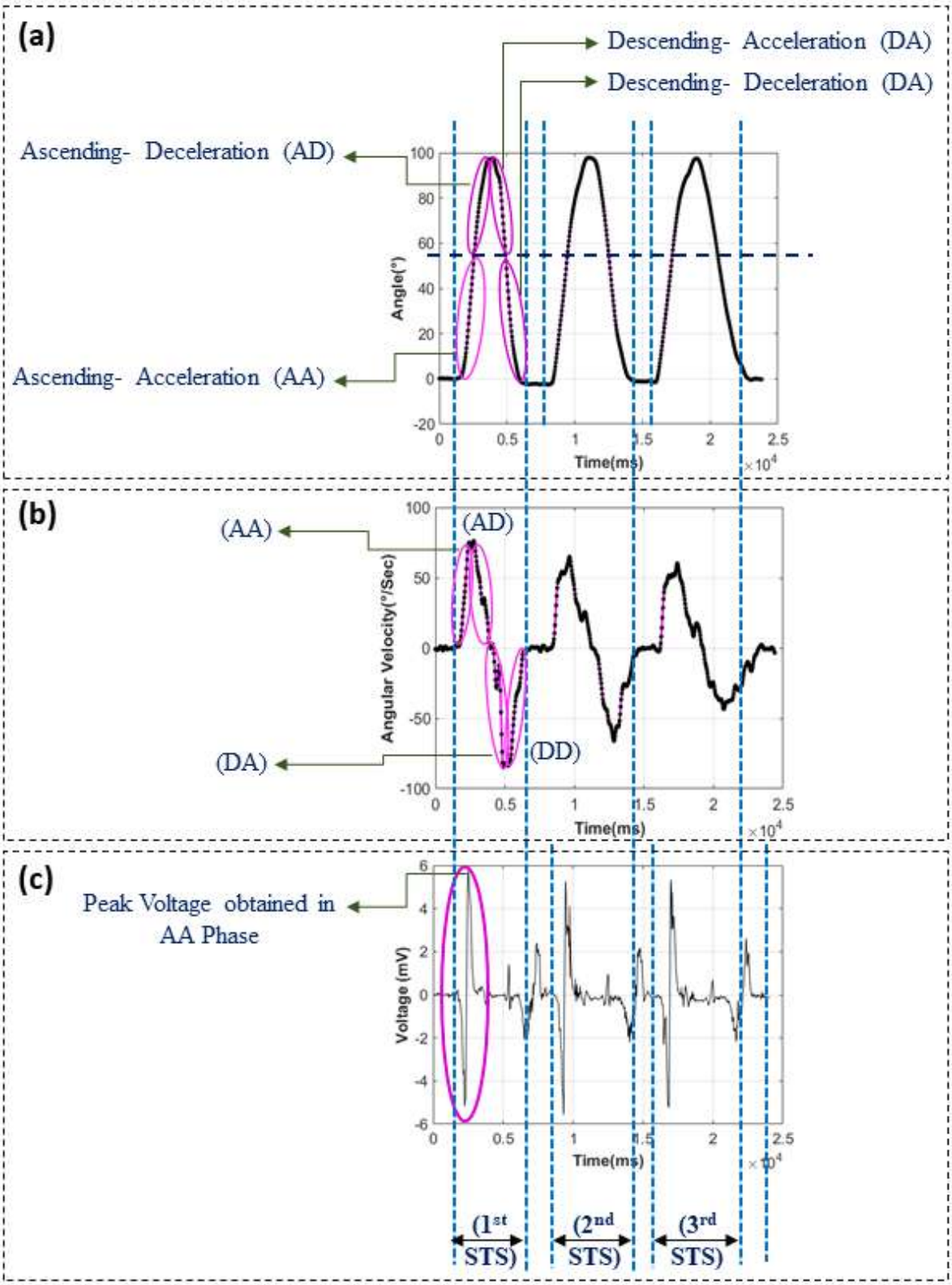

Figure 4.6: Joint Angle Based Vibroarthrography: (a) Joint Angle, (b) Joint Angular Velocity, (c) Voltage Output.

signal amplitude together. Also, it initially divides the spectrum into small segments and then combinedly shows the frequency distributions throughout the recorded signal with its amplitude distribution.

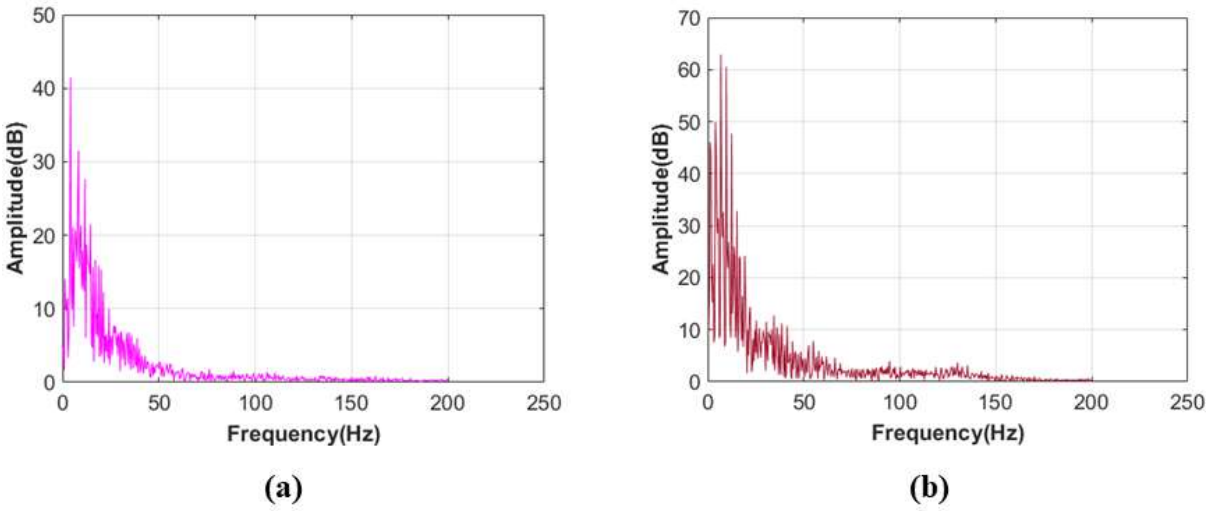

Figure 4.7: Frequency Analysis: (a) Healthy Knee, (b) Pathological Knee.

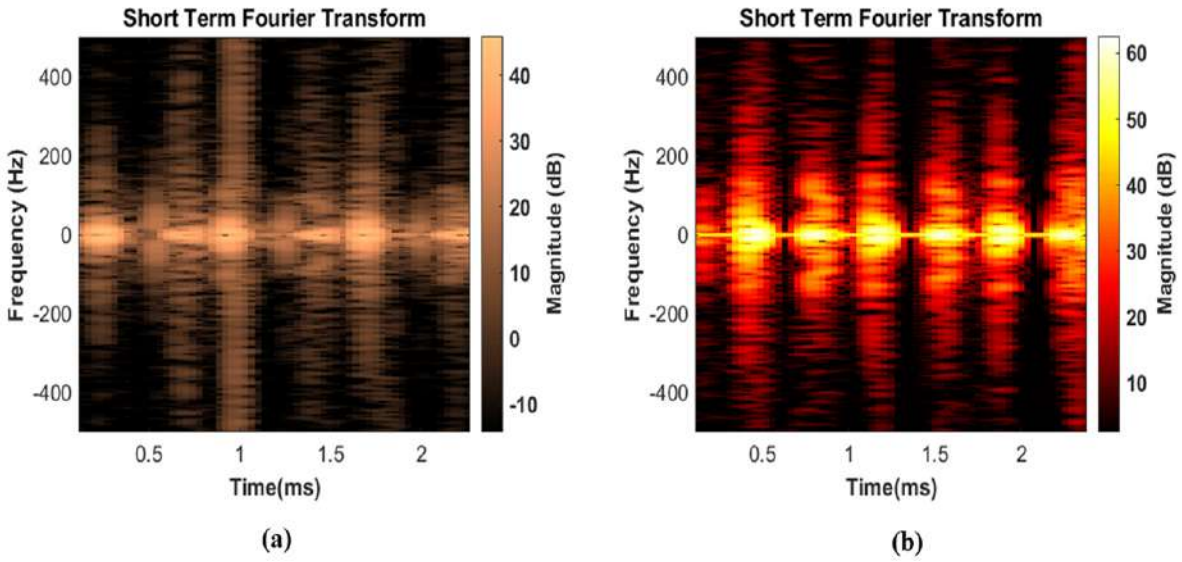

Figure 4.8: Frequency Spectogram: (a) Healthy Knee, (b) Pathological Knee.

Fig. 4.7(a) and, 4.7(b) show the FFT of the vibroarthrographic signals, collected when a healthy and an unhealthy subject performed the weight-bearing S-T-S exercise while STFT is shown in Fig. 4.8(a) and, 4.8(b) respectively. As shown in Fig. 4.7(a) and, 4.7(b), there are peak-frequency components when a subject performs a movement in a standing

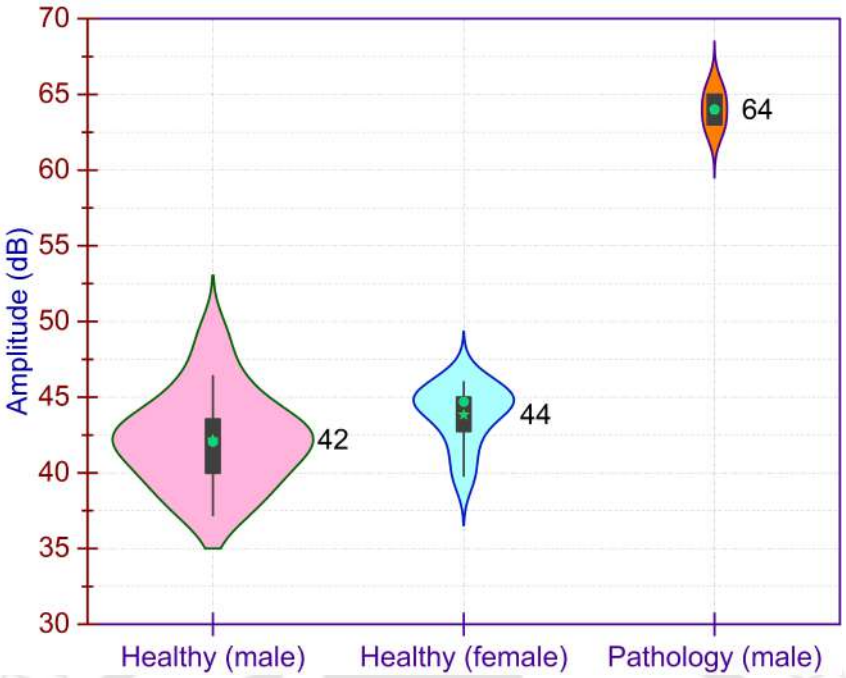

Figure 4.9: Violin Plots for Different Subject Groups.

position from the sitting position which is also justified by the higher voltage value as shown in Fig. 4.6 during the same phase. Fig. 4.7(a) and, 4.7(b) show the difference in frequency peaks between the healthy and unhealthy subjects, respectively. It is observed that in both the cases the obtained peak frequencies are different and less than 100 *Hz* but there is a significant difference in the signal amplitude. These results are in line with the published literature (Ye *et al.*) [188]. In Fig. 4.8(a) and, 4.8(b), the spectrogram of STFT of the output voltage of a healthy and an unhealthy subject is shown respectively to provide the time-localized frequency information in which frequency components of a signal vary over time. It is also been observed that the peak amplitude obtained for a healthy subject is 43 *dB* and for a pathological subject is 63 *dB* approximately which is shown in the following graphs.

Fig. 4.9 shows the violin plots for the sixteen healthy (male), eight healthy (female), and two pathologies (male) subjects. Here, the maximum amplitude (in *dB* level) data is considered with a kernel density distribution with a box plot. kernel density distribution,

a statistical technique is used to map the real-valued function to the weighted average of the observed neighboring data. The plots show the median (a green dot on the violin plot) with the interquartile range (a black bar at the center of the plot). In these plots, the corresponding mean (a green star on the violin plot) of the amplitudes is also shown with its magnitude for each group. From the violin plots, the maximum amplitude of acoustic emission obtained from the fabricated device is obtained to be in the range of 40-45 *dB* and 60-65 *dB* for the healthy subjects and pathology subjects, respectively.

4.3.3 Spectral Density Analysis

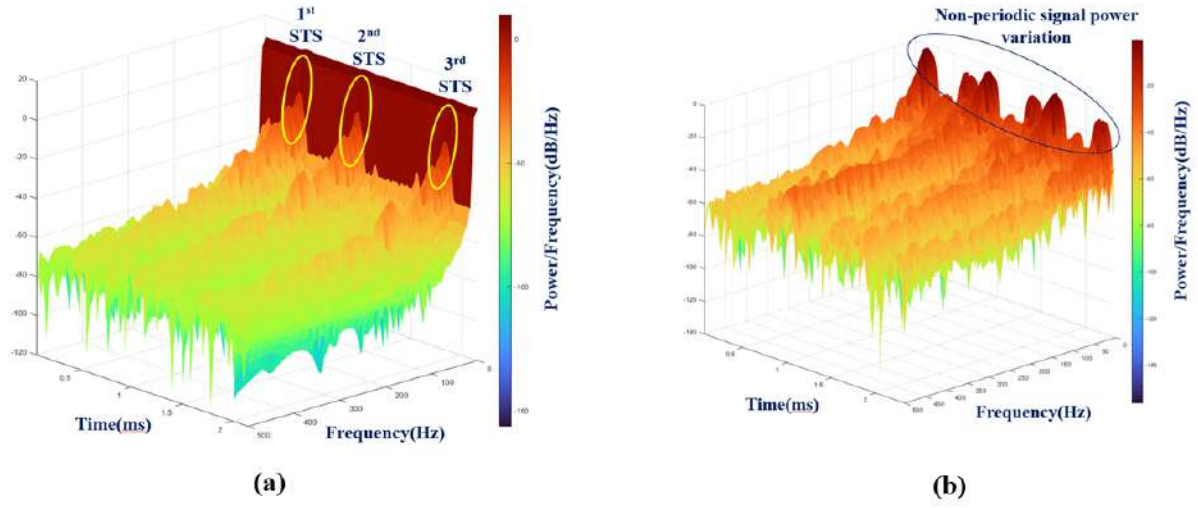

Figure 4.10: Power Spectral Density: (a) Healthy Knee, (b) Pathological Knee.

Power spectral density (PSD) is used to quantify the spectral power over the interested frequency band. It also gives the signal power variations over the time scale of the order of *1/Hz*. Fig. 4.10(a) and, 4.10(b) represents the waterfall plot or a time-frequency observation in the form of the spectrogram. Here the signal duration in *s* and contained frequencies in *Hz* are represented in the XY plane while Z-axis represents power spectral density (PSD) obtained from a pathological knee during the experiments in the *(dB/Hz)* scale for each time-frequency frame. In Fig. 4.10(a), it is observed that the spectral

signal power distribution for a healthy knee the gain in frequency is obtained at three certain locations in the time duration and it is because of the particular joint articulation. However, the pathological knee exhibits continuous frequencies as shown in Fig. 4.10(b) over the different frequencies from 0 Hz to 500 Hz. It represents the continuous generation of the vibration signals during the joint articulation throughout the signal acquisition period (0 s-2.5 s) and indicates the unhealthy knee joint condition.

4.4 Summary

In summary, a contact microphone-based wearable device has been successfully fabricated using an Arduino Nano microcontroller and other necessary electronic components in this work. The primary circuit is tested and calibrated and further converted into a printed circuit board. The device is successfully tested on healthy and pathological subjects by analyzing their knee joint sounds by employing vibroarthrography. Raw joint signals are stored in the device. After analog to digital conversion and postprocessing of the data in MATLAB R2021a version software, essential signal features are obtained. Sensor output up to 6 mV along with the joint articulation in the range of 0°-90° is obtained in all subjects during experiments. The signal time-frequency analysis reveals a significant difference between a healthy and pathological knee and indicates that the pathological knee emits a continuous vibration signal during data sampling. It can be concluded that healthy subjects emit the lower decibel level of amplitude (40-45 dB) compared to that of pathological subjects (60-65 dB).

Chapter 5

Quantitative and Parametric Study of Knee Joint Health Assessment Using Commercial Acoustic Sensors in Osteoarthritis

5.1 Introduction

This chapter presents a novel diagnosis approach to sensor-based acoustic emission for the assessment of the dynamic integrity of the human knee joint, along with its efficacy on healthy and osteoarthritic subjects. A total of 121 humans with increasing ages from different healthy to OA knee conditions participated in this study. Various signal parameters like acoustic hit, decibel, signal rise time, signal duration, absolute energy, and signal strength are determined along with the joint angles in sit-stand-sit activity. Descriptive statistical analysis is established using four phases of S-T-S movements. Bilateral symmetry of acoustic hits in both legs is obtained among the healthy subjects. Direct signal parameters, acoustic hits, and decibels are found to be increased with significant differences among the healthy and OA subject groups. Further, for detailed group characterization, time and energy signal parameters are statistically analyzed and observed with a very high percentage increment in the OA group compared with healthy subjects. Cumulative probability index analysis establishes a linear and non-linear trend among the groups, and OA subjects are identified with the most deviated feature patterns

in AE detection. From the study outcomes, a strong basis is formed for the development of sensor-based wearable systems in the early diagnosis of OA.

5.2 Methods

5.2.1 Data Acquisition System, Sensor Calibration and Placement

The acoustic monitoring system used in this work is AEwin^{TM} USB AE Node type setup manufactured by the 'Physical Acoustics Corporation USA'. It is a commercial sensor system that provides piezoelectric nanosensors and a data acquisition unit with wideband operational frequency ranges (125 *kHz*-700 *kHz*) of acoustic emission at a higher data sampling rate. It incorporates an analog-to-digital conversion (ADC) type signal processing unit that operates at 18 bits with 20 million samples per second (MSPS). The resonance frequency of the sensor is 300 *kHz*, and its peak sensitivity is 62 *dB*. After installation of the sensor system and before data collection, it is mandatory to calibrate the sensors. As shown in Fig. 5.1, two nanosensors (25.5 *mm* in diameter and 15.2 *mm* in thickness) are attached using hypoallergenic medical adhesive tape on the medial side of each leg. The anatomical landmark is fixed anterior to the medial patella retinaculum and inferior to the patella for the AE data collection (Shark *et al.*) [150]. The piezoelectric sensors are tested using the standard 'Hsu-Nielsen' pencil lead-breaking method before data acquisition. It is a standard approach for simulating the source of AE signals in which 0.5 *mm* mechanical pencil lead is broken at a 7.5 *cm* distance between the source and sensor, and calibration is performed at 100 *dB* amplitude as a standard output (Karvelis *et al.*) [189]. There is a limitation to conduct this procedure on human

skin because subjects may feel pain during lead breaking on the skin, so the test is performed on a flat surface where sensors are attached using medical tape. AE system records the burst energy of the source due to acoustic emission and captures it in the form of a hit. During the test run, several hits are recorded and each hit has a unique waveform. This waveform is in the form of signal voltage (mV) w.r.t time (μs), and the peak of the voltage represents the intensity of AE in the test.

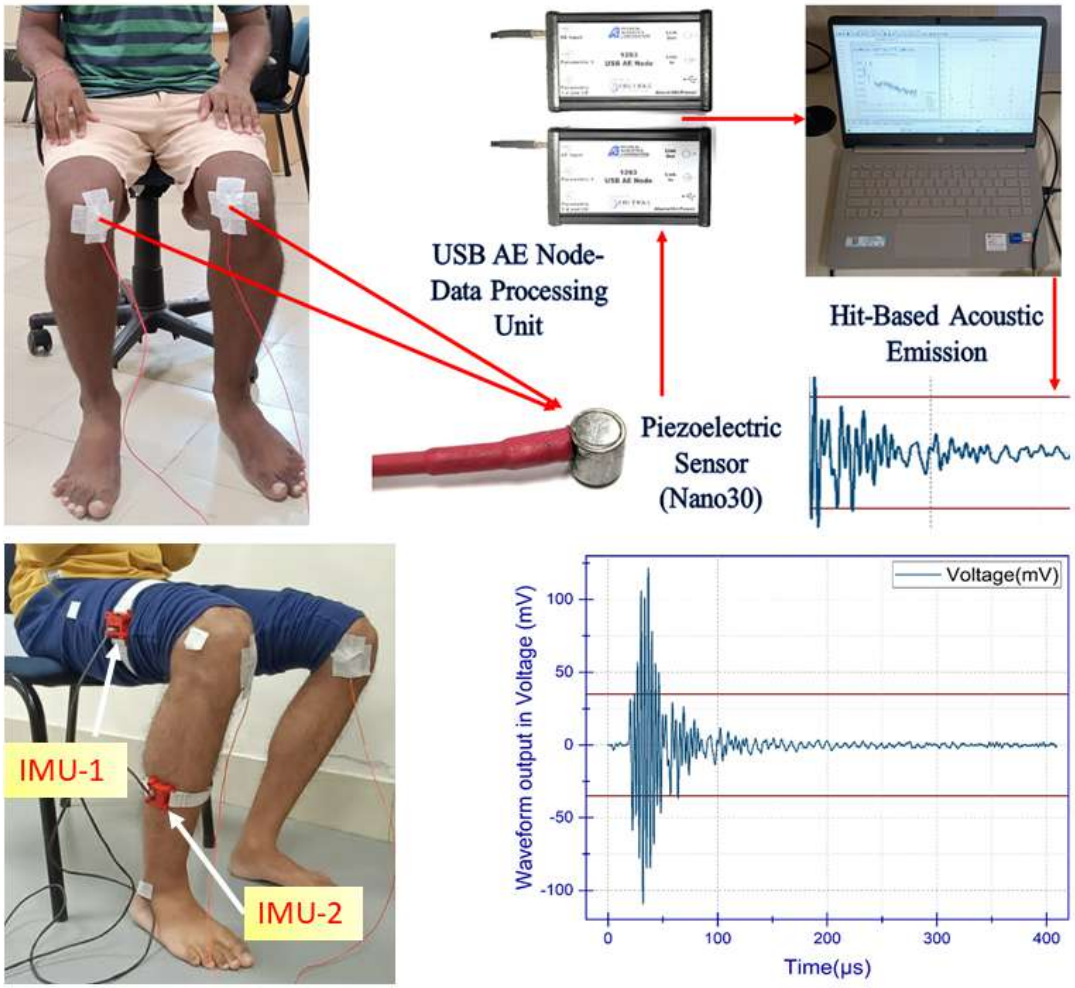

Figure 5.1: AEwin^{TM} Data Acquisition System with Subject Trial.

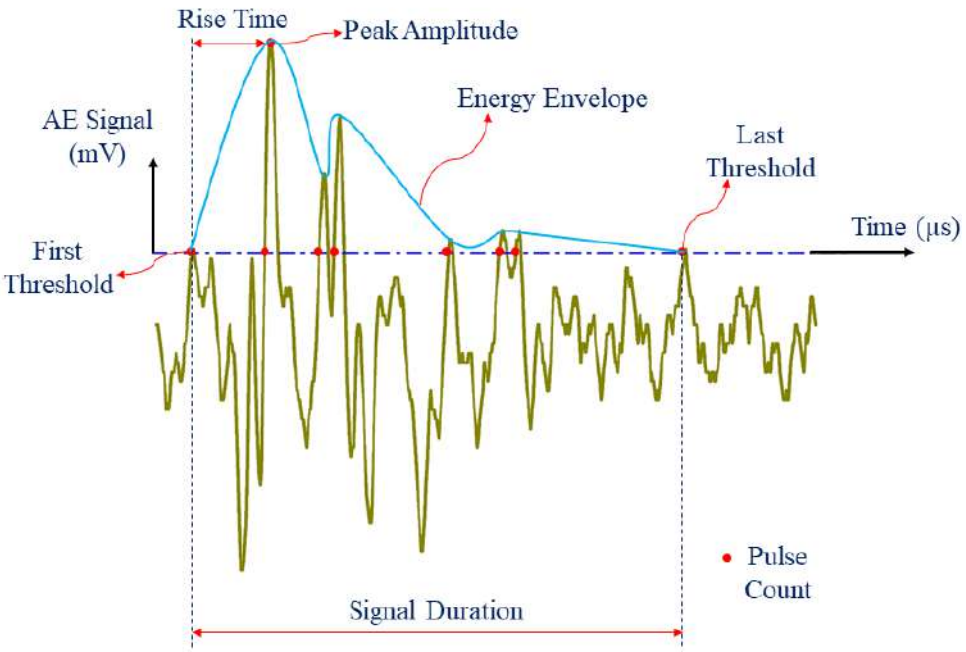

Figure 5.2: Standard Parameters of an AE Waveform.

5.2.2 Study Design and Participants

In the current study, AE signal features are analyzed for different subject groups. A typical standard waveform of a single hit is represented in Fig. 5.2, in which prime signal features are mentioned. Here, six major signal features like the number of Hits, Signal Amplitude (dB), Duration (ms), Rise Time (ms), Signal Strength ($nV\text{-}s$), and Absolute Energy (fJ) are studied and further evaluated in quantitative statistical analysis for individual subject groups. To highlight the disparities in AE features between knee joints in excellent condition, where frictions are minimal, and osteoarthritic knee joints, four participant groups having different age groups participated in this study. A total of one hundred twenty-one subjects are recruited with healthy knee and OA knee symptoms. Each participant has given written ethical consent and followed the standard inclusion-exclusion criteria. Data is collected from the young candidates at the Gait and motion analysis laboratory, IIT Guwahati, for the H1 (mean age: 28.77, SD: 4.78 *years*) and H2

(mean age: 48.88, SD: 4.89 *years*) groups while H3 (mean age: 67.83, SD: 6.92 *years*) and OA (mean age: 49.45, SD: 7.99 *years*) candidates are recruited at Mariapatty, a physical health center in Assam which is located in the remote area of Kamrup district in North Guwahati. The study is approved by the Institute Human Ethical Committee (IHEC), IIT Guwahati.

5.2.3 Clinical and AE Data Collection

During the initial assessment, anthropometric and clinical information is collected, such as age, sex, BMI, pain, function, and stiffness scores using WOMAC. Before the final data collection, each subject underwent substantial training in the usage of the equipment and data collection methodologies in order to ensure consistent protocol use. Starting in a seated posture with their backs on the chair and their knees bent at 90 degrees, the participants conducted sit-stand-sit (S-T-S) activities. In one S-T-S movement, four different joint motion phases are obtained. These are ascending acceleration (AA), ascending deceleration (AD), descending acceleration (DA), and descending deceleration (DD). The AE and joint angles are captured simultaneously from both knees. Three sets of three S-T-S motions are recorded in each test. Every subject is advised to move as naturally as possible at their convenience. The detailed description of the participants (abbreviated as S 1 to S 121) anthropometric data and direct signal outputs are summarized in the Tables of the Appendix A.1 contents.

5.3 Results and Discussion

5.3.1 Acoustic Hit Distribution and Joint Motion Phase Identification

In this work, the primary output of the acoustic sensor is an acoustic hit. Figure 5.3 shows the acoustic hit distribution in different subject groups where the coordinate of each point represents the number of hits in individual legs. The distribution of hits is represented on the Y-axis for the left leg in all subjects, while the right leg for individual groups is represented on the X-axis. The spread of hits in Fig. 5.3(a) shows an increasing trend with the group order, and the closed cluster dispersion of hits shows the bilateral symmetry of the acoustic emission from the subject legs, which means that the subjects emit a nearly equal number of hits during S-T-S activity. The data distribution from Fig. 5.3(a) is further analyzed to find the mean and range of hits in each group, as shown in Fig. 5.3(b), where the acoustic data from summarized statistics are graphically represented in the box plot.

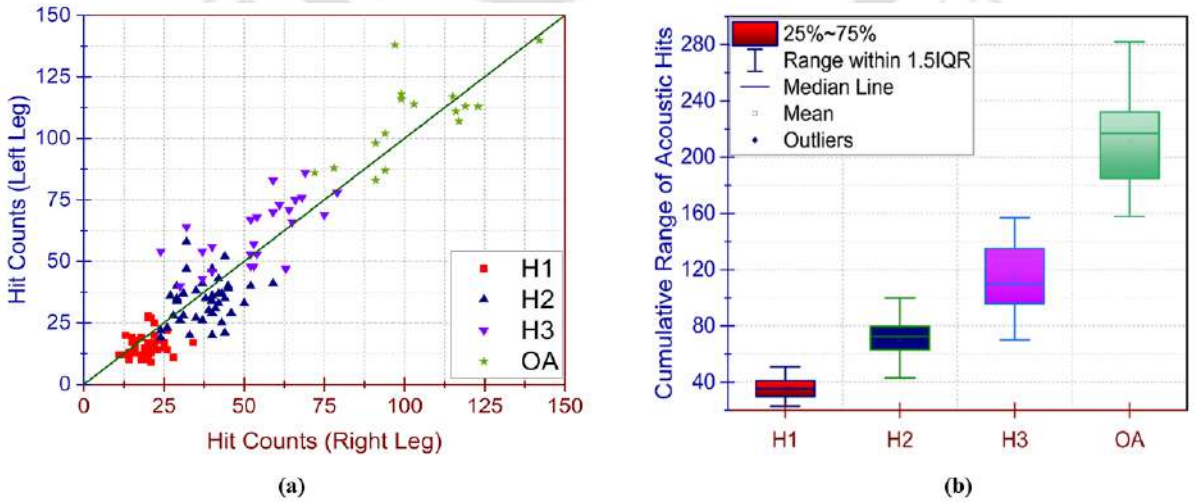

Figure 5.3: (a) AE Hit Distribution in All Subjects (Leg-Vise); (b) Range of Hits for Different Groups.

During three S-T-S cycles in each trial for individual groups H1, H2, H3, and OA, the obtained mean and standard deviation values of AE hits are 36±7, 72±13, 115±25 and 211±32 respectively. A significant increment in acoustic hits is observed among the different subject groups. The highest number of acoustic hits are obtained in the OA subject group. A study published by Shark *et al.* [150], on the early adulthood healthy group, late adulthood healthy group, and late adulthood OA group participants in which authors used a similar sensor system AEwin^{TM} to the current work with different PCI connection and S9204 model acoustic sensor. The study has identical observations to the present work, and the authors reported in their findings that the early adulthood healthy group emitted a comparatively lower number of hits than the late adulthood healthy group, while the OA group participants emitted maximum acoustic hits. In another study by Mascaro *et al.* [190], the authors reported that osteoarthritic knees produce 6–10 times more acoustic emissions than healthy knees. Similar observations are found in the current work.

During the activity and along with the AE data collection, an indigenously developed digital goniometer *(DG_IITG_V0)* as discussed in the Chapter 3, is also placed on the leg to record the knee joint angle and its angular velocity to identify the joint angle at which the acoustic hits are generated. The purpose of this experiment is to record a joint angle-based acoustic emission for motion phase identification using joint angular velocity. In Fig. 5.4, the overlapping of acoustic hits on varying angles with simultaneously varying angular velocity is plotted in the same time interval for a subject. A similar kind of combined knee joint angular velocity, joint angle, and acoustic hits are analyzed for every subject. Here, the velocity diagram shows the four phases in a cycle. Since the variation of velocity and angle are plotted in the same time interval, thus, it can distinguish each

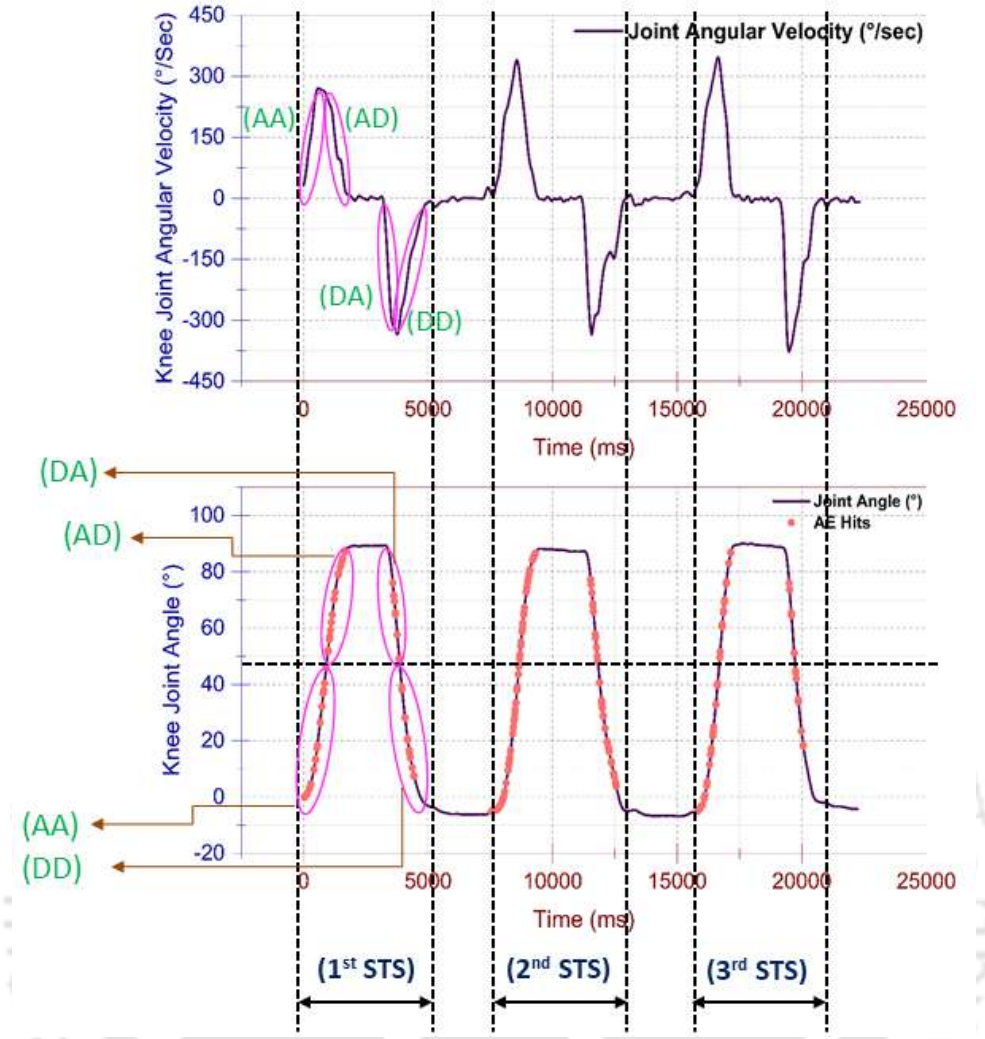

Figure 5.4: Joint Angle and Angular Velocity-Based Acoustic Emission.

phase in the joint angle while comparing with the joint angular velocity diagram. After identifying each phase in the joint angle, the number of hits for every phase can be obtained from the overlapped graph of hits and angle. Similar observations are obtained for all subjects from each group.

Figure 5.5 shows the bilateral plots of descriptive analysis for the distribution of the number of acoustic hits in each phase of the S-T-S activity and in each group during the data collection. There are four bilateral plots for each subject and from each group showing the joint movement phases together. A symmetrical pair of knees is identified by the point nearer to the bilateral line, representing similar acoustic hits obtained from the

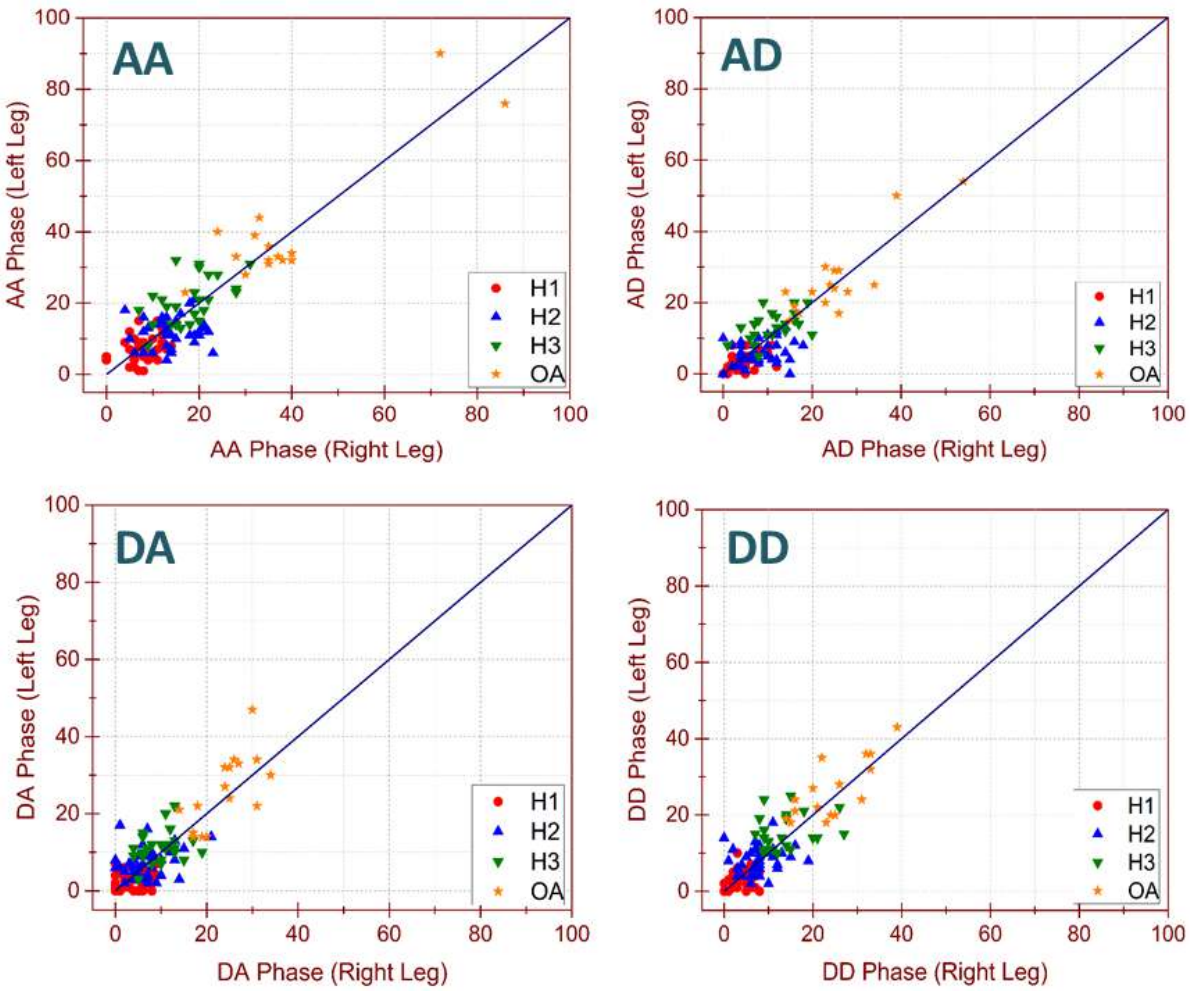

Figure 5.5: Phase-Wise AE Hit Distribution in All Subject Groups.

left and right knee in an individual phase. The group vise AE hits distribution is further analyzed. It is observed that the H1 subject group emits a symmetrical, repeated, and lower number of hits in all movement phases. With the increasing age of the subjects from the H2 and H3 groups, the acoustic hits also increase in numbers, but the hit distribution pattern deviates slightly from the symmetry. A different observation is made in OA subject groups as the knee condition turns towards OA, the highest acoustic hits are observed with dispersed deviation from bilateral symmetry in all movement phases. Among all joint movement phases, it is observed that the AA phase shows a maximum number of hits for all groups and each subject. In the study published by Mascaro *et al.* [190], the authors used (S9204, 50–200 *kHz*, Physical Acoustics Ltd. Cambridge, UK)

with two pre-amplifiers and reported that healthy knees produce less than 25 AE hits per movement and OA knees can produce 150–250 AE hits per movement. At the same time, this number is higher in the AA phase of S-T-S activity. The present study results are found to be in line with the previously published research [190].

5.3.2 Group Index Plots for AE Features

Since the current research is focused on a group of human subjects and in the case of any individual subject trial, the sensor receives a large number of acoustic hits according to the joint health condition. Hence, different signal parameters are analyzed to differentiate among the groups based on leg-wise AE signal features for detailed characterization. Here, a total of six AE signal features, Number of Hits, Signal Amplitude (dB), Rise Time (ms), Signal Duration (ms), Absolute Energy (fJ), and Signal Strength ($nV\text{-}s$) are analyzed as shown in 5.6. It is feasible to visualize the clusters of information through their quartiles using the box plots so for the statistical representation of these features, diamond group index charts are plotted to differentiate between the left and right leg among the four subject groups. It is observed from Fig. 5.6(a) and, Fig. 5.6(b) that the acoustic hits and decibels values are gradually increasing with the increasing age groups from healthy to OA in both the legs and showing almost a symmetrical output. The highest hits and decibels are obtained in OA subject groups. Further, Fig. 5.6(c) and, Fig. 5.6(d) show the variation in signal Rise Time (ms) and Signal Duration (ms). It is observed that minimal duration signals are obtained in groups H1, H2, and H3 and with their corresponding shorter rise time. It shows that healthy knees emit lesser acoustic emissions for very small durations. However, the trend is found to be increasing among healthy subject groups. It is previously published by Mascaro *et al.* [190] that OA knees

can produce ten times longer duration signals compared to healthy knees. In the case of OA subjects, longer duration signals with higher rise time values are obtained, which means that the OA knees emit higher acoustic emission due to poor joint condition and higher joint surface friction. The essence of time-dependent parameters is simultaneously reflected by energy parameters as shown in Fig. 5.6(e) and, Fig. 5.6(f), where signal absolute energy and signal strength are found to be almost negligible among healthy groups, while in the case of OA subject groups, this is drastically increased.

This indicates that the most degraded knee joint condyle surfaces produce high frictional energy. These time and energy-dependent observations are evident and validated from the previously published research by Sakib *et al.* [191], in which the authors identified a natural pattern of signal features among the subjects with OA and without OA where signal strength and absolute energy identified as a potential biomarker for knee OA detection using AE. This multidimensional feature-based quantitative assessment is useful for the subject group and signal feature characterization regarding their mean and standard deviations. The more descriptive observations of feature percentage increments from healthy to OA subject groups is shown in Fig. 5.7, where the energy-dependent parameters are found with significant increments in OA subjects.

In this study, the WOMAC questionnaire is also used to assess the pain, stiffness, and physical function before collecting the AE data from each participant. The WOMAC score is calculated, and it is observed that with the increasing age in the groups, the obtained score is also increasing. The mean score in H1 (6.75±10.83), H2 (22.58±11.87), H3 (35.40±12.74), and in OA is (38.06±13.01) observed. The WOMAC scores of all individual subjects are reported in the Appendix A.1. It is noted that the increasing WOMAC score is age-associated and highest in severe knee health in OA subjects.

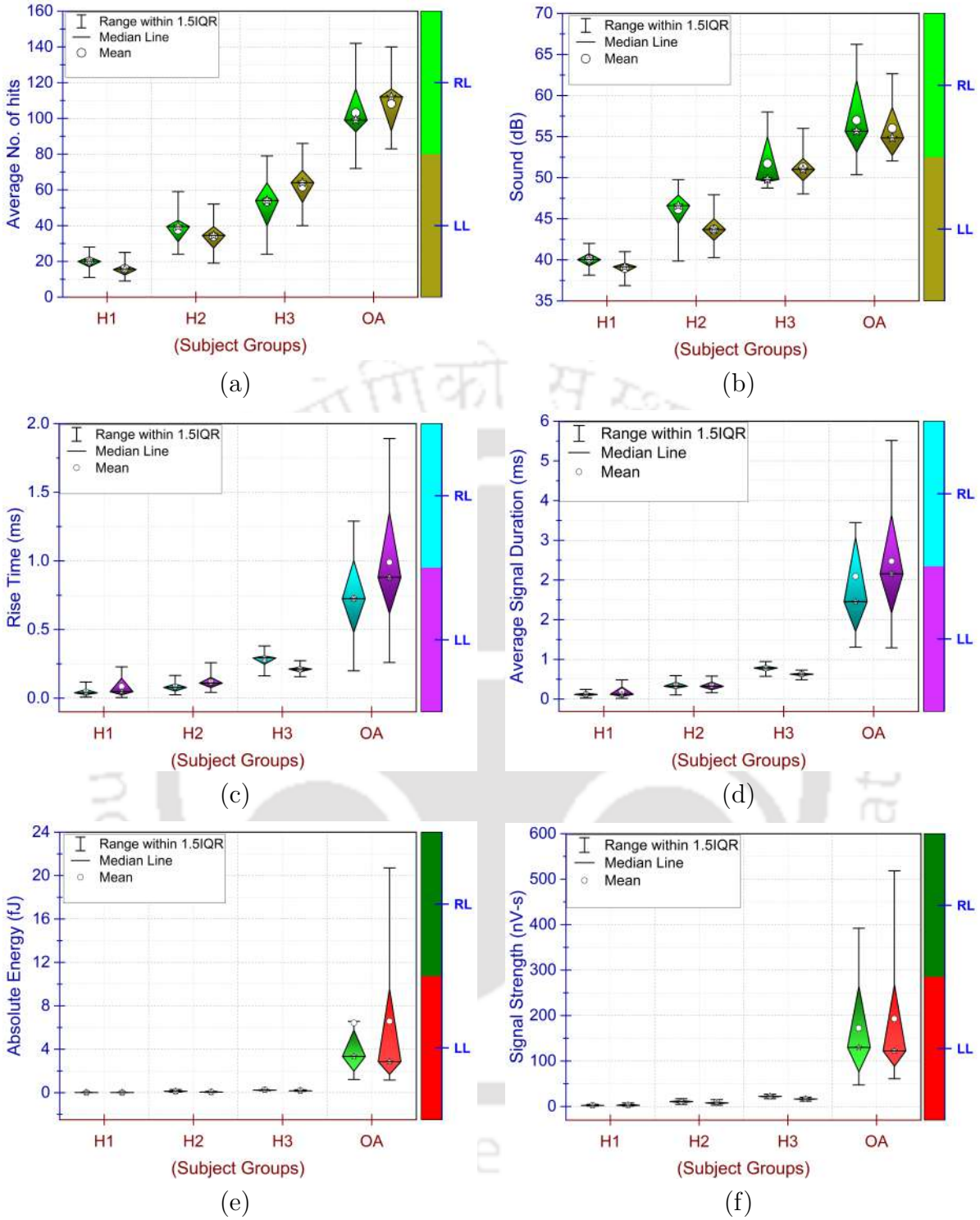

Figure 5.6: Diamond Box Plots for AE Signal Features: (a) AE Hits, (b) Amplitude (dB), (c) Rise Time (ms), (d) Duration (ms), (e) Absolute Energy (fJ), (f) Signal Strength (nV-s).

5.3.3 Cumulative Probability Index plots for AE features

The cumulative density function (CDF) plots are generated for AE features using the exponential probability density function. These plots represent proportions and percentiles

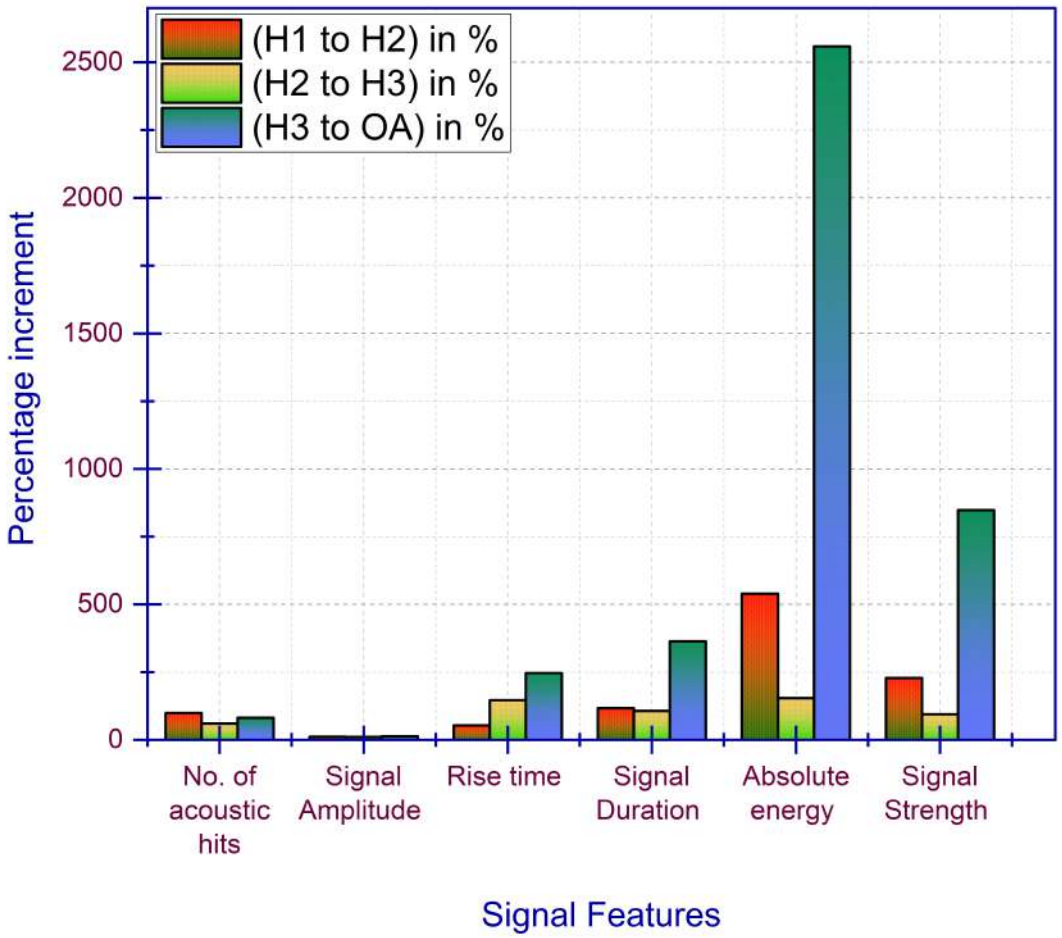

Figure 5.7: Percentage Increment in Signal Features (Cumulative Both-Leg) from Healthy to OA Subject Group.

for data ranges and are helpful to identify the most occurred values by comparing the sample distribution of all subjects in their subgroups. It also determines the lower and upper bounds of AE features in their respective ranges. As shown in Fig. 5.8(a) and, Fig. 5.8(b), H1 and H2 groups show almost similar and linearly increasing trends for hits and decibel features, which defines the well-fitted distribution of the data. These subject groups emit uniform hits and decibels during S-T-S activity. In the case of the number of hits, H3 is almost linear, but OA subject groups are found with a deviation of the probability of occurrence at the tail section, which shows lower proportions in the sample distribution in a few subjects. For the case of signal amplitude, the H3 subject group shows a slight deviation in the head and tail section, which means a few subjects show

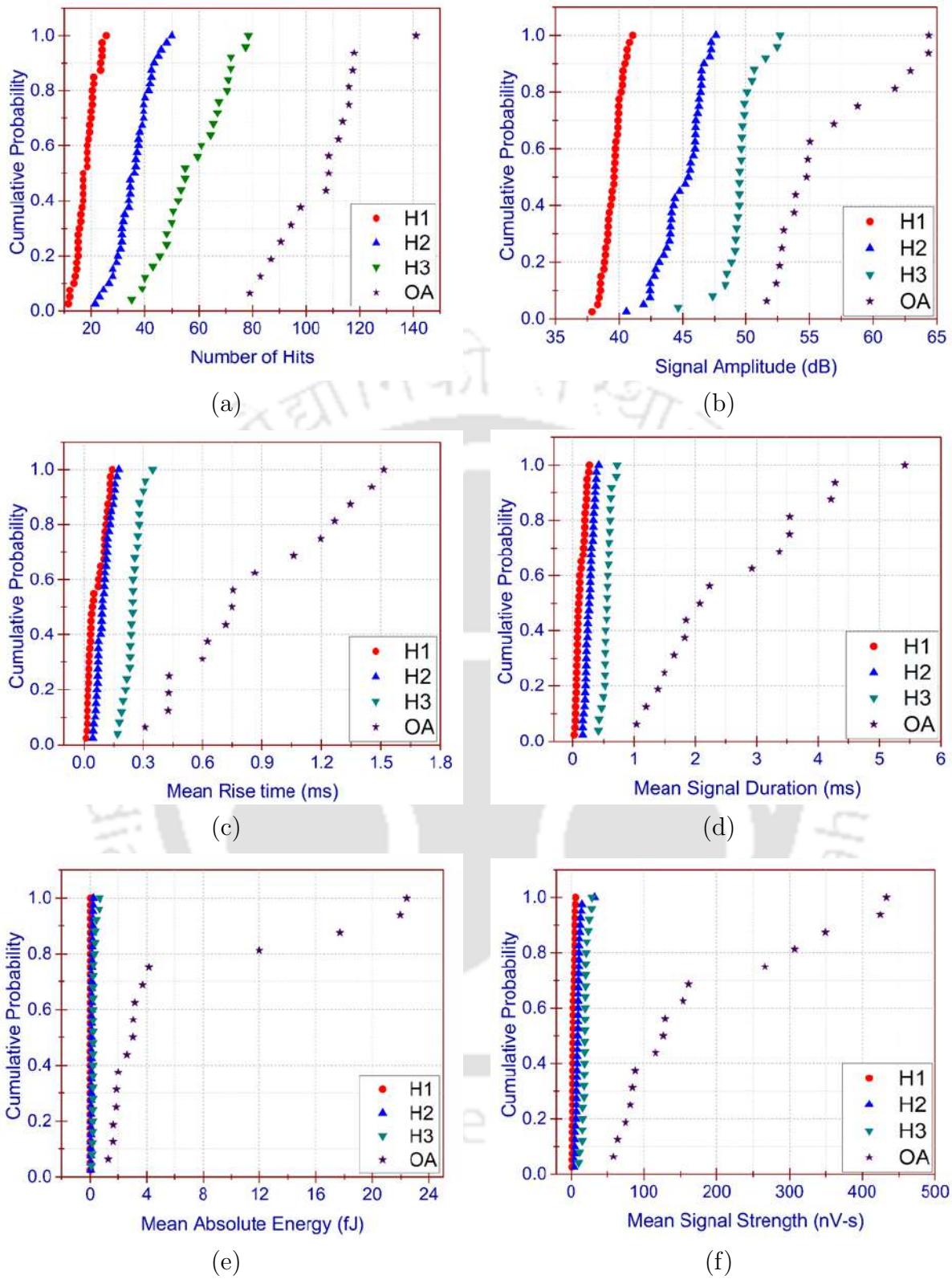

Figure 5.8: Gaussian Probability Plots for:(a) AE Hits, (b) Amplitude (dB), (c) Rise Time (ms), (d) Duration (ms), (e) Absolute Energy (fJ), (f) Signal Strength (nV-s).

decibel deviation among the others in the same H3 group, but in the case of OA, the trend is highly deviated. Results are non-uniformly distributed, which means OA subjects emit the highest and random decibels during S-T-S activity. In the case of mean rise time and signal duration, H1, H2, and H3 subject groups show a good linearly increasing trend, which indicates uniform data distribution over the group sample and shows stable and small duration signals in all healthy subjects. OA subject groups are scattered in CDF for the same time-dependent features and follow the non-linear trend, as shown in Fig. 5.8(c) and, Fig. 5.8(d).

Shark *et al.* [150] reported a significant increment in signal features from healthy to OA subjects. During the AE biomarker identification in their study, the authors reported a very high increment in absolute energy from healthy (21.76 aJ) to OA (8.7x10^4 aJ). Moreover, Sakib *et al.* [191] also reported a significant increment in absolute energy and signal strength from healthy to OA in their findings. The results from the present work in CDF are shown in Fig. 5.8(e) and, Fig. 5.8(f), where absolute energy and signal strength increase with the highest difference between healthy and OA subjects. Simultaneously, the OA subjects showed a nonlinear variation in these energy parameters, indicating the random burst of energy in different OA subjects with poor knee health. The current research observations are aligned with previously published research [150, 191].

5.4 Summary

The present study shows an overall AE signal feature distribution trend in healthy and osteoarthritic subject groups. Initially, the scattering of waveform hits in both legs in all subject groups is identified to observe the distribution of signal bursts during S-T-S activity. H1 and H2 Healthy subjects emit an almost similar number of hits from

both legs, while the increasing age in H3 and the subjects from the OA group show bilateral asymmetry. Another critical observation is made by superimposing the angular data on acoustic hits having different data sampling rates to study the joint motion phases based on AE analysis. Here, the hits are evenly distributed with joint angles throughout the cycle. The AA phase of weight-bearing S-T-S activity is the most critical and dominating joint motion phase in which the AE sensors recorded the highest hits. Another observation from the bilateral plots for phase-wise hit distribution is that the symmetry of hit distribution is consistent in all healthy groups except OA knee, where the hits are asymmetrically distributed.

Furthermore, different inherent signal parameters corresponding to each signal waveform are obtained, and based on these parameters, the distinction between all healthy age groups and osteoarthritic subject groups is assessed. The average decibel values are observed to be distributed from the 35 dB threshold to 65 dB signal amplitude, increasing from H1 to OA subject groups. However, the H2 and H3 subject groups are closer in range distribution from 40 dB to 55 dB. It is clearly distinguished that the higher decibel values of signal amplitude are achieved in OA subject groups. A substantial increment in the mean signal parameter values is achieved in all features with increasing age groups and OA people. A sudden increment in absolute energy and signal strength is observed in the OA subject group compared to healthy people. This tremendous absolute energy and signal strength change is the prime evidence of degraded joint health and is considered a suitable biomarker for OA detection. Results from the cumulative probability index plots show the linearity in healthy groups in quantitative assessment and differentiated groups in AE assessment. While the features from OA subjects show an asymmetric pattern, which is evident for OA knee. Furthermore, all obtained signal features differ-

entiate among all the subject groups in this study and can be accepted as adaptive AE biomarkers for OA detection.

Chapter 6

Classification of Knee Osteoarthritis Using Commercial Acoustic Sensors and its Validation Through X-Ray Imaging

6.1 Introduction

The objective of this research is to assess the feasibility and effectiveness of a non-invasive and non-radiographic tool for the quantitative evaluation of the different stages of knee osteoarthritis using an acoustic emission system and validate from respective radiographic (X-ray) findings in human subjects from the North-Eastern region of India. This novel approach is implicated by capturing the sound waves generated from the knee using acoustic emission signal features as biomarkers for the diagnosis of different stages of OA. A total of sixty-three OA knee participants with radiographic evidence are examined through the acoustic sensors placed at their medial tibiofemoral knee locations. Joint angle-based signal features are detected for biomarker identification under the sit-stand-sit (S-T-S) data collection protocol. Joint space narrowing (JSN) of the knee for individual subjects is calculated through image processing, and AE findings are validated from Kellgren-Lawrence (KL) grades from KL-1 to KL-4 with JSN. The average knee joint sound level is obtained as 60 dB in KL-1 subject groups, 64 dB in KL-2, 71 dB in KL-3, and the highest 76 dB in KL-4 subject groups. Very high absolute energy and longer duration

signals are obtained in the KL-4 subject's knees compared to other OA grades. The Principal Component Analysis (PCA) analysis identified the signal Amplitude (dB) as a primary biomarker for OA detection. The study findings lead to the acoustic emission is a promising diagnostic tool in OA detection and provides a non-invasive management of knee OA.

6.2 Materials and Methods

6.2.1 Experimental Set-up

In this work, the sound generated due to the frictional contact from the sliding between the femoral condyle and tibial condyle, followed by the gliding of the knee joint, is recorded during the weight-bearing activity by using the same commercial sensor system used in the previous work as mentioned in the Chapter 5. To achieve an adequate acoustic coupling between the knee skin surface and sensor, a thin layer of 'Aquasonic gel' is applied on the knee joint skin, and the sensors are placed on the knee above the medial tibial condyle (Khokhlova *et al.*) [192]. The machine thresholds used for data acquisition are considered as 35 dB, a frequency range of 10 kHz to 700 kHz, and a 20 MHz sampling frequency, which is achieved with respect to 1 μV reference voltage level (Schluter *et al.*) [193].

6.2.2 Study Design and Participants

A total of sixty-three confirmed OA subjects from North-East India with X-ray KL scores of 1 or higher are recruited after obtaining their written ethical consent. KL score is an established radiographic system for OA knee grading consisting of four features: bone-

end deformation, subchondral sclerosis, osteophyte formation on the joint edges or tibial spines, and joint space narrowing (JSN) (Steenkamp *et al.*) [194]. JSN on radiography is typically attributed to cartilage loss, and a decreased joint space is linked to more meniscal tears and persistent knee discomfort (Chan *et al.*) [195]. Anterior-posterior (AP) view of knee joint X-rays is analyzed, and the JSN is estimated individually for each OA subject using an image processing method. The AE features are validated with radiographic findings, and AE biomarkers are identified in a quantitative assessment manner for the early diagnosis of OA. The anthropometric information is recorded for all subjects (abbreviated as S 1 to S 63) individually before the data collection, which is summarized in the Tables of the Appendix A.2 contents.

AE measurements of the participants are done at the gait and motion analysis laboratory, IIT Guwahati, and three independent hospitals of Guwahati Neurological Research Centre (GNRC) Guwahati at GNRC-Dispur, GNRC-Sixmile, and GNRC-North Guwahati while conducting knee health check-up camps. Data collection is done after getting IHEC approval from IIT Guwahati and GNRC. The AE data acquisition system consists of two high-frequency piezoelectric broadband sensors. An AEwin^{TM} data processing software is used for knee joint sound recording and display. These sensors are placed on the medial side of the tibiofemoral joint. Joint angles during the S-T-S posture (0°-90°) are simultaneously measured using IMU based indigenously developed digital goniometer *(DG_IITG_V0)*. Joint space narrowing (JSN) is measured from the radiographic evidence of individual subjects, which are post-processed through image processing software 'ImageJ'.

6.2.3 Inclusion-Exclusion Criteria

Each subject is carefully examined before data collection and followed by the inclusion and exclusion criteria as per the guidelines of the Institute Human Ethical Committee (IHEC) IIT Guwahati and GNRC Guwahati.

The subject's inclusion criteria are as follows:

- The age group varies from 30 to 80, including males and females.
- The subjects must have radiological evidence of OA knee.
- Must be able to read and understand English, Hindi, Assamese, or any other Indian language and demonstrate the ability and willingness to follow the protocol and complete the questionnaires and diaries.
- Manual dexterity is sufficient to perform all tasks required by the participants.
- Willingness to wear the knee joint acoustic wave capturing system for the examination during sit-stand-sit motions.
- Able to travel as the data collection takes place at different places by conducting camps, where participants attended the data collection sessions.

The subject's exclusion criteria are as follows:

- Current musculoskeletal injury and infection.
- People with secondary osteoarthritis or any previous knee surgery.
- Unable to follow instructions or cognitive deficits.

- Subjects with cardiovascular risk or under any treatment of major health issues.
- Subjects having any kind of implants.
- Unable to perform tasks due to current medical conditions like contagious diseases, balance and coordination disorders, any active infection, unhealed wounds or ulcers, and sensory deficit of lower limbs.
- Subject unable to perform sit-stand-sit motions due to any reason.

6.2.4 Clinical and AE Data Collection

All the subjects underwent clinical assessment, including past and present medical history, age, sex, Body mass index (BMI), and Western Ontario and McMaster Universities Osteoarthritis Index (WOMAC) score for pain, function, and stiffness. The collected X-ray images are analyzed through image processing software 'ImageJ', and JSN is measured for individual subjects. Fig. 6.1 differentiates the OA grades from the radiograph of the individual subjects, who participated in this study. These grades are based on the primary findings like the presence of JSN, osteophytes, and sclerosis in the X-ray. The purpose of JSN identification is to find the KL grades for different OA groups and further validate them with AE signal features.

During the AE data collection protocol, the subject is asked to sit on a chair with knees bent at 90° and arms crossed across the chest. In one trial, the subject is asked to perform three S-T-S cycles synchronized with a metronome in approximately 25-30 *s*. A total number of three trials are recorded for each subject. Simultaneously, knee joint kinematic parameters are recorded using an indigenously developed inertial measurement unit (IMU) sensor-based digital goniometer to assess joint angle-based AE (Mascaro *et*

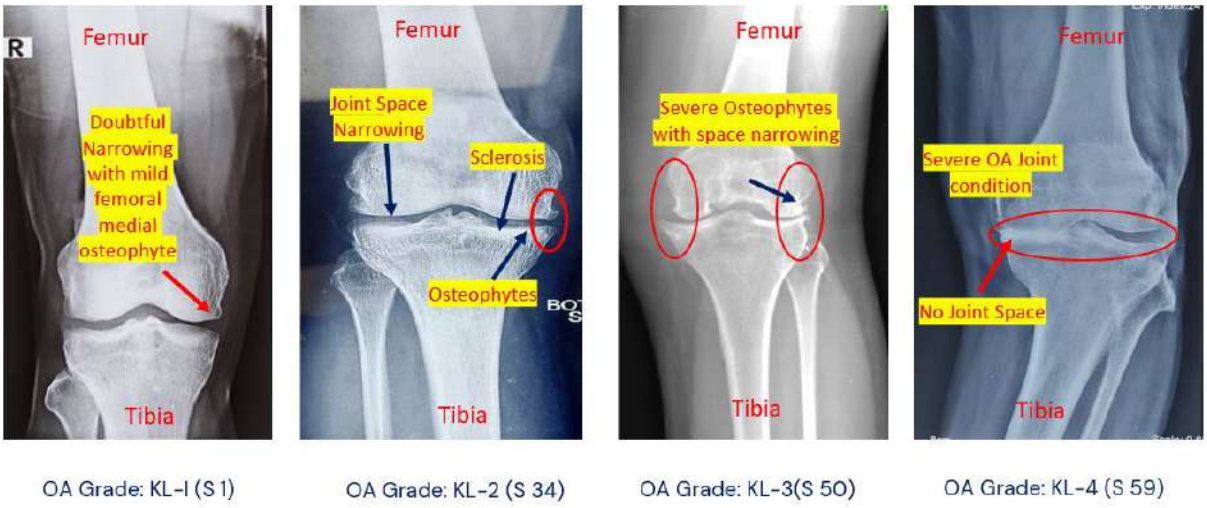

Figure 6.1: Osteoarthritic Changes Observed in X-ray (AP View) for Confirmation of KL Grades.

al.) [190]. All subjects are asked to perform the S-T-S exercise according to their comfort.

6.2.5 Semi-Quantitative Measurement of Knee OA from X-ray

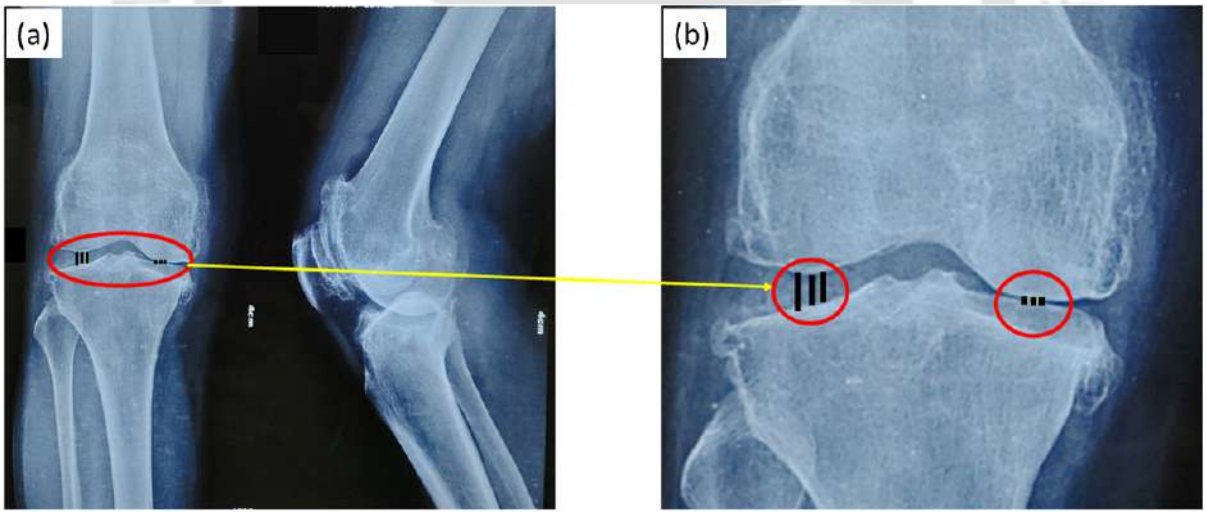

Figure 6.2: (a) AP and Lateral View of OA Knee (S5, KL-3); (b) Enlarged AP View Showing Three Vertical Measurements of JSN in Both Medial and Lateral Condyle.

Initially, the X-ray images of all the individuals are collected. The radiographic scale is calibrated with the 'ImageJ' software to find the JSN. It is achieved by fixing the calibrated scale as a global reference on the radiograph, and with reference to it, the three vertical measurements are taken at the mid-intercondylar space of the more affected

zone (medial or lateral) of the OA knee as shown in Fig. 6.2. The line is drawn in the translucent area, which is between the transopaque area of both femoral and tibial condyles. The length of the drawn line is then individually determined using the 'ImageJ' measuring tool. Finally, JSN is calculated as a mean of the three sets of measurements, which is further helpful for differentiating among the KL grades (Steenkamp *et al.*) [194].

6.3 Results

6.3.1 Evaluation of Number of Hits and Sound Decibel

Figure 6.3(a) shows a relation between the KL grade obtained from radiographic images through clinical assessments and the acoustic hits during three S-T-S activities in all subjects. The observations are described through the violin plots, showing a statistical evaluation of the obtained data in interquartile ranges with means and median interpretations. These plots are helpful in visualizing the data density and entire data distribution with their symmetry and skewness. It is observed that the number of acoustic hits increased with the severity of the condition of knee OA i.e. KL-1 (81±12), KL-2 (105±9), and KL-3 (137±12), and the highest acoustic hits, 167±11, are obtained in KL grade 4.

Figure 6.3(b) is the statistical representation of the average decibel values obtained in different OA groups during the joint articulation. It is observed that the least mean decibel of 60±2 dB is obtained in KL grade-1 subject groups, which is found to be increased with the progression of KL grades 64±2 in KL-2, 71±2 in KL-3 and the highest mean decibel value, i.e., 76±1 dB, is obtained in KL grade 4 subject group. It is identified from Fig. 6.3(a) and, Fig. 6.3(b) that the obtained feature ranges in the violin plots are overlapped. A very few subjects are found with similar feature ranges for different KL

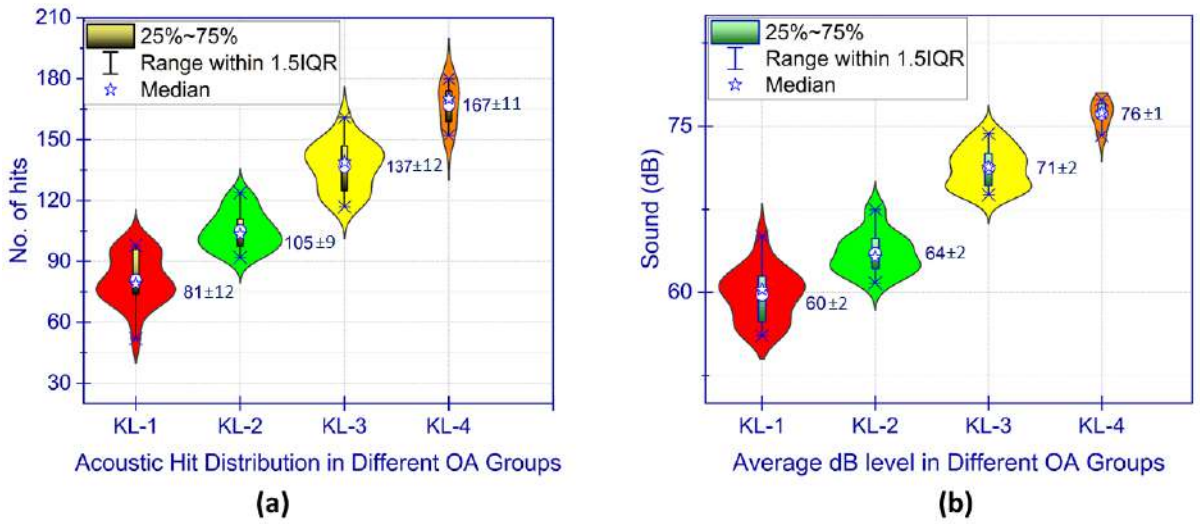

Figure 6.3: (a) Acoustic Hit Distribution Among OA Groups; (b) Obtained Decibel Levels in Different OA Groups.

groups, but they are clearly differentiated from the X-ray findings. So, the mean value interpretations are considered to distinguish among the different OA subject groups to obtain signal features.

Since the acoustic hits are studied with (0°-90°) S-T-S motion in all subjects, the analysis is further carried out for different joint motion phases. A subject performs four different phases during each S-T-S activity, namely ascending acceleration (AA), ascending deceleration (AD), descending acceleration (DA), and descending deceleration (DD). Figure 6.4 describes the average number of acoustic hits obtained in individual phases in different OA groups. The important observation is that the AA and DD phases contain the maximum number of acoustic hits in the weight-bearing activity. This is quite apparent because the subject carries maximum body weight while standing from the chair in the AA phase and sitting on the chair in the DD phase. The obtained AE hits and decibel values are distinguished among the different OA groups.

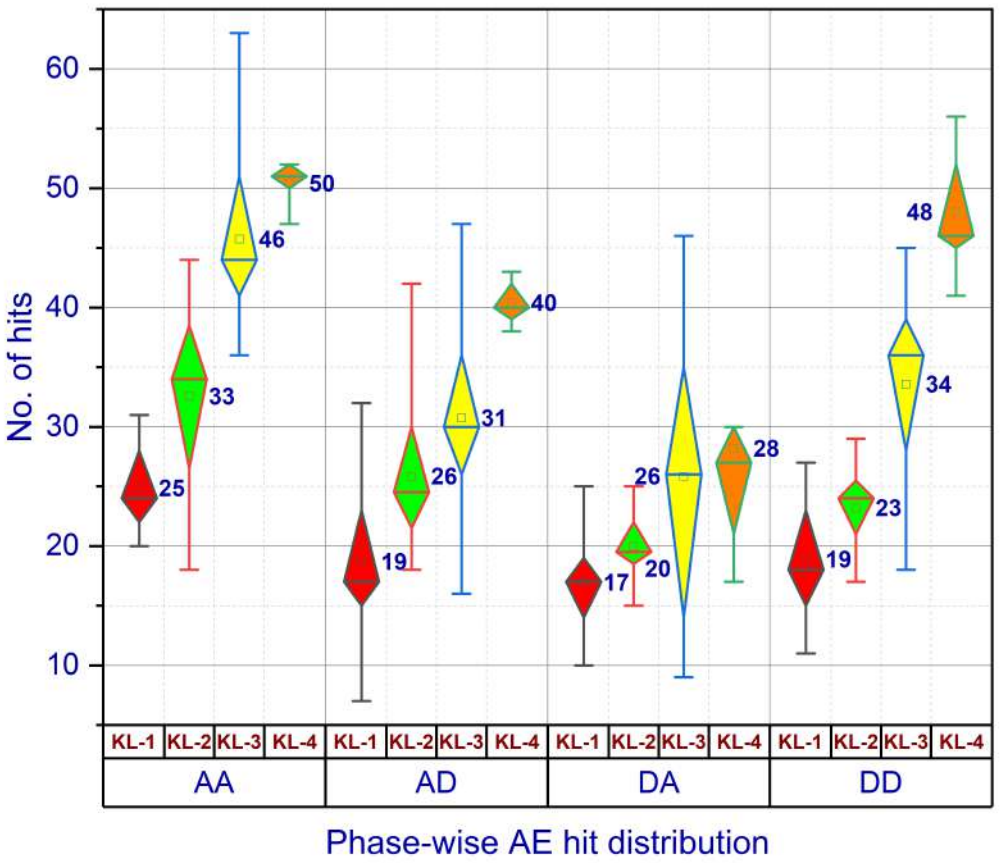

Figure 6.4: Acoustic Hit Distribution in Joint Motion Phases.

6.3.2 Inherent Signal Features: Signal Duration, Absolute Energy, and Average Frequency Estimation with JSN

The study is also focused on the inherent signal parameters, which are analyzed to differentiate among the OA groups. From joint acoustic signals, the time-dependent feature (Average Signal Duration) in *ms*, energy-dependent feature (Average Absolute Energy) in femtojoule *fJ*, and frequency feature (Average Frequency) in *kHz* are reported in Fig. 6.5(a), Fig. 6.5(b), and Fig. 6.5(c), respectively. Signal duration is a feature that signifies the total time over which the signal is active above the first and last threshold crossings and justifies how long an acoustic event is relevant. Signal duration also refers to the signal counts or pulse emitted, which measures the number of threshold crossings

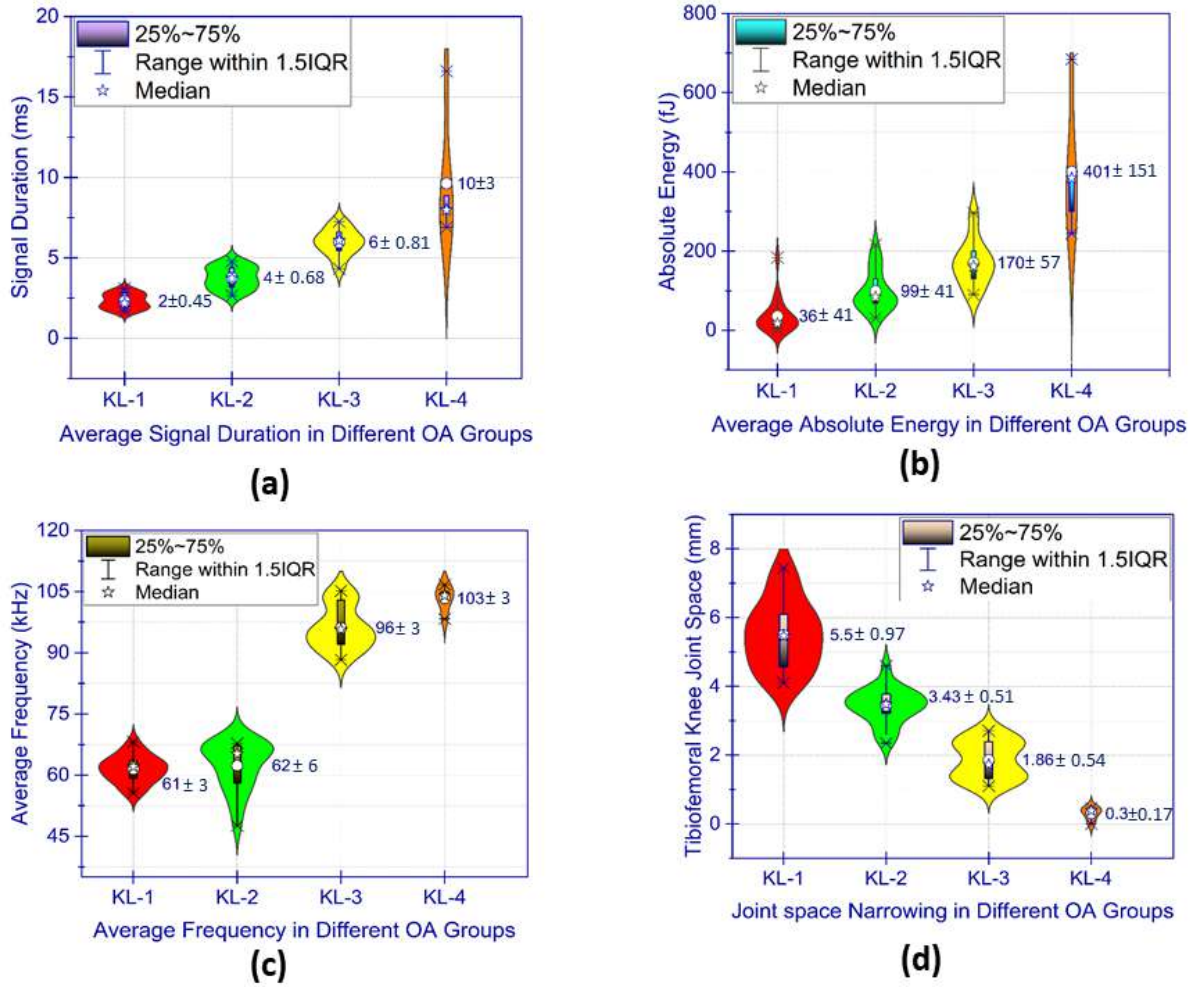

Figure 6.5: Statistical Observations: (a) Average Signal Duration; (b) Average Absolute Energy; (c) Average Frequency; (d) Average JSN in Different OA Groups.

of a waveform.

The signal duration is increased from its lowest value in KL grade 1 to approximately five times higher in KL grade 4, as shown in Fig. 6.5(a). It is observed that the least mean duration, 2±0.45 *ms*, is obtained in KL grade-1 subject groups, which is found to be increased with the progression of KL grades, 4±0.68 in KL-2, 6±0.81 in KL-3, and the highest mean duration, i.e., 10±3 *ms*, is obtained in KL grade 4 subject group. Fig. 6.5(b) shows the absolute energy trends in all OA groups and observed that the minimum of 36±41 *fJ* in KL-1, 99±41 *fJ* in KL-2, 170±57 *fJ* in KL-3, is obtained, and the highest energy signals at 401±151 *fJ* are recorded from the badly damaged knee

health condition in the KL-4 group subjects. Fig. 6.5(c) shows the average frequency that provides an estimate of the characteristic frequency of the complete signal and depends on signal counts and duration. It can be interpreted as the number of counts over a signal duration during an acoustic event. Almost similar mean frequencies, 61±3 *kHz* and 62±6 *kHz*, are obtained in KL-1 and KL-2 subjects groups, while 96±3 *kHz* and 103±3 *kHz* are obtained in KL-3 and KL-4 groups, respectively.

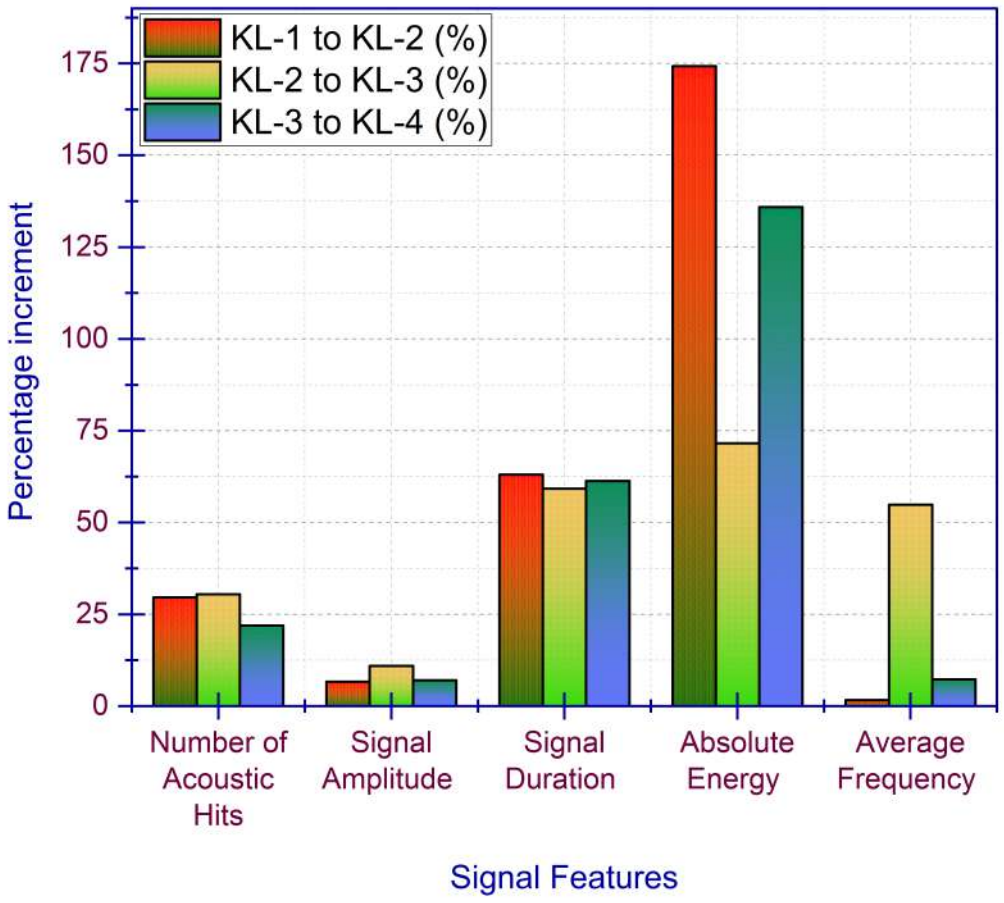

Figure 6.6: Percentage Increment in Signal Features with Increasing KL Grades of Different OA Groups.

The present study showed a significant difference in average frequencies between higher (KL-3, KL-4) and lower (KL-1, KL-2) grade subject groups. However, there is not much difference between KL-1 to KL-2 groups and KL-3 to KL-4 subject groups individually. Since all the signal parameters in different OA groups are validated with the radiographic

findings, the calculated JSN is statically analyzed, as shown in Fig. 6.5(d), where a decreased trend of JSN compared with AE features is obtained. The obtained JSN values are 5.5±0.97 *mm*, 3.43±0.51 *mm*, 1.86±0.54 *mm*, and 0.3±0.17 *mm* in KL-1, KL-2, KL-3 and KL-4 subject groups respectively. Figure 6.6 summarizes the percentage variation among the signal features in all OA groups with their increasing KL grades. It is observed that an approximate uniform percentage variation occurred in the number of hits, signal amplitude, and signal duration with the increasing KL grades, while a non-uniform with sudden rise is obtained in the absolute energy from KL-1 to KL-2 and KL-3 to KL 4. Similarly, the frequency feature of the signal is interrelated during joint articulation and is the outcome of more AE bursts inside the knee joint. When the grade increases from KL 2 to KL 3, it indicates the severe degradation of the knee joint. The average frequency obtained from Fig. 6.6 shows the highest percentage variation between the group KL 2 to KL 3, and it is due to the presence of osteophytes, JSN, sclerosis, and possible bone deformity.

6.3.3 Principal Component Analysis (PCA)

In this section, an unsupervised machine learning approach is used, which is a very prominent method to analyze high-dimensional data by reducing the data dimensionality. The Principal Component Analysis (PCA) is the technique where the data dimensionality is reduced by generating orthogonal principal components that contain the maximum variances in ascending or descending order among the features, and the most dominant feature is identified as an output among all four OA groups and five different signal features. In the context of current PCA analysis for acoustic emission parameters related to knee osteoarthritis, several preliminary steps are crucial for ensuring accurate

and meaningful results. These steps included data standardization, correlation matrix computation, and eigenvalue extraction. The scree plot, which is a critical tool in PCA, helps in determining the optimal number of principal components to retain. Following is the detailed explanation incorporating these preliminary processes:

Data Standardization

Standardization is performed to normalize the data, ensuring that each variable contributes equally to the PCA. This step is vital because it transforms the data to have a mean of zero and a standard deviation of one. The variables in the dataset, including No. of Acoustic Hits, Amplitude (dB), Average Frequency (kHz), Duration (ms), and Absolute Energy (fJ), are standardized to remove units and scale differences. This allowed for a fair comparison of their contributions to the principal components.

Correlation Matrix Computation

The standardized data is used to compute the correlation matrix, which shows the relationships between the variables. This matrix is fundamental in PCA as it helps identify how variables are interrelated. The correlation matrix revealed strong correlations among variables, such as a high correlation between Amplitude (dB) and No. of Acoustic Hits is (0.89), which is expected from the nature of the data.

Eigenvalue Extraction

Eigenvalues represent the amount of variance captured by each PC. These values are critical for understanding the importance of each component. Eigenvalues are computed from the correlation matrix, showing that PC1 had an eigenvalue of 4.26, explaining 85.36% of the variance, while subsequent components have smaller variance.

Scree Plot Analysis

The scree plot is generated using the OriginPro-2021 software, displaying the eigenvalues of the principal components in descending order. This plot helps visualize the variance explained by each component and aids in selecting the number of components to retain. As shown in Fig. 6.7, the scree plot exhibited a sharp drop in eigenvalues from the first to the second principal component. PC1, with the highest eigenvalue (4.26), accounts for the majority of the variance (85.36%). The plot shows an 'elbow' after the second principal component, where the eigenvalue decline levels off. This point indicates that additional components beyond the second contribute minimal additional variance. The eigenvalues for PC3, PC4, and PC5 were significantly lower, explaining only a small fraction of the total variance (PC3: 3.27%, PC4: 1.87%, PC5: 1.23%). This justifies excluding these components from further analysis.

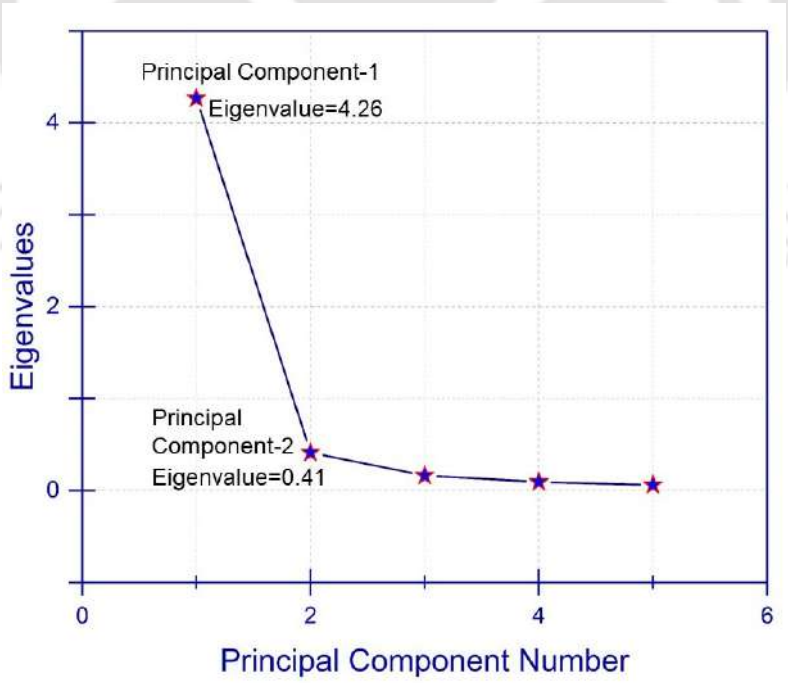

Figure 6.7: Scree plot for Principal Component determination.

Biplot Analysis

Fig. 6.8 shows a biplot and confidence ellipse plot of the PCA outcomes. The feature vectors are shown in Fig. 6.8(a), in which the arrow direction indicates feature variation in the principal component space while its length indicates the variance magnitude of the original data along with that feature. The eigenvectors are associated with the percentage of maximum variances PC1 (85.36%), which are listed in Table 6.1. The higher eigenvector value in either direction (+ve or -ve) associated with PC1 variance shows the most dominating feature in the signal among different OA groups.

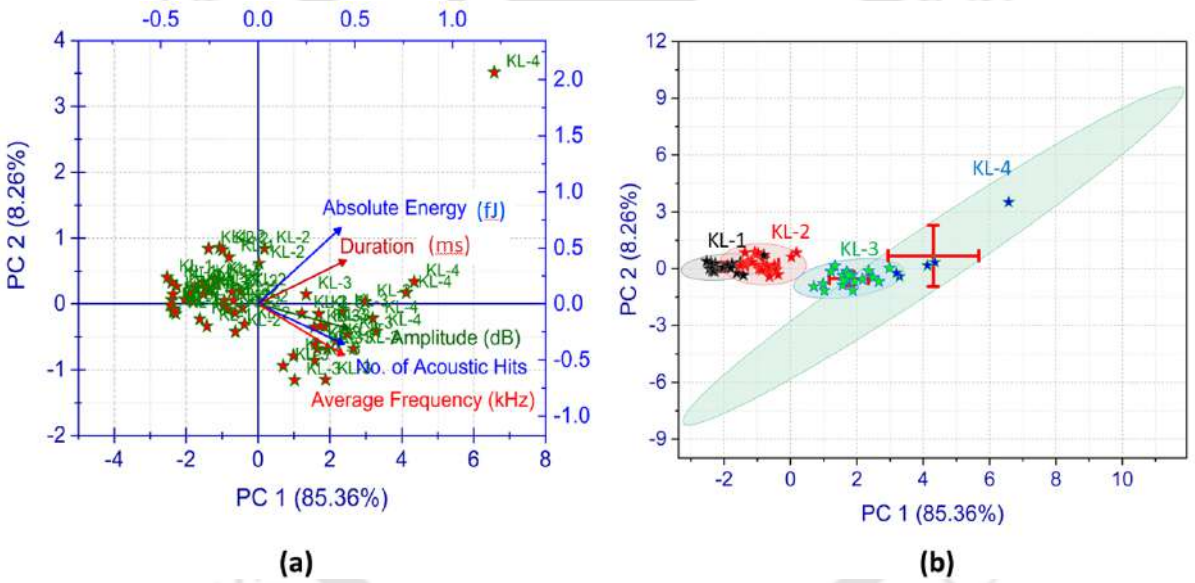

Figure 6.8: (a) Biplot of Acoustic Features in PCA Analysis; (b) Confidence Interval Plot.

Table 6.1: Listing of loading coefficients of eigenvectors in PC 1 (85.36%) for all acoustic features

S.N	Loading coefficient on PC1 (85.36%)	Acoustic Signal Features
1	0.467	Amplitude (dB)
2	0.453	Duration (ms)
3	0.444	No. of Acoustic Hits
4	0.443	Average Frequency (kHz)
5	0.426	Absolute Energy (fJ)

Table 6.1 shows the order of feature dominance with their corresponding eigenvector. It is observed that the signal Amplitude (dB) is the most dominant feature, having the highest loading coefficient of PC1 eigenvector magnitude with maximum variance, which can be selected as a biomarker in early OA detection for participants in different OA groups. Furthermore, Fig. 6.8(b) shows the confidence ellipse for a 95% confidence interval, indicating the group-wise feature association and uncertainty in feature association. The ellipse orientation shows the standard deviation and covariance structure distribution of the feature data in the PCA space. The size of the ellipse is the indication of data concentration in that particular group. Individual KL grade groups are identified with associated feature datasets in their ellipse. It is observed that higher data variability is present among the features of OA grade-4 subject groups, which is apparent because most random vibrations or joint sounds are captured from KL-4 grade subjects.

6.4 Discussion

The current findings described that AE has a potential application scope in the detection of OA in humans. When the knee joint has OA at different grades, the cartilage is degenerated due to friction between the femoral and tibial condyles. A weight-bearing activity imparts the maximum loaded joint articulation, resulting in narrowed joint space, and as an outcome, higher AE hits are generated from the condyle surfaces. In this work, the number of AE hits is distinguished from KL-1 to KL-4 subject groups in three S-T-S cycles in each subject individually, where a significant increasing trend in their mean values is identified to differentiate the OA groups. Furthermore, based on the distribution of the acoustic hits in a single cycle of the weight-bearing activity, obtained results showed the highest number of hits in the AA and DD phases. These phases are

identified as suitable biomarkers in the first and last quadrant duration of a single S-T-S cycle w.r.t. acoustic hits. Previously, AE has also been used to distinguish among the people with healthy and OA knee conditions based on the number of hits for different age groups, and it was revealed that acoustic hits increased with increasing age and OA knee stages (Shark *et al.*) [150], (Sakib *et al.*) [191]. Since the AE hit is a function of signal waveform and in each trial, the number of waveforms obtained is equal to the number of acoustic hits. The AE is measured in decibels (dB), and it is a function of voltage gain in the signal. The dB values of a waveform are obtained by using Equation 6.1 where Vout is the waveform output for a single hit in mV, and Vref is the system reference voltage with a preset value of 1 mV.

$$dB = 20 \cdot \log_{10}\left(\frac{V_{out}}{V_{ref}}\right) \tag{6.1}$$

The outcomes of the absolute energy showed an increment among the OA groups, approximately three times from KL-1 to KL-2, two times from KL-2 to KL-3, and two and half times from KL-3 to KL-4 as shown in Fig. 6.6. This significant increment is helpful in differentiating between the OA groups. Here, the absolute energy is identified as a suitable biomarker for OA grading. Similar to the current findings, a previous study revealed the potential of absolute energy between healthy and OA subjects, and absolute energy was identified as a suitable biomarker for OA knee detection (Sakib *et al.*) [191].

Furthermore, the progression of knee OA started with doubtful JSN and possible osteophytic lipping from the KL-1 grade. It gradually increased with confirmed osteophytes and definite JSN in KL-2, where the AE signal bursts are noticed. The deformed condyle surfaces produced higher frequencies with the progression of multiple osteophytes, sclerosis, and severe JSN verified from the radiographs of the OA subjects. Here, it is notable

that the obtaining of the frequency parameter depends on various factors in AE methodology like data sampling rate, sensor system sensitivity, type of the sensor used, signal filtering and processing, noise and interface, data processing units, and most importantly, sensor placement on the knee joint. Different authors reported the different ranges of frequencies among the healthy and OA knees, and it entirely depends on the effectiveness of the sensor system (Choi *et al.*) [145], (Verma *et al.*) [196]. In this study, KL-1 and KL-2 grades attain almost similar and lower mean frequencies relating to the joint health condition. However, it is found to be increased in KL grade 3. Due to the restricted joint movements in KL-4, the frequencies are also not significantly increased compared to the KL-3 subject group, and the frequency feature is not identified as a suitable biomarker to differentiate among the OA groups. Since the AE features are further validated with JSN from radiographic findings, where the recommended JSN according to the International Knee Documentation Committee (IKDC) form for states of the grade evaluation is to be > 4 *mm* for grade 1, 2-4 *mm* for grade 2, and < 2 *mm* for grade 3 (Kohn *et al.*) [197].

Moreover, the two-dimensional PCA findings are insightful in this work for identifying suitable OA biomarkers from different KL-grade groups. Biplot illustrated the relationship between the signal features and OA groups. Longer feature vector with small angles between the feature vectors shows a positive correlation among the features. Signal amplitude (dB) is identified as the most suitable biomarker in OA detection, with the highest loading coefficient in PCA analysis. However, the cluster and feature variances are observed in Fig. 6.8(b), where the confidence ellipse differentiates among the OA groups according to the KL grades, and the order of feature dominance is identified with a lesser loading coefficient difference in Table 6.1. A previous study reported the results of three components of PCA in their work, similar to the current findings, and they re-

vealed the observation regarding obtained broad-spaced clusters of signal features and suggested a further group cluster formation can be achieved based on knee pathological conditions (Shark *et al.*) [150]. The present study provides a cluster-based group identification among all the features and validates that all features are segregated among the OA groups.

6.5 Summary

In Summary, Sensor-based OA detection in a weight-bearing activity and S-T-S movement protocol involves a unique procedure to evaluate the knee joint integrity. The sensor captures higher frictional energy during the S-T-S activity. Ascending acceleration and descending deceleration modes of S-T-S activities consist of the maximum number of acoustic hits in each KL grade group. They are identified as the significant phases for AE biomarkers in OA detection. The highest dB values are obtained in the KL-4 grade group, which is identified with the most dominating feature subsets. Longer signal durations are also captured with the increasing KL grades. The AE frequency is not recognized as a dominating feature for OA detection among the KL grade groups. A very high increment in the absolute energy in the most degenerated knees in the KL-4 OA grade group subjects is a suitable biomarker. JSN observation from X-rays is a significant differentiation among the OA knee groups and varies among the AE features and OA groups. Further, the PCA results showed that the signal amplitude (dB) is the most dominating feature identified among all the subject groups and signal features. The present study outcomes reveal the importance of knee joint AE and their direct and indirect signal features in selecting biomarkers to differentiate between knee OA grades. Finally, the present research outcomes are heading towards a successful multidimensional AE feature validation in

a quantitative assessment among different OA grade subjects from the North-Eastern region of India, and signal parameters are identified as a feasible AE biomarker.

Chapter 7

In-house Development of Knee Health Monitoring Device Using Acoustic Technology

7.1 Introduction

The aim of this work is to conduct the human knee joint health assessment by using acoustic emissions (AE) technology. As discussed in Chapter 1, osteoarthritis is a prevalent disease in people nowadays. Knee health assessment is related to the proper functioning of bones like the femur, tibia, fibula, and patella, along with all soft tissues like ligaments, meniscus, and cartilage. In Chapter 4, a contact microphone-based wearable system for knee OA detection is developed, but in that work, different limitations are observed like the frequency sensing range of the sensor, data sampling and processing limitations in the Arduino Nano board, and the sensitivity of the sensor in OA detection. Further, as discussed in Chapter 5, and Chapter 6, a commercial nano piezoelectric sensor system is used to identify the different signal features from healthy and OA subjects from different age groups. That commercial sensor system is a costly setup, and is not affordable every time. So, the present study is focused on developing a cost-effective, small, and portable wearable system for OA detection. In the present work, a high-speed data processing board, Raspberry Pi 4 is used as an alternative to the Arduino Nano which has an excellent sampling rate that offers several benefits. The very first advantage of the Raspberry

Pi 4 is that it has a significant boosting power in data processing, and having the feature of a quad-core ARM Cortex-A72 CPU with different RAM options with 2 *GB*, 4 *GB*, and 8 *GB*. In this device, an 8 *GB* RAM is used for data processing which enhances the system's performance. It has dual HDMI outputs and USB 3.0 ports for external storage access, faster data transfer, and improved connectivity. It also supports a Gigabit Ethernet port which provides faster network connectivity and is advantageous for high-speed data transfer for a local network. The Raspberry Pi 4 model supports 2.4 *GHz* and 5 *GHz* Wi-Fi bands, as well as Bluetooth 5.0. for IoT (Internet on Things) based applications. Apart from this, the device includes an HDMI 7-inch LCD, keyboard, mouse, and other peripherals for interfacing audio sensors. The fabricated system is well-suitable for early diagnosis of the OA which is always helpful in preventing a severe health condition by taking preventive actions after recording and analyzing the vibroarthrographic signals originating from the knee joint. The general application of this wearable device is that it can be used by any person in their daily life from any age group to detect osteoarthritis.

7.2 Working Principle

Figure 7.1 shows a flow chart of the working principle of the wearable device. The device proposed in this research is capable of working with two types of audio modules. First is a general audio microphone which can be directly interfaced with the Raspberry Pi 4 using a USB port. The second is the audio vibration module which needs an external circuit to convert and amplify the signal. Since Raspberry Pi can be interfaced with any peripheral device, it also includes external circuitry. For this work, a circuit board is designed, which connects with the Raspberry Pi for audio sensor application. This circuit board includes an audio amplifier and an analog-to-digital converter. Furthermore, the

vibration sensor senses vibration and converts it into an analog electrical signal. Then the signal is fed to an amplifier which amplifies the signal according to the requirement. The signal coming out of the vibration sensor is in the range of millivolts which is too low and TL072 IC is a perfect low-cost amplifier that can amplify the signal to the range of volts.

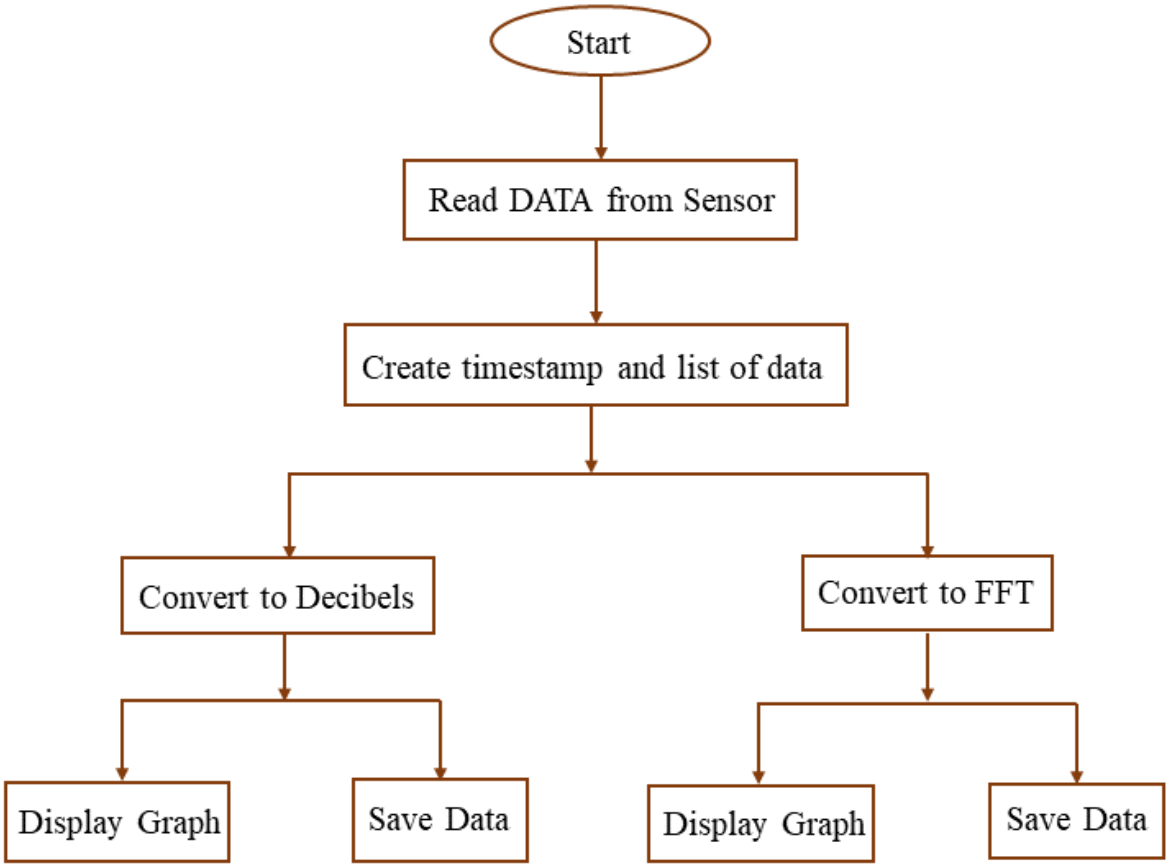

Figure 7.1: Flow chart of the working principle of the Wearable Device.

The resulting analog signal is then fed into an analog-to-digital converter (ADC) MCP3008 to convert to a digital form so the Raspberry Pi can read it. This ADC can be directly interfaced with any Raspberry Pi. For displaying and analysis of sound signals, codes are written in Python programming language. The display of the device is a GUI (Graphical user interface) designed to be as simple as possible with buttons for different pages. Each page can display different graphs for multiple audio signals. The

first page simply displays the continuous raw sound data in the graph of Decibels (dB) *vs* Time (ms). The second page displays a graph that represents frequency domain analysis that is formed by the FFT (Fast Fourier Transform) method. The FFT graph shows the peak frequency along with the dominant frequencies of the data.

7.3 Listing of the Features and Elements of the Developed Device

As shown in Fig. 7.2, the device includes a lavalier II microphone, TL072 operational amplifier, MCP3008 analog to digital converter, Raspberry Pi 4 with 8 GB RAM, HDMI 7-inch LCD, printed circuit board (PCB), keyboard, mouse, and other peripherals for interfacing audio sensors. Following are the detailed description of the individual components:

7.3.1 Lavalier II Microphone:

The Lavalier II is a premium lavalier microphone that is suitable for audio and video applications. It has a unique low-profile design with a flat capsule which includes a amounting clip. The omnidirectional polar pattern of this microphone picks up crystal-clear, detailed audio from all directions. It has a 3.5 mm TRS locking connector which can be integrated other peripheral components.

7.3.2 TL072 Operational Amplifier:

The TL072 is a low-noise JFET-input operational amplifier (op-amp) that is designed for use in a wide range of analog applications. It is a dual op-amp that contains two

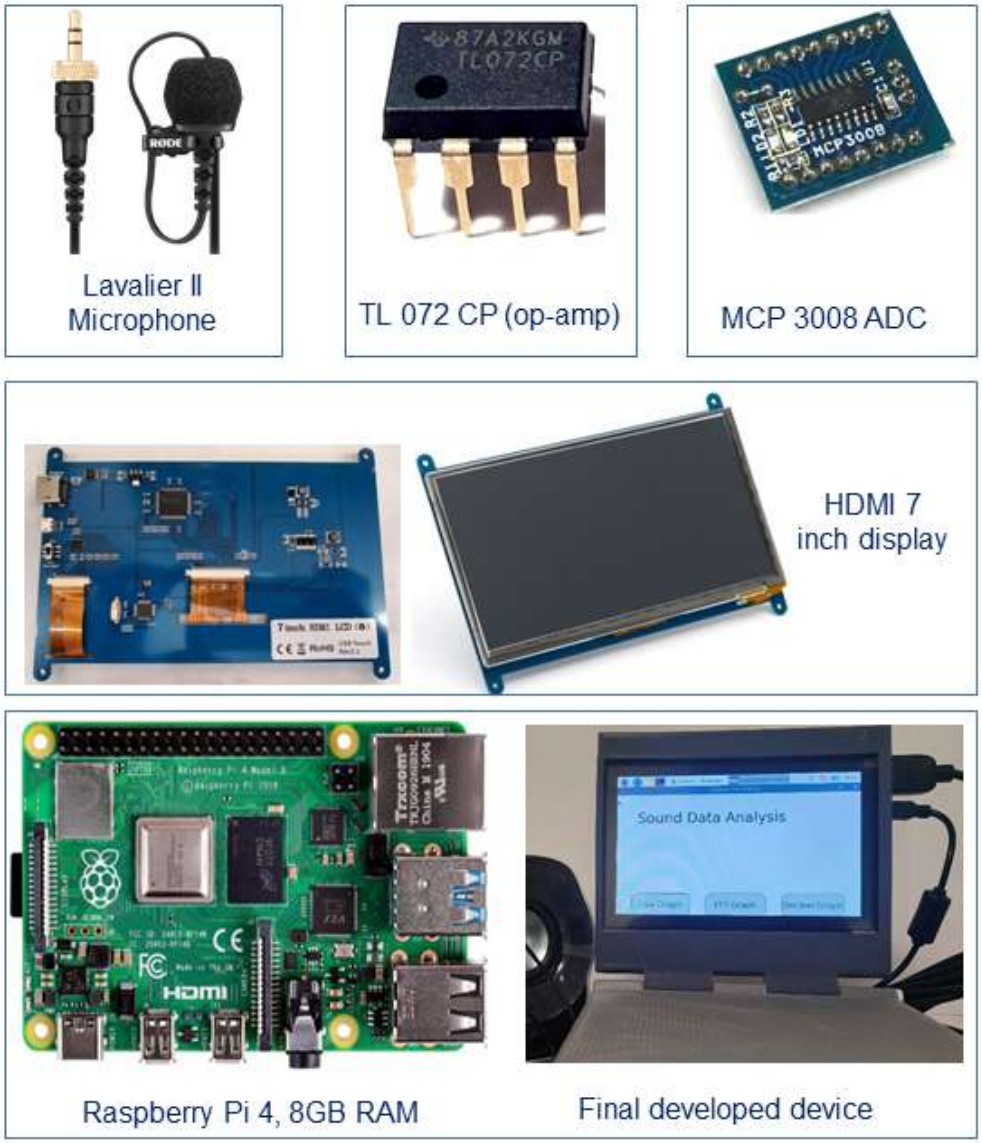

Figure 7.2: Major Components Used in the Wearable Device Fabrication.

separate amplifiers in a single package. The TL072 is known for its low noise, high gain bandwidth product, and low distortion, which makes it well-suited for audio applications such as preamplifiers, mixers, and equalizers.

7.3.3 Analog-to-Digital Converter (MCP3008):

MCP3008 is an 8-channel 10-bit analog-to-digital converter (ADC) IC (Integrated Circuit) manufactured by Microchip Technology. It is widely used in electronic applications

where analog signals need to be converted into digital signals for further processing and analysis. MCP3008 is a versatile and reliable ADC used in many DIY electronics applications, including data logging, temperature sensing, and audio signal processing. It provides a cost-effective and easy-to-use solution for converting analog signals into digital signals for further processing and analysis.

7.3.4 Raspberry Pi 4:

The Raspberry Pi 4 is the fourth generation of the Raspberry Pi single-board computer. It was released in June 2019 and is designed to be a versatile and affordable computer used for various applications. Raspberry Pi 4 can be powered by a 5 V micro-USB power supply, and it has a power consumption of up to 7.5 W, depending on the model and usage. It is a powerful and versatile computer used for many applications, including robotics, home automation, media centers, game consoles, and many more.

7.3.5 HDMI 7-inch LCD

An HDMI 7-inch LCD is a small display screen that can be connected to a device with an HDMI output, such as a computer, media player, or game console. It typically has a resolution of 800x480 pixels and a 16:9 aspect ratio and is perfect for watching videos and playing games. The display is usually compact and lightweight, which makes it easy to carry and set up. An HDMI 7-inch LCD is a valuable and versatile display solution for various applications.

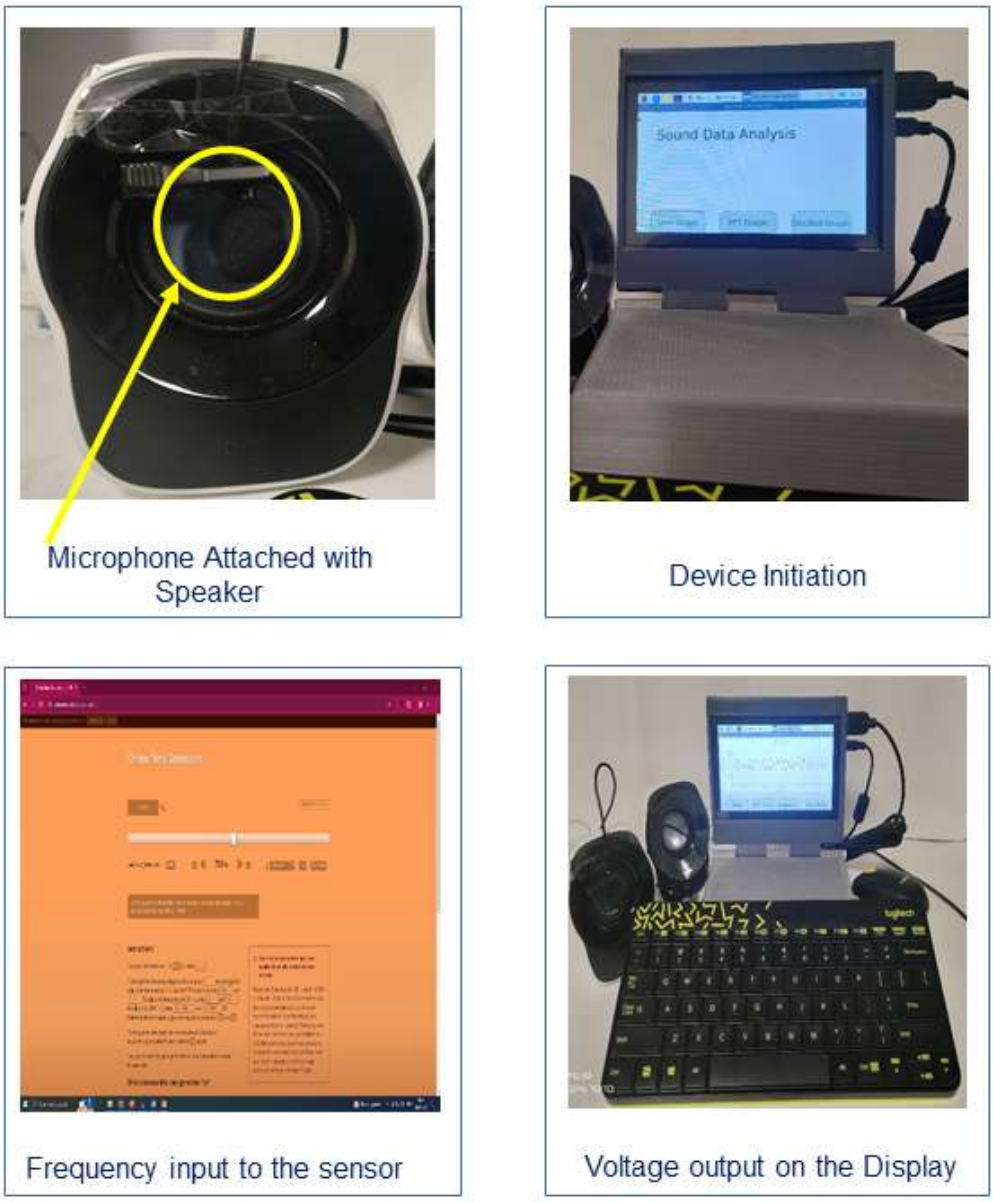

Figure 7.3: Device Test Procedure.

7.4 Device Calibration and Perfomance Testing

As shown in Fig 7.3, the fabricated device is successfully calibrated, and tested for different sound frequency ranges. For this procedure, an online tone generator is used using a laptop and a speaker to which the acoustic microphone is attached. The microphone surface is kept in front of the diaphragm of the speaker and tested on different generated sinusoidal sound waves of different frequencies. The aim of this experiment is to

validate the input frequency from the tone generator with the output of the contact microphone and the results are verified on the screen of the fabricated device. The arbitrarily generated sound waves at different frequencies are verified repeatedly with different magnitudes. In the next phase of device performance analysis, healthy and osteoarthritic human subject trials are proposed.

7.5 Proposed Major Advantages of the Developed Device

- The current development is a compact and portable wearable device that can be used anywhere, like at work or at home.
- It is a low-cost device, and no skilled operator is required to apply the sensor on the knee joint.
- It provides a purely non-invasive OA detection method and is free from harmful radiation.
- Real-time disease detection using the sensor methodology is adopted in the invention, which is helpful for the early detection of OA.

Chapter 8

Research Summary

For the first time, this study is conducted in the North Esatern region of India. In this research work, the acoustic emission methodology is found to be significantly advanced for understanding the non-invasive diagnostic procedure for knee osteoarthritis. The use of acoustic sensors to capture and analyze the sounds emitted by the knee joints has shown great promise in providing valuable insight into the early stages of degenerative joint disorder. The outcomes of information derived from the sensors in terms of the signal features including distinctive acoustic patterns associated with cartilage degradation and biomechanical alterations opens a new scope of visualization of osteoarthritis detection and its preventive care. The potential of acoustic methodology is not only limited to diagnostic applications but also it can be used for the monitoring of the disease progression. Despite these advancements, challenges such as ambient noise interference, sensor calibration, and standardization of data acquisition protocols also need to be addressed in a detailed manner to ensure the reliability and reproducibility of results. Looking ahead, the future of knee joint vibroarthrography research holds exciting possibilities like, multimodal sensor technologies, combined with advances in artificial intelligence and data analytics, may further enhance the diagnostic accuracy and clinical utility of knee joint vibroarthrography. The exploration of the acoustic signatures associated with different stages of knee osteoarthritis and its validation from radiological findings represent a promising avenue for future investigations. In summary, the research on knee

joint vibroarthrography has demonstrated its potential as a non-invasive, sensitive, and dynamic tool for knee osteoarthritis detection and monitoring. As the field progresses, it is anticipated that knee joint vibroarthrography will play a pivotal role in revolutionizing the diagnostic landscape of knee osteoarthritis, and will offer the valuable information to the clinicians for early intervention and personalized patient care.

8.1 Synoptic Conclusions From The Present Work

This section summarizes the chapter-wise outcomes of this research work and future research directions. The major conclusions are encapsulated below:

1. **Development of an IMU-Based Digital Goniometer for Knee Joint Analysis:**
    - The fabrication and calibration of the digital goniometer using IMU sensors and electronic components have been successfully completed.
    - The validation process demonstrated that the digital goniometer accurately measures knee joint angles during various movements.
    - Comparison with established methods like video motion analysis has shown promising results, indicating the reliability of the digital goniometer for knee joint kinematics analysis.

2. **Development of a Wearable Device for Knee Joint Sound Detection Using Contact Microphone:**
    - The wearable device incorporating a contact microphone and Arduino Nano has been successfully fabricated.

- Preliminary testing confirmed the functionality and comfort of the device during use.
- Signal feature analysis showed a promising outcome among healthy and osteoarthritic subjects, and they are successfully categorized based on sound decibels.

3. **Comparing Knee Joint Angle-Based Acoustic Emissions in Healthy and OA Subjects in a Quantitative Evaluation:**

   - Knee joint angle-based acoustic emissions are successfully detected from 121 subjects after their recruitment and consent, demonstrated the feasibility of the methodology in capturing acoustic signals associated with knee joint movements.
   - Analysis of the bilateral plots revealed distinct patterns of acoustic emissions between healthy and osteoarthritis subject groups. These groups are identified as significantly different based on the number of acoustic hits captured by the sensors in S-T-S activity.
   - Analysis of time-dependent and energy-dependent signal parameters revealed significant differences between healthy and osteoarthritis (OA) subject groups. Specifically, OA subjects exhibited higher levels of these parameters. This indicates a potential association with compromised knee health conditions in individuals with OA.
   - Cumulative density function plots further underscored the differences between healthy and OA subject groups, revealing a non-uniform trend in the data distribution for the OA group. This observation signifies distinct acoustic

emission patterns associated with different knee health conditions.

4. **Identifying Biomarkers for OA Detection in Different KL Grades:**

   - The study has expanded to include OA individuals with confirmed KL grades obtained from X-rays, allowing for a comprehensive analysis of knee joint health across different degenerative stages.
   - In OA subjects, specific phases of S-T-S activities, such as ascending acceleration and descending deceleration, exhibit the highest number of acoustic hits, indicating their potential as significant phases for identifying AE biomarkers.
   - Signal durations increase with higher KL grades, suggesting a correlation between disorder severity and signal characteristics.
   - Remarkably elevated absolute energy levels are observed in knees with advanced OA (KL grade 4), indicating significant joint degeneration.
   - Image processing analysis revealed a progressive decrease in joint space narrowing with increasing KL grades, particularly pronounced in KL grade 4 subjects, signifying severe knee degeneration.
   - Acoustic emission frequency is not a predominant feature for OA detection across different KL grade groups, highlighting the importance of other signal features.
   - Principal Component Analysis identified signal amplitude (dB) as the most suitable biomarker for distinguishing OA subjects among all KL grades, underscoring its significance in OA detection and classification.

8.2 Futute Scope of Work

The future studies based on this work can be in following aspects:

- Since the AE system used in this research is an expensive sensor and data acquisition configuration, further research can be focused on developing different low-cost acoustic sensors and small-scale data acquisition systems in the form of knee health assessment wearable devices for taken-home healthcare systems.
- This research work is carried out on the population from the North-Eastern region in India. However, other states and places with different demographic and anthropometric conditions can also be explored.
- Patellofemoral sites can be examined to distinguish between OA groups in different activities.
- Other body joints and secondary OA can also be examined using AE sensors.
- Current sensor-based AE methodology can be used for the monitoring of the subjects under different rehabilitation conditions.
- Wireless and mobile application-based wearable devices can also be developed for OA detection.

Appendix A

Appendix

A.1 The Details of the Total 121 Subjects, Participated in this Study and Categorized into Healthy and Osteoarthritic Subject Groups based on their Age and Knee Health Conditions.

Table A.1: Anthropometric and other parameters of 40 subjects (H1 Group).

Subjects	Age	Sex (M/F)	BMI	Pain (20)	Stiffness (8)	Physical Function (68)	WOMAC score (96)	AE Hits (RL)	AE Hits (LL)	Average Amplitude (dB)
S 1	28	M	23.88	0	0	0	0	18	19	78
S 2	29	M	19.58	0	0	0	0	22	16	77
S 3	25	M	21.11	0	0	0	0	25	16	79
S 4	37	M	30.10	0	0	0	0	20	28	81
S 5	26	M	23.90	0	0	0	0	21	27	79
S 6	33	M	28.66	1	1	5	7	26	14	82
S 7	20	F	22.98	0	0	0	0	22	25	78
S 8	28	M	19.91	0	0	0	0	16	18	80
S 9	20	M	20.23	0	0	0	0	13	20	79
S 10	28	M	17.74	0	0	0	0	20	27	79

Table A.1: Continued on next page

Table A.1: continued from previous page

Subjects	Age	Sex (M/F)	BMI	Pain (20)	Stiffness (8)	Physical Function (68)	WOMAC score (96)	AE Hits (RL)	AE Hits (LL)	Average Amplitude (dB)
S 11	20	M	18.54	0	0	0	0	25	16	76
S 12	30	M	26.13	1	0	3	4	25	17	80
S 13	28	F	18.97	0	0	0	0	20	17	80
S 14	20	F	25.42	0	0	0	0	22	20	80
S 15	24	M	37.42	5	0	8	13	16	15	81
S 16	35	F	31.62	0	0	0	0	28	11	81
S 17	29	M	39.95	1	0	2	3	34	17	81
S 18	38	F	36.75	5	0	16	21	20	14	82
S 19	26	F	31.57	2	1	6	9	23	18	81
S 20	35	F	18.16	0	0	0	0	15	17	79
S 21	29	F	19.23	1	0	6	7	25	15	79
S 22	22	F	20.48	4	2	12	18	15	19	78
S 23	29	M	25.63	3	2	10	15	26	22	77
S 24	32	F	21.47	6	0	19	25	18	12	77
S 25	30	M	22.17	3	0	6	9	12	12	80
S 26	33	M	22.60	10	6	6	22	14	13	79
S 27	28	M	25.53	2	0	12	14	23	14	80
S 28	35	F	33.52	3	1	5	9	21	16	78

Table A.1: Continued on next page

Table A.1: continued from previous page

Subjects	Age	Sex (M/F)	BMI	Pain (20)	Stiffness (8)	Physical Function (68)	WOMAC score (96)	AE Hits (RL)	AE Hits (LL)	Average Amplitude (dB)
S 29	26	M	27.98	2	0	6	8	21	9	77
S 30	28	F	20.39	3	3	5	11	19	13	79
S 31	28	F	27.65	10	7	39	56	19	10	77
S 32	21	M	24.33	0	0	0	0	21	13	78
S 33	26	M	24.31	0	0	0	0	11	12	78
S 34	37	M	23.32	0	0	0	0	22	17	78
S 35	30	M	18.84	0	0	0	0	19	15	78
S 36	24	M	21.31	4	3	12	19	14	10	80
S 37	27	F	20.26	0	0	0	0	20	10	79
S 38	24	M	27.83	0	0	0	0	16	13	81
S 39	30	M	22.71	0	0	0	0	18	10	80
S 40	35	M	24.94	0	0	0	0	19	11	78

Table A.1: It ends from the previous page.

Table A.2: Anthropometric and other parameters of 40 subjects (H2 Group).

Subjects	Age	Sex (M/F)	BMI	Pain (20)	Stiffness (8)	Physical Function (68)	WOMAC score (96)	AE Hits (RL)	AE Hits (LL)	Average Amplitude (dB)
S 41	52	F	27.41	5	0	6	11	29	35	81
S 42	53	M	26.12	2	0	12	14	35	27	86
S 43	42	M	30.16	3	1	11	15	40	47	88
S 44	45	M	28.88	1	0	4	5	39	30	88
S 45	52	F	25.98	11	4	28	43	46	29	85
S 46	52	F	18.36	3	2	18	23	26	23	84
S 47	57	F	24.88	5	2	21	28	45	40	88
S 48	53	F	22.48	6	3	26	35	42	43	85
S 49	56	F	17.31	3	3	21	27	43	37	88
S 50	50	F	21.93	5	2	24	31	40	29	89
S 51	48	F	27.69	4	4	6	14	44	21	92
S 52	47	M	22.60	3	2	13	18	40	34	87
S 53	42	M	25.15	7	2	18	27	42	37	89
S 54	40	F	22.22	7	0	20	27	52	40	92
S 55	42	M	30.98	5	0	16	21	59	41	94
S 56	54	F	22.37	8	4	23	35	31	37	94
S 57	44	M	38.19	3	0	9	12	37	41	94

Table A.2: Continued on next page

Table A.2: continued from previous page

Subjects	Age	Sex (M/F)	BMI	Pain (20)	Stiffness (8)	Physical Function (68)	WOMAC score (96)	AE Hits (RL)	AE Hits (LL)	Average Amplitude (dB)
S 58	51	M	34.68	1	0	4	5	32	47	93
S 59	40	F	38.63	3	0	8	11	43	25	93
S 60	53	M	30.13	5	1	14	20	40	20	93
S 61	53	F	24.45	6	0	28	34	42	33	95
S 62	52	F	33.48	3	2	24	29	27	36	93
S 63	50	F	24.80	7	4	16	27	38	35	85
S 64	40	F	29.14	8	2	28	38	41	31	92
S 65	48	F	33.29	7	2	23	32	44	52	86
S 66	48	F	30.06	3	0	9	12	40	36	90
S 67	44	F	31.15	3	0	12	15	50	33	92
S 68	54	F	20.27	6	2	22	30	29	34	87
S 69	42	M	23.67	5	0	21	26	45	39	92
S 70	53	M	29.30	1	1	4	6	30	26	92
S 71	47	F	24.69	7	1	32	40	31	28	91
S 72	58	M	25.83	1	0	0	1	29	40	88
S 73	48	M	24.57	3	2	9	14	32	58	91
S 74	47	F	22.51	2	0	0	2	44	35	93
S 75	52	F	28.84	7	0	21	28	33	20	92

Table A.2: Continued on next page

Table A.2: continued from previous page

Subjects	Age	Sex (M/F)	BMI	Pain (20)	Stiffness (8)	Physical Function (68)	WOMAC score (96)	AE Hits (RL)	AE Hits (LL)	Average Amplitude (dB)
S 76	48	F	26.01	7	4	31	42	24	22	93
S 77	48	F	24.03	5	2	19	26	24	19	90
S 78	44	F	21.10	6	2	20	28	35	38	86
S 79	48	F	23.15	1	0	5	6	37	26	91
S 80	57	M	31.64	8	6	31	45	28	28	93

Table A.2: It ends from the previous page.

Table A.3: Anthropometric and other parameters of 25 subjects (H3 Group).

Subjects	Age	Sex (M/F)	BMI	Pain (20)	Stiffness (8)	Physical Function (68)	WOMAC score (96)	AE Hits (RL)	AE Hits (LL)	Average Amplitude (dB)
S 81	64	M	24.22	9	4	30	43	64	71	97
S 82	75	F	26.71	11	4	28	43	65	66	99
S 83	61	F	17.98	7	3	27	37	69	86	100
S 84	66	F	22.64	10	3	23	36	79	78	100
S 85	66	F	20.00	5	2	20	27	66	75	99
S 86	83	M	25.14	9	4	26	39	68	76	99
S 87	70	F	18.37	5	2	19	26	75	69	99
S 88	65	F	18.97	12	4	32	48	52	67	99
S 89	67	F	25.22	12	5	21	38	61	73	99
S 90	65	F	18.73	6	2	22	30	59	70	95
S 91	61	M	15.62	4	2	14	20	40	56	97
S 92	69	M	18.67	5	2	12	19	63	47	89
S 93	70	F	25.79	8	4	18	30	52	53	98
S 94	63	F	23.73	5	2	15	22	52	48	99
S 95	67	F	23.56	5	3	15	23	54	53	105
S 96	69	M	33.78	7	0	29	36	53	48	100
S 97	60	M	31.61	10	0	28	38	40	46	98

Table A.3: Continued on next page

The Details of the Total 121 Subjects, Participated in this Study and Categorized into Healthy and Osteoarthritic Subject Groups based on their Age and Knee Health Conditions.

Table A.3: continued from previous page

Subjects	Age	Sex (M/F)	BMI	Pain (20)	Stiffness (8)	Physical Function (68)	WOMAC score (96)	AE Hits (RL)	AE Hits (LL)	Average Amplitude (dB)
S 98	73	F	31.57	5	0	26	31	37	43	99
S 99	62	F	30.38	5	2	35	42	59	83	103
S 100	79	F	26.63	9	6	51	66	37	54	101
S 101	61	F	31.52	12	4	42	58	24	54	99
S 102	62	M	27.39	10	0	30	40	54	68	98
S 103	84	F	23.19	12	5	38	55	32	64	101
S 104	68	M	22.84	7	2	21	30	53	57	100
S 105	63	M	24.19	1	1	6	8	30	40	105

Table A.3: It ends from the previous page.

Table A.4: Anthropometric and other parameters of 16 subjects (OA Group).

Subjects	Age	Sex (M/F)	BMI	Pain (20)	Stiffness (8)	Physical Function (68)	WOMAC score (96)	AE Hits (RL)	AE Hits (LL)	Average Amplitude (dB)
S 106	43	M	26.45	4	1	17	22	94	102	110
S 107	61	F	39.06	15	7	39	61	142	140	118
S 108	43	M	38.44	2	3	12	17	123	113	110
S 109	66	F	37.09	7	4	30	41	97	138	110
S 110	49	M	29.12	7	2	21	30	103	114	106
S 111	63	M	28.66	7	4	32	43	117	107	108
S 112	37	F	28.76	10	6	39	55	116	111	103
S 113	55	F	28.08	10	0	24	34	115	117	105
S 114	37	M	25.82	4	0	27	31	78	88	106
S 115	50	M	22.65	15	5	42	62	72	86	105
S 116	60	M	27.01	6	2	22	30	99	118	114
S 117	49	F	26.67	5	2	26	33	99	116	108
S 118	52	F	44.63	4	0	25	29	119	113	129
S 119	46	F	44.19	11	6	30	47	94	87	123
S 120	42	F	42.35	5	1	21	27	91	83	129
S 121	48	F	38.69	9	5	33	47	91	98	126

Table A.4: It ends from the previous page.

A.2 The Details of the Total 63 Osteoarthritic Subjects with Different KL Grades, Participated in this Study and have Confirm Radiographic Evidences.

Table A.5: Anthropometric and other parameters of 19 subjects (OA-KL grade-1).

Subjects	Age	Sex (M/F)	BMI	Pain (20)	Stiffness (8)	Physical Function (68)	WOMAC score (96)	JSN (mm)	Signal Amplitude (dB)	No. of Hits
S1	50	M	22.65	15	5	42	62	6.09	61.50	79
S2	38	F	30.95	8	5	30	43	5.1	62.15	52
S3	50	F	31.00	5	0	24	29	7.44	60.47	67
S4	47	M	22.64	7	0	17	24	6.96	59.27	69
S5	37	F	24.88	3	3	7	13	5.09	65.08	90
S6	55	F	19.82	14	4	41	59	6.03	62.65	96
S7	50	M	25.92	2	0	3	5	6.02	58.48	72
S8	45	F	22.98	9	4	27	40	7.05	60.39	96
S9	54	F	37.76	6	0	35	41	5.55	57.34	96
S10	55	M	31.01	2	0	13	15	4.57	60.81	98
S11	49	M	42.16	6	2	19	27	5	56.63	76
S12	46	F	28.39	4	0	11	15	5.11	59.92	75
S13	60	M	22.21	4	4	28	36	4.15	58.50	77
S14	47	F	29.71	8	4	45	57	4.1	60.61	75
S15	70	F	34.00	10	4	25	39	6.17	56.83	81

Table A.5: Continued on next page

Table A.5: continued from previous page

Subjects	Age	Sex (M/F)	BMI	Pain (20)	Stiffness (8)	Physical Function (68)	WOMAC score (96)	JSN (mm)	Signal Amplitude (dB)	No. of Hits
S16	38	M	22.67	4	1	10	15	4.45	61.45	86
S17	57	M	28.34	6	2	19	27	5.47	56.07	81
S18	56	F	26.91	3	3	24	30	4.26	60.24	97
S19	55	M	27.99	3	2	11	16	5.88	56.70	74

Table A.5: It ends from the previous page.

Table A.6: Anthropometric and other parameters of 20 subjects (OA-KL grade-2).

Subjects	Age	Sex (M/F)	BMI	Pain (20)	Stiffness (8)	Physical Function (68)	WOMAC score (96)	JSN (mm)	Signal Amplitude (dB)	No. of Hits
S20	43	M	38.41	2	3	12	17	3.36	67.48	102
S21	37	F	28.76	10	6	39	55	2.35	60.84	119
S22	58	F	27.49	4	3	21	28	3.96	61.71	101
S23	54	F	23.92	9	2	27	38	4.6	62.78	109
S24	54	F	26.39	11	2	26	39	3.81	64.75	110
S25	60	M	36.98	9	6	48	63	2.61	61.07	109
S26	45	F	27.24	8	4	31	43	3.33	64.98	104
S27	52	F	31.83	1	1	9	11	3.37	67.47	103
S28	56	F	36.98	8	2	28	38	3.15	63.58	100
S29	49	F	27.43	3	0	16	19	3.47	64.29	116
S30	45	F	39.24	4	0	24	28	3.59	62.57	105
S31	39	F	35.00	3	0	5	8	3.49	65.08	112
S32	66	M	30.82	9	6	37	52	3.28	62.07	94
S33	47	M	25.16	3	3	26	32	3.77	62.03	97
S34	39	M	26.21	3	4	22	29	3.78	62.56	93
S35	53	M	21.39	4	3	16	23	2.95	65.04	124
S36	54	M	24.33	4	2	16	22	3.52	64.06	98

Table A.6: Continued on next page

Table A.6: continued from previous page

Subjects	Age	Sex (M/F)	BMI	Pain (20)	Stiffness (8)	Physical Function (68)	WOMAC score (96)	JSN (mm)	Signal Amplitude (dB)	No. of Hits
S37	55	M	27.99	3	2	11	16	3.73	62.19	92
S38	80	M	23.74	5	3	14	22	3.92	63.83	121
S39	70	M	27.64	7	5	23	35	2.65	62.45	97

Table A.6: It ends from the previous page.

Table A.7: Anthropometric and other parameters of 19 subjects (OA-KL grade-3).

Subjects	Age	Sex (M/F)	BMI	Pain (20)	Stiffness (8)	Physical Function (68)	WOMAC score (96)	JSN (mm)	Signal Amplitude (dB)	No. of Hits
S40	59	F	24.24	12	4	32	48	1.49	73.23	131
S41	66	F	37.09	5	4	37	46	1.73	74.26	137
S42	63	M	28.66	9	5	37	51	2.71	71.39	161
S43	55	F	28.08	13	4	34	51	1.14	72.13	121
S44	61	F	25.97	9	5	27	41	1.25	68.82	120
S45	68	F	28.23	12	4	31	47	1.32	71.12	125
S46	72	M	24.60	7	3	23	33	1.44	74.33	150
S47	60	F	26.08	8	2	31	41	1.69	68.97	142
S48	69	M	26.40	12	6	50	68	2.45	71.31	148
S49	65	M	20.81	10	6	40	56	2.24	72.28	139
S50	38	F	39.03	8	2	24	34	2.47	69.79	129
S51	65	M	30.08	14	3	49	66	2.14	71.87	141
S52	50	F	26.90	8	4	41	53	1.1	68.93	140
S53	40	F	26.30	10	5	38	53	1.25	69.65	117
S54	42	M	26.53	7	5	47	59	2.39	72.54	135
S55	80	M	23.74	5	3	14	22	2.13	69.74	147
S56	70	M	27.64	7	5	23	35	2.65	73.42	148

Table A.7: Continued on next page

Table A.7: continued from previous page

Subjects	Age	Sex (M/F)	BMI	Pain (20)	Stiffness (8)	Physical Function (68)	WOMAC score (96)	JSN (mm)	Signal Amplitude (dB)	No. of Hits
S57	55	F	24.56	11	5	45	61	2.32	69.46	123
S58	59	F	30.26	10	6	48	64	1.51	69.95	145

Table A.7: It ends from the previous page.

Table A.8: Anthropometric and other parameters of 05 subjects (OA-KL grade-4).

Subjects	Age	Sex (M/F)	BMI	Pain (20)	Stiffness (8)	Physical Function (68)	WOMAC score (96)	JSN (mm)	Signal Amplitude (dB)	No. of Hits
S59	65	M	30.08	14	3	49	66	0	75.69	170
S60	59	F	30.26	10	6	48	64	0.43	77.40	174
S61	78	M	25.22	13	7	49	69	0.46	76.98	152
S62	65	M	28.55	16	5	45	66	0.39	74.18	159
S63	70	M	27.29	12	7	47	66	0.22	76.20	180

Table A.8: It ends from the previous page.

WOLTERS KLUWER HEALTH, INC. LICENSE
TERMS AND CONDITIONS

Feb 29, 2024

This Agreement between IIT Guwahati -- Dhirendra Verma ("You") and Wolters Kluwer Health, Inc. ("Wolters Kluwer Health, Inc.") consists of your license details and the terms and conditions provided by Wolters Kluwer Health, Inc. and Copyright Clearance Center.

License Number	5738150635750
License date	Feb 29, 2024
Licensed Content Publisher	Wolters Kluwer Health, Inc.
Licensed Content Publication	Current Sports Medicine Reports
Licensed Content Title	Current Progress in Meniscal Repair and Postoperative Rehabilitation
Licensed Content Author	Scott Pyne
Licensed Content Date	Oct 1, 2002
Licensed Content Volume	1
Licensed Content Issue	5
Type of Use	Dissertation/Thesis
Requestor type	University/College
Sponsorship	No Sponsorship
Format	Print and electronic
Will this be posted online?	Yes, on a secure website
Portion	Figures/tables/illustrations
Number of figures/tables/illustrations	2
Author of this Wolters Kluwer	No

article	
Will you be translating?	No
Intend to modify/change the content	No
Title of new work	DEVELOPMENT OF WEARABLE SYSTEMS FOR THE DETECTION AND CLASSIFICATION OF KNEE OSTEOARTHRITIS AND ITS VALIDATION THROUGH RADIOGRAPHIC IMAGES
Institution name	IIT GUWAHATI
Expected presentation date	May 2024
Portions	Figure 1, Figure 2
Requestor Location	IIT Guwahati Amingaon Guwahati, 781039 India Attn: IIT Guwahati
Publisher Tax ID	13-2932696
Total	0.00 USD
Terms and Conditions	

ELSEVIER LICENSE TERMS AND CONDITIONS

Feb 29, 2024

This Agreement between IIT Guwahati -- Dhirendra Verma ("You") and Elsevier ("Elsevier") consists of your license details and the terms and conditions provided by Elsevier and Copyright Clearance Center.

License Number	5738450474348
License date	Feb 29, 2024
Licensed Content Publisher	Elsevier
Licensed Content Publication	The Lancet
Licensed Content Title	Rheumatoid arthritis
Licensed Content Author	Andrea Di Matteo,Joan M Bathon,Paul Emery
Licensed Content Date	25 November–1 December 2023
Licensed Content Volume	402
Licensed Content Issue	10416
Licensed Content Pages	15
Start Page	2019
End Page	2033
Type of Use	reuse in a thesis/dissertation
Portion	figures/tables/illustrations
Number of figures/tables/illustrations	1
Format	both print and electronic
Are you the author of this Elsevier article?	No
Will you be translating?	No

Title of new work	DEVELOPMENT OF WEARABLE SYSTEMS FOR THE DETECTION AND CLASSIFICATION OF KNEE OSTEOARTHRITIS AND ITS VALIDATION THROUGH RADIOGRAPHIC IMAGES
Institution name	IIT GUWAHATI
Expected presentation date	May 2024
Portions	Figure 1
Requestor Location	IIT Guwahati Amingaon Guwahati, 781039 India Attn: IIT Guwahati
Publisher Tax ID	GB 494 6272 12
Total	0.00 USD
Terms and Conditions	

ELSEVIER LICENSE
TERMS AND CONDITIONS

Feb 29, 2024

This Agreement between IIT Guwahati -- Dhirendra Verma ("You") and Elsevier ("Elsevier") consists of your license details and the terms and conditions provided by Elsevier and Copyright Clearance Center.

License Number	5738140719157
License date	Feb 29, 2024
Licensed Content Publisher	Elsevier
Licensed Content Publication	The Lancet
Licensed Content Title	Ankylosing spondylitis
Licensed Content Author	Jürgen Braun,Joachim Sieper
Licensed Content Date	21–27 April 2007
Licensed Content Volume	369
Licensed Content Issue	9570
Licensed Content Pages	12
Start Page	1379
End Page	1390
Type of Use	reuse in a thesis/dissertation
Portion	figures/tables/illustrations
Number of figures/tables/illustrations	1

Format	both print and electronic
Are you the author of this Elsevier article?	No
Will you be translating?	No
Title of new work	DEVELOPMENT OF WEARABLE SYSTEMS FOR THE DETECTION AND CLASSIFICATION OF KNEE OSTEOARTHRITIS AND ITS VALIDATION THROUGH RADIOGRAPHIC IMAGES
Institution name	IIT GUWAHATI
Expected presentation date	May 2024
Portions	Figure 3
Requestor Location	IIT Guwahati Amingaon Guwahati, 781039 India Attn: IIT Guwahati
Publisher Tax ID	GB 494 6272 12
Total	0.00 USD

TH-3463_176103116

BMJ PUBLISHING GROUP LTD. LICENSE
TERMS AND CONDITIONS

Feb 29, 2024

This Agreement between IIT Guwahati -- Dhirendra Verma ("You") and BMJ Publishing Group Ltd. ("BMJ Publishing Group Ltd.") consists of your license details and the terms and conditions provided by BMJ Publishing Group Ltd. and Copyright Clearance Center.

License Number	5738140900093
License date	Feb 29, 2024
Licensed Content Publisher	BMJ Publishing Group Ltd.
Licensed Content Publication	Annals of the Rheumatic Diseases
Licensed Content Title	Neurovascular mechanisms as a possible cause of remission of rheumatoid arthritis in hemiparetic limbs
Licensed Content Author	G Keyszer,Th Langer,M Kornhuber,B Taute,G Horneff
Licensed Content Date	Oct 1, 2004
Licensed Content Volume	63
Licensed Content Issue	10
Type of Use	Dissertation/Thesis
Requestor type	Individual
Format	Print and electronic
Portion	Figure/table/extract

Number of figure/table/extracts	1
Descriptionof figure/table/extracts	Figure 1
Will you be translating?	No
Circulation/distribution	10
Title of new work	DEVELOPMENT OF WEARABLE SYSTEMS FOR THE DETECTION AND CLASSIFICATION OF KNEE OSTEOARTHRITIS AND ITS VALIDATION THROUGH RADIOGRAPHIC IMAGES
Institution name	IIT GUWAHATI
Expected presentation date	May 2024
Portions	Figure 1
Requestor Location	IIT Guwahati Amingaon Guwahati, 781039 India Attn: IIT Guwahati
Publisher Tax ID	GB674738491
Total	0.00 USD
Terms and Conditions	

TH-3463_176103116

ELSEVIER LICENSE
TERMS AND CONDITIONS

Feb 29, 2024

This Agreement between IIT Guwahati -- Dhirendra Verma ("You") and Elsevier ("Elsevier") consists of your license details and the terms and conditions provided by Elsevier and Copyright Clearance Center.

License Number	5738141039988
License date	Feb 29, 2024
Licensed Content Publisher	Elsevier
Licensed Content Publication	Computerized Medical Imaging and Graphics
Licensed Content Title	Fully automatic knee osteoarthritis severity grading using deep neural networks with a novel ordinal loss
Licensed Content Author	Pingjun Chen,Linlin Gao,Xiaoshuang Shi,Kyle Allen,Lin Yang
Licensed Content Date	Jul 1, 2019
Licensed Content Volume	75
Licensed Content Issue	n/a
Licensed Content Pages	9
Start Page	84
End Page	92
Type of Use	reuse in a thesis/dissertation
Portion	figures/tables/illustrations

Number of figures/tables/illustrations	1
Format	both print and electronic
Are you the author of this Elsevier article?	No
Will you be translating?	No
Title of new work	DEVELOPMENT OF WEARABLE SYSTEMS FOR THE DETECTION AND CLASSIFICATION OF KNEE OSTEOARTHRITIS AND ITS VALIDATION THROUGH RADIOGRAPHIC IMAGES
Institution name	IIT GUWAHATI
Expected presentation date	May 2024
Portions	Figure 1
Requestor Location	IIT Guwahati Amingaon Guwahati, 781039 India Attn: IIT Guwahati
Publisher Tax ID	GB 494 6272 12
Total	0.00 USD

Terms and Conditions

Bibliography

[1] David T Felson, Yuqing Zhang, Marian T Hannan, Allan Naimark, Barbara Weissman, Piran Aliabadi, and Daniel Levy. Risk factors for incident radiographic knee osteoarthritis in the elderly. the framingham study. *Arthritis Rheumatol.*, 40(4):728–733, 1997.

[2] Uyen-Sa DT Nguyen, Yuqing Zhang, Yanyan Zhu, Jingbo Niu, Bin Zhang, and David T Felson. Increasing prevalence of knee pain and symptomatic knee osteoarthritis: survey and cohort data. *Annals of internal medicine*, 155(11):725–732, 2011.

[3] Yuqing Zhang and Joanne M Jordan. Epidemiology of osteoarthritis. *Clinics in geriatric medicine*, 26(3):355–369, 2010.

[4] Elena Losina, Alexander M Weinstein, William M Reichmann, Sara A Burbine, Daniel H Solomon, Meghan E Daigle, Benjamin N Rome, Stephanie P Chen, David J Hunter, Lisa G Suter, et al. Lifetime risk and age at diagnosis of symptomatic knee osteoarthritis in the us. *Arthritis care & research*, 65(5):703–711, 2013.

[5] Kanto Nagai, Tomomasa Nakamura, and Freddie H Fu. The diagnosis of early osteoarthritis of the knee using magnetic resonance imaging. *Annals of Joint*, 3, 2018.

[6] Ervin Nippolainen, Rubina Shaikh, Vesa Virtanen, Lassi Rieppo, Simo Saarakkala, Juha Töyräs, and Isaac O Afara. Near infrared spectroscopy enables differentiation

of mechanically and enzymatically induced cartilage injuries. *Ann. Biomed. Eng.*, 48(9):2343–2353, 2020.

[7] Vikki Wylde, P Dieppe, S Hewlett, and ID Learmonth. Total knee replacement: is it really an effective procedure for all? *The Knee*, 14(6):417–423, 2007.

[8] Ernest Blodgett. Auscultation of the knee joint. *Boston Med. Surg. J.*, 146(3):63–66, 1902.

[9] A Peylan. Direct auscultation of the joints; preliminary clinical observations. *Rheumatism*, 9(4):77–81, 1953.

[10] Mamerto Chu, Ivan Gradisar, and Richard Mostardi. A noninvasive electroacoustical evaluation technique of cartilage damage in pathological knee joints. *Med. Biol. Eng. Comput.*, 16(4):437–442, 1978.

[11] RA Mollan, GC McCullagh, and RI Wilson. A critical appraisal of auscultation of human joints. *Clin. Orthop. Relat. Res.*, (170):231–237, 1982.

[12] Nima Befrui, Jens Elsner, Achim Flesser, Jacqueline Huvanandana, Oussama Jarrousse, Tuan Nam Le, Marcus Müller, Walther HW Schulze, Stefan Taing, and Simon Weidert. Vibroarthrography for early detection of knee osteoarthritis using normalized frequency features. *Med. Biol. Eng. Comput.*, 56(8):1499–1514, 2018.

[13] Robert Karpiński, Anna Machrowska, and Marcin Maciejewski. Application of acoustic signal processing methods in detecting differences between open and closed kinematic chain movement for the knee joint. *Appl. Comput. Sci.*, 15, 2019.

[14] Dhirendra Kumar Verma, Poonam Kumari, and Subramani Kanagaraj. Engineer-

ing aspects of incidence, prevalence, and management of osteoarthritis: a review. *Annals of Biomedical Engineering*, 50(3):237–252, 2022.

[15] Jawad F Abulhasan and Michael J Grey. Anatomy and physiology of knee stability. *J. Funct. Morphol. Kinesiol.*, 2(4):34, 2017.

[16] J Tortora Gerard. *Principles of Anatomy and Physiology 14th Edition*. Incorporated, 2013.

[17] Daniel Constantin and Cristian Molder. The analysis of the knee joint movement. *MTA Review*, XXVI:117–122, 06 2016.

[18] Yunfeng Wu, Sridhar Krishnan, and Rangaraj M Rangayyan. Computer-aided diagnosis of knee-joint disorders via vibroarthrographic signal analysis: a review. *Crit. Rev. Biomed. Eng.*, 38(2), 2010.

[19] David L Hamblen and Hamish Simpson. *Adams's Outline of Orthopaedics E-Book*. Elsevier Health Sciences, 2009.

[20] Michael AR Freeman and V Pinskerova. The movement of the normal tibio-femoral joint. *J. Biomech.*, 38(2):197–208, 2005.

[21] Faye H Chen, Kathleen T Rousche, and Rocky S Tuan. Technology insight: adult stem cells in cartilage regeneration and tissue engineering. *Nat. Clin. Pract. Rheum.*, 2(7):373–382, 2006.

[22] Alice J Sophia Fox, Asheesh Bedi, and Scott A Rodeo. The basic science of articular cartilage: structure, composition, and function. *Sports health*, 1(6):461–468, 2009.

[23] Lijie Zhang, Jerry Hu, and Kyriacos A Athanasiou. The role of tissue engineering

in articular cartilage repair and regeneration. *Crit. Rev. Biomed. Eng.*, 37(1-2), 2009.

[24] Shaw Akizuki, Van C Mow, Francisco Müller, Julio C Pita, David S Howell, and Daniel H Manicourt. Tensile properties of human knee joint cartilage: I. influence of ionic conditions, weight bearing, and fibrillation on the tensile modulus. *Journal of Orthopaedic Research*, 4(4):379–392, 1986.

[25] Jerry Hu. *Chondrocyte self-assembly and culture in bioreactors*. PhD thesis, Rice University, 2005.

[26] M Majewski, Habelt Susanne, and Steinbrück Klaus. Epidemiology of athletic knee injuries: a 10-year study. *The knee*, 13(3):184–188, 2006.

[27] Bing Yu and William E Garrett. Mechanisms of non-contact acl injuries. *British journal of sports medicine*, 41(suppl 1):47–51, 2007.

[28] Sivashankar Chandrasekaran, David Ma, Jennifer M Scarvell, Kevin R Woods, and Paul N Smith. A review of the anatomical, biomechanical and kinematic findings of posterior cruciate ligament injury with respect to non-operative management. *The Knee*, 19(6):738–745, 2012.

[29] Scott W Pyne. Current progress in meniscal repair and postoperative rehabilitation. *Curr Sports Med Rep*, 1(5):265–271, 2002.

[30] Mena Mesiha, David Zurakowski, Jamil Soriano, Jason H Nielson, Bertram Zarins, and Martha M Murray. Pathologic characteristics of the torn human meniscus. *The American journal of sports medicine*, 35(1):103–112, 2007.

[31] Anuradha V Khadilkar and Rubina M Mandlik. Epidemiology and treatment of osteoporosis in women: an indian perspective. *International journal of women's health*, 7:841–850, 2015.

[32] Christopher JL Murray, Theo Vos, Rafael Lozano, Mohsen Naghavi, Abraham D Flaxman, Catherine Michaud, Majid Ezzati, Kenji Shibuya, Joshua A Salomon, Safa Abdalla, et al. Disability-adjusted life years (dalys) for 291 diseases and injuries in 21 regions, 1990–2010: a systematic analysis for the global burden of disease study 2010. *The lancet*, 380(9859):2197–2223, 2012.

[33] Kelli D Allen and Yvonne M Golightly. Epidemiology of osteoarthritis: state of the evidence. *Curr. Opin. Rheumatol.*, 27(3):276, 2015.

[34] Joseph A Buckwalter, Henry J Mankin, and Alan J Grodzinsky. Articular cartilage and osteoarthritis. *Instr. Course. Lect.*, 54:465–480, 2005. PMID:15952258.

[35] Hyun Ah Kim, Mi-La Cho, Hye Young Choi, Chang Sik Yoon, Joo Yeon Jhun, Hey Jwa Oh, and Ho-Youn Kim. The catabolic pathway mediated by toll-like receptors in human osteoarthritic chondrocytes. *Arthritis Rheumatol.*, 54(7):2152–2163, 2006.

[36] Ru Liu-Bryan, Kenneth Pritzker, Gary S Firestein, and Robert Terkeltaub. Tlr2 signaling in chondrocytes drives calcium pyrophosphate dihydrate and monosodium urate crystal-induced nitric oxide generation. *J. Immunol.*, 174(8):5016–5023, 2005.

[37] Susan E Sweeney and Gary S Firestein. Rheumatoid arthritis: regulation of synovial inflammation. *The international journal of biochemistry & cell biology*, 36(3):372–378, 2004.

[38] Howard Anthony Bird. *Arthritis: Your Comprehensive Guide to Pain Management, Medication, Diet, Exercise, Surgery, and Physical Therapies*. DK, 2009.

[39] Andrea Di Matteo, Joan M Bathon, and Paul Emery. Rheumatoid arthritis. *The Lancet*, 402(10416):2019–2033, 2023.

[40] Jürgen Braun and Joachim Sieper. Ankylosing spondylitis. *The Lancet*, 369(9570):1379–1390, 2007.

[41] G Keyszer, Th Langer, M Kornhuber, B Taute, and G Horneff. Neurovascular mechanisms as a possible cause of remission of rheumatoid arthritis in hemiparetic limbs. *Annals of the Rheumatic Diseases*, 63(10):1349–1351, 2004.

[42] TR Mikuls, JT Farrar, WB Bilker, S Fernandes, and KG Saag. Suboptimal physician adherence to quality indicators for the management of gout and asymptomatic hyperuricaemia: results from the UK general practice research database (GPRD). *Rheumatology*, 44(8):1038–1042, 2005.

[43] EUR Smith, C Diaz-Torne, F Perez-Ruiz, and LM March. Epidemiology of gout: an update. *Best Practice & Research Clinical Rheumatology*, 24(6):811–827, 2010.

[44] Mohammadhossein Ebrahimi, Simo Ojanen, Ali Mohammadi, Mikko A Finnilä, Antti Joukainen, Heikki Kröger, Simo Saarakkala, Rami K Korhonen, and Petri Tanska. Elastic, viscoelastic and fibril-reinforced poroelastic material properties of healthy and osteoarthritic human tibial cartilage. *Ann. Biomed. Eng.*, 47(4):953–966, 2019.

[45] Mohammadhossein Ebrahimi, Mikael J Turunen, Mikko A Finnilä, Antti Joukainen, Heikki Kröger, Simo Saarakkala, Rami K Korhonen, and Petri Tanska. Structure–

function relationships of healthy and osteoarthritic human tibial cartilage: Experimental and numerical investigation. *Ann. Biomed. Eng.*, 48(12):2887–2900, 2020.

[46] Mohammadhossein Ebrahimi, Mikko AJ Finnilä, Aleksandra Turkiewicz, Martin Englund, Simo Saarakkala, Rami K Korhonen, and Petri Tanska. Elastic, dynamic viscoelastic and model-derived fibril-reinforced poroelastic mechanical properties of normal and osteoarthritic human femoral condyle cartilage. *Ann. Biomed. Eng.*, pages 1–13, 2021.

[47] Amin Komeili, Baaba Sekyiwaa Otoo, Ziad Abusara, Scott Sibole, Salvatore Federico, and Walter Herzog. Chondrocyte deformations under mild dynamic loading conditions. *Ann. Biomed. Eng.*, 49(2):846–857, 2021.

[48] Sotcheadt Sim, Insaf Hadjab, Martin Garon, Eric Quenneville, Patrick Lavigne, and Michael D Buschmann. Development of an electromechanical grade to assess human knee articular cartilage quality. *Ann. Biomed. Eng.*, 45(10):2410–2421, 2017.

[49] Mehdi Shekarforoush, Paris Vakiel, Michael Scott, Gregory Muench, David A Hart, and Nigel G Shrive. Relative surface velocity of the tibiofemoral joint and its relation to the development of osteoarthritis after joint injury. *Ann. Biomed. Eng.*, 48(2):695–708, 2020.

[50] Lise De Moor, Elien Beyls, and Heidi Declercq. Scaffold free microtissue formation for enhanced cartilage repair. *Ann. Biomed. Eng.*, 48(1):298–311, 2020.

[51] Roseline Menezes and Treena L Arinzeh. Comparative study of electrospun scaffolds containing native gags and a gag mimetic for human mesenchymal stem cell chondrogenesis. *Ann. Biomed. Eng.*, 48(7):2040–2052, 2020.

[52] Bethany Almeida, Yingying Wang, and Anita Shukla. Effects of nanoparticle properties on kartogenin delivery and interactions with mesenchymal stem cells. *Ann. Biomed. Eng.*, 48(7):2090–2102, 2020.

[53] Michael Neidlin, Efthymia Chantzi, George Macheras, Mats G Gustafsson, and Leonidas G Alexopoulos. A novel multiplex based platform for osteoarthritis drug candidate evaluation. *Ann. Biomed. Eng.*, 48:2438–2448, 2020.

[54] Chandra Prakash Pal, Pulkesh Singh, Sanjay Chaturvedi, Kaushal Kumar Pruthi, and Ashok Vij. Epidemiology of knee osteoarthritis in india and related factors. *Indian journal of orthopaedics*, 50:518–522, 2016.

[55] Eman A M Alkady, Zahraa I Selim, Marwa M Abdelaziz, Fatma A El-Hafeez, et al. Epidemiology and socioeconomic burden of osteoarthritis. *Journal of Current Medical Research and Practice*, 8(1):7, 2023.

[56] Sion Glyn-Jones, AJR Palmer, R Agricola, AJ Price, TL Vincent, H Weinans, and AJ Carr. Osteoarthritis. *The Lancet*, 386(9991):376–387, 2015.

[57] Mizanur Rahaman Sk, Mukesh Phalak, Joe Jacob, Tushar Chaudhari, Anteshwar Birajdar, Bibin Selvin, Shubham Taori, Sagar Gurnani, and Shivam Patel. Functional outcome of early osteoarthritis of the knee joint treated with prp. *Journal of Pharmaceutical Negative Results*, pages 9432–9438, 2022.

[58] Aderonke Omobonike Akinpelu, Temitope Olugbenga Alonge, Babatunde Ayo Adekanla, and Adesola Christiana Odole. Prevalence and pattern of symptomatic knee osteoarthritis in nigeria: A community-based study. *Internet Journal of Allied Health Sciences and Practice*, 7(3):10, 2009.

[59] Sharon L Brennan-Olsen, S Cook, MT Leech, Steven J Bowe, Paul Kowal, N Naidoo, IN Ackerman, RS Page, SM Hosking, JA Pasco, et al. Prevalence of arthritis according to age, sex and socioeconomic status in six low and middle income countries: analysis of data from the world health organization study on global ageing and adult health (sage) wave 1. *BMC Musculoskelet. Disord.*, 18(1):1–12, 2017.

[60] JH Kellgren and JS1006995 Lawrence. Radiological assessment of osteo-arthrosis. *Ann. Rheum. Dis.*, 16(4):494, 1957.

[61] Pingjun Chen, Linlin Gao, Xiaoshuang Shi, Kyle Allen, and Lin Yang. Fully automatic knee osteoarthritis severity grading using deep neural networks with a novel ordinal loss. *Comput. Med. Imag. Grap.*, 75:84–92, 2019.

[62] Ilana Ackerman. Western ontario and mcmaster universities osteoarthritis index (womac). *Aust. J. Physiother.*, 55(3):213, 2009.

[63] Barbara Gandek. Measurement properties of the western ontario and mcmaster universities osteoarthritis index: a systematic review. *Arthrit. Care. Res.*, 67(2):216–229, 2015.

[64] Sara McConnell, Pamela Kolopack, and Aileen M Davis. The western ontario and mcmaster universities osteoarthritis index (womac): a review of its utility and measurement properties. *Arthrit. Care. Res.*, 45(5):453–461, 2001.

[65] Rohit Yadav, Ajay Kumar Verma, Arjun Uppal, Hemant Singh Chahar, Jaydeep Patel, and Chandra Prakash Pal. Prevalence of primary knee osteoarthritis in the urban and rural population in india. *Indian Journal of Rheumatology*, 17(3):239–243, 2022.

[66] Tahbildar P Gogoi B P Buragohain C R, Kalita P. Prevalence of primary osteoarthritis of knee in tea garden community of jorhat district, assam. *IP Int J Orthop Rheumatol*, 9(1):25–29, 2023.

[67] Y Ghodke, A Chopra, P Shintre, K Joshi, and B Patwardhan. O58 the association of gene polymorphism in methotrexate (mtx) metabolic pathway with toxicity related to mtx therapy in rheumatoid arthritis (ra). *Indian Journal of Rheumatology*, 3(3):S29–S30, 2008.

[68] M Haque, S Masum, M Haqe, M Islam, M Rahman, et al. Pattern of osteoarthritis among ethnic people residing hilly area: a cross sectional ethnic community based study. *MOJ Orthop Rheumatol*, 3(1):00076, 2015.

[69] Y Nagaosa, P Lanyon, and M Doherty. Characterisation of size and direction of osteophyte in knee osteoarthritis: a radiographic study. *Ann. Rheum. Dis.*, 61(4):319–324, 2002.

[70] Rose S Fife, Kenneth D Brandt, Ethan M Braunstein, Barry P Katz, K Donald Shelbourne, Lorrie A Kalasinski, and Sarah Ryan. Relationship between arthroscopic evidence of cartilage damage and radiographic evidence of joint space narrowing in early osteoarthritis of the knee. *Arthritis Rheumatol.*, 34(4):377–382, 1991.

[71] John Bedson and Peter R Croft. The discordance between clinical and radiographic knee osteoarthritis: a systematic search and summary of the literature. *BMC Musculoskelet. Disord.*, 9(1):1–11, 2008.

[72] CE Chaisson, DR Gale, E Gale, L Kazis, K Skinner, and DT Felson. Detecting radiographic knee osteoarthritis: what combination of views is optimal? *Rheumatology*, 39(11):1218–1221, 2000.

[73] AJ Teichtahl, Anita E Wluka, Miranda L Davies-Tuck, and Flavia M Cicuttini. Imaging of knee osteoarthritis. *Best Pract. Res.: Clin. Rheumatol.*, 22(6):1061–1074, 2008.

[74] AS Doria. State-of-the-art imaging techniques for the evaluation of haemophilic arthropathy: present and future. *Haemophilia*, 16:107–114, 2010.

[75] I Möller, D Bong, E Naredo, E Filippucci, I Carrasco, C Moragues, and Annamaria Iagnocco. Ultrasound in the study and monitoring of osteoarthritis. *Osteoarthr. Cartil.*, 16:S4–S7, 2008.

[76] Eiji Tanaka, Yao Liu, Linze Xia, Naoko Ogasawara, Takuma Sakamaki, Fumiya Kano, Noboru Hashimoto, Xingmei Feng, and Akihito Yamamoto. Effectiveness of low-intensity pulsed ultrasound on osteoarthritis of the temporomandibular joint: a review. *Ann. Biomed. Eng.*, 48(8):2158–2170, 2020.

[77] Md Belayet Hossain, Belinda Pingguan-Murphy, Hum Yan Chai, Maheza Irna Mohd Salim, Dyah Ekashanti Octorina Dewi, Eko Supriyanto, and Khin Wee Lai. Improved ultrasound imaging for knee osteoarthritis detection. In *Medical Imaging Technology*, pages 1–40. Springer, 2015.

[78] Win Min Oo and Myat Thae Bo. Role of ultrasonography in knee osteoarthritis. *JCR-J. Clin. Rheumatol.*, 22(6):324–329, 2016.

[79] Annamaria Iagnocco and Esperanza Naredo. Osteoarthritis: research update and clinical applications. *Rheumatology*, 51(suppl_7):vii2–vii5, 2012.

[80] M Østergaard, M Court-Payen, P Gideon, S Wieslander, M Cortsen, I Lorenzen,

and O Henriksen. Ultrasonography in arthritis of the knee: a comparison with mr imaging. *Acta Radiol.*, 36(1):19–26, 1995.

[81] Ali Guermazi, Daichi Hayashi, Frank W Roemer, and David T Felson. Osteoarthritis: a review of strengths and weaknesses of different imaging options. *Rheum. Dis. Clin. N. Am.*, 39(3):567–591, 2013.

[82] MA Bredella, PF Tirman, CG Peterfy, M Zarlingo, JF Feller, FW Bost, JP Belzer, TK Wischer, and HK Genant. Accuracy of t2-weighted fast spin-echo mr imaging with fat saturation in detecting cartilage defects in the knee: comparison with arthroscopy in 130 patients. *Am. J. Roentgenol.*, 172(4):1073–1080, 1999.

[83] F Eckstein, J Westhoff, H Sittek, KP Maag, M Haubner, S Faber, KH Englmeier, and M Reiser. In vivo reproducibility of three-dimensional cartilage volume and thickness measurements with mr imaging. *Am. J. Roentgenol.*, 170(3):593–597, 1998.

[84] M van Leersum, ME Schweitzer, F Gannon, G Finkel, S Vinitski, and DG Mitchell. Chondromalacia patellae: an in vitro study. comparison of mr criteria with histologic and macroscopic findings. *Skeletal Radiol.*, 25(8):727–732, 1996.

[85] Peter MM Cashman, Richard I Kitney, Munir A Gariba, and Mary E Carter. Automated techniques for visualization and mapping of articular cartilage in mr images of the osteoarthritic knee: a base technique for the assessment of microdamage and submicro damage. *IEEE T. Nanobiosci.*, 99(1):42–51, 2002.

[86] Mika E Mononen, Mimmi K Liukkonen, and Rami K Korhonen. Utilizing atlas-based modeling to predict knee joint cartilage degeneration: data from the osteoarthritis initiative. *Ann. Biomed. Eng.*, 47(3):813–825, 2019.

[87] Ali Mohammadi, Katariina AH Myller, Petri Tanska, Jukka Hirvasniemi, Simo Saarakkala, Juha Töyräs, Rami K Korhonen, and Mika E Mononen. Rapid ct-based estimation of articular cartilage biomechanics in the knee joint without cartilage segmentation. *Ann. Biomed. Eng.*, 48(12):2965–2975, 2020.

[88] Hattie C Cutcliffe, Keithara M Davis, Charles E Spritzer, and Louis DeFrate. The characteristic recovery time as a novel, noninvasive metric for assessing in vivo cartilage mechanical function. *Ann. Biomed. Eng.*, 48(12):2901–2910, 2020.

[89] Xingde Li, Scott Martin, Costas Pitris, Ravi Ghanta, Debra L Stamper, Michelle Harman, James G Fujimoto, and Mark E Brezinski. High-resolution optical coherence tomographic imaging of osteoarthritic cartilage during open knee surgery. *Arthritis Res. Ther.*, 7(2):1–6, 2005.

[90] Christopher Rashidifard, Christopher Vercollone, Scott Martin, Bin Liu, and Mark E Brezinski. The application of optical coherence tomography in musculoskeletal disease. *Arthritis*, 2013, 2013.

[91] Constance R Chu, Ashley Williams, David Tolliver, C Kent Kwoh, Stephen Bruno III, and James J Irrgang. Clinical optical coherence tomography of early articular cartilage degeneration in patients with degenerative meniscal tears. *Arthritis Rheum.*, 62(5):1412–1420, 2010.

[92] Mobin Ibne Mokbul. Optical coherence tomography: basic concepts and applications in neuroscience research. *J. Med. Eng.*, 2017, 2017.

[93] Fleming Lund and Bo E Nilsson. Arthroscopy of the patello-femoral joint. *Acta Orthop. Scand.*, 51(1-6):297–302, 1980.

[94] LP Li and W Herzog. Arthroscopic evaluation of cartilage degeneration using indentation testing influence of indenter geometry. *Clin. Biomech.*, 21(4):420–426, 2006.

[95] DJ Ogilvie-Harris and DP Fitsialos. Arthroscopic management of the degenerative knee. *Arthroscopy*, 7(2):151–157, 1991.

[96] Subhas Chandra Mukhopadhyay. Wearable sensors for human activity monitoring: A review. *IEEE Sens. J.*, 15(3):1321–1330, 2014.

[97] Massimiliano Donno, Elia Palange, Fabio Di Nicola, Giovanni Bucci, and Fabrizio Ciancetta. A new flexible optical fiber goniometer for dynamic angular measurements: Application to human joint movement monitoring. *IEEE T. Instrum. Meas.*, 57(8):1614–1620, 2008.

[98] L Bilro, JG Oliveira, JL Pinto, and RN Nogueira. A reliable low-cost wireless and wearable gait monitoring system based on a plastic optical fibre sensor. *Meas. Sci. Technol.*, 22(4):045801, 2011.

[99] Chee Kian Lim, Zhiqiang Luo, I-Ming Chen, and Song Huat Yeo. A low cost wearable optical-based goniometer for human joint monitoring. *Front. Mech. Eng.*, 6(1):13–22, 2011.

[100] Dragan Z Stupar, Jovan S Bajic, Lazo M Manojlovic, Miloš P Slankamenac, Ana V Joza, and Miloš B Zivanov. Wearable low-cost system for human joint movements monitoring based on fiber-optic curvature sensor. *IEEE Sens. J.*, 12(12):3424–3431, 2012.

[101] Jyri Rantala, Jaana Hännikäinen, and Jukka Vanhala. Fiber optic sensors for wearable applications. *Pers. Ubiquitous Comput.*, 15(1):85–96, 2011.

[102] Min Li, Bo He, Xingang Zhao, Jun Xie, Wei Yao, and Guanghua Xu. A wearable fiber-optic sensor for monitoring human elbow and wrist joint motion. *Adv. Robotics*, pages 1–13, 2020.

[103] Paris Vakiel, Mehdi Shekarforoush, Christopher R Dennison, Michael Scott, Cyril B Frank, David A Hart, and Nigel G Shrive. Stress measurements on the articular cartilage surface using fiber optic technology and in-vivo gait kinematics. *Ann. Biomed. Eng.*, 48(12):2836–2845, 2020.

[104] Amir Mobini, Saeed Behzadipour, and Mahmoud Saadat Foumani. Accuracy of kinect's skeleton tracking for upper body rehabilitation applications. *Disabil. Rehabilitation. Assist. Technol.*, 9(4):344–352, 2014.

[105] Wan Zharfan Wan Zainal Abiddin, R Jailani, Abdul Rahman Omar, and Ihsan M Yassin. Development of matlab kinect skeletal tracking system (mksts) for gait analysis. In *2016 IEEE Symposium on Computer Applications & Industrial Electronics (ISCAIE)*, pages 216–220. IEEE, 2016.

[106] Muhammad Usama Islam, Hasan Mahmud, Faisal Bin Ashraf, Iqbal Hossain, and Md Kamrul Hasan. Yoga posture recognition by detecting human joint points in real time using microsoft kinect. In *2017 IEEE Region 10 humanitarian technology conference (R10-HTC)*, pages 668–673. IEEE, 2017.

[107] Ziren Wang, Guoliang Liu, and Guohui Tian. Human skeleton tracking using information weighted consensus filter in distributed camera networks. In *2017 Chinese Automation Congress (CAC)*, pages 4640–4644. IEEE, 2017.

[108] Orasa Patsadu, Chakarida Nukoolkit, and Bunthit Watanapa. Human gesture recognition using kinect camera. In *2012 ninth international conference on computer science and software engineering (JCSSE)*, pages 28–32. IEEE, 2012.

[109] Jeroen HM Bergmann, Salzitsa Anastasova-Ivanova, Irina Spulber, Vivek Gulati, Pantelis Georgiou, and Alison McGregor. An attachable clothing sensor system for measuring knee joint angles. *IEEE Sens. J.*, 13(10):4090–4097, 2013.

[110] Peter T Gibbs and HHarry Asada. Wearable conductive fiber sensors for multi-axis human joint angle measurements. *J. Neuroeng. Rehabil.*, 2(1):1–18, 2005.

[111] Saba Bakhshi and Mohammad H Mahoor. Development of a wearable sensor system for measuring body joint flexion. In *2011 International Conference on Body Sensor Networks*, pages 35–40. IEEE, 2011.

[112] Guido Gioberto. Garment-integrated wearable sensing for knee joint monitoring. In *Proceedings of the 2014 ACM International Symposium on Wearable Computers: Adjunct Program*, pages 113–118, 2014.

[113] Massimo Totaro, Tommaso Poliero, Alessio Mondini, Chiara Lucarotti, Giovanni Cairoli, Jesùs Ortiz, and Lucia Beccai. Soft smart garments for lower limb joint position analysis. *Sensors*, 17(10):2314, 2017.

[114] Sang-Mi Jeong, Youngsoo Kang, Taekyung Lim, and Sanghyun Ju. Hydrophobic microfiber strain sensor operating stably in sweat and water environment. *Adv. Mater. Interfaces*, 5(24):1801376, 2018.

[115] Sangki Park, Seongcheol Ahn, Jingzhe Sun, Divij Bhatia, Dukhyun Choi, Kap Seung Yang, Jihyun Bae, and Jong-Jin Park. Highly bendable and rotational textile

structure with prestrained conductive sewing pattern for human joint monitoring. *Adv. Funct. Mater.*, 29(10):1808369, 2019.

[116] H Montazerian, A Dalili, AS Milani, and M Hoorfar. Piezoresistive sensing in chopped carbon fiber embedded pdms yarns. *Compos. B. Eng.*, 164:648–658, 2019.

[117] Saba Bakhshi, Mohammad H Mahoor, and Bradley S Davidson. Development of a body joint angle measurement system using imu sensors. In *2011 Annual International Conference of the IEEE Engineering in Medicine and Biology Society*, pages 6923–6926. IEEE, 2011.

[118] Julien Favre, BM Jolles, Rachid Aissaoui, and K Aminian. Ambulatory measurement of 3d knee joint angle. *J. Biomech.*, 41(5):1029–1035, 2008.

[119] Julien Favre, Rab Aissaoui, Brigitte M Jolles, Jacques A de Guise, and Kamiar Aminian. Functional calibration procedure for 3d knee joint angle description using inertial sensors. *J. Biomech.*, 42(14):2330–2335, 2009.

[120] Thomas Seel and Thomas Schauer. Imu-based joint angle measurement made practical. In *Proceedings of the 4th European Conference on Technically Assisted Rehabilitation*, 2013.

[121] Sarvenaz Salehi, Gabriele Bleser, Attila Reiss, and Didier Stricker. Body-imu autocalibration for inertial hip and knee joint tracking. In *Proceedings of the 10th EAI International Conference on Body Area Networks*, pages 51–57, 2015.

[122] Vincent Bonnet, Vladimir Joukov, Dana Kulić, Philippe Fraisse, Nacim Ramdani, and Gentiane Venture. Monitoring of hip and knee joint angles using a single inertial

measurement unit during lower limb rehabilitation. *IEEE Sens. J.*, 16(6):1557–1564, 2015.

[123] Laura Susana Vargas-Valencia, Arlindo Elias, Eduardo Rocon, Teodiano Bastos-Filho, and Anselmo Frizera. An imu-to-body alignment method applied to human gait analysis. *Sensors*, 16(12):2090, 2016.

[124] Alessandro Tognetti, Federico Lorussi, Nicola Carbonaro, and Danilo De Rossi. Wearable goniometer and accelerometer sensory fusion for knee joint angle measurement in daily life. *Sensors*, 15(11):28435–28455, 2015.

[125] Daniel J Crews. *Real-time estimation of knee angle, heel-strike, and toe-off events for gait rehabilitation devices*. California State University, Long Beach, 2017. M.S. Thesis.

[126] Zhi Chao Ong, YC Seet, Shin Yee Khoo, and Siamak Noroozi. Development of an economic wireless human motion analysis device for quantitative assessment of human body joint. *Measurement*, 115:306–315, 2018.

[127] A Steindler. Auscultation of joints. *J. Bone Jt. Surg.*, 19(1):121–136, 1937.

[128] John Hunter and HC Brooks. Study of recorded noise in normal and pathologic knee joints of human subjects. *J. Lab. Clin. Med.*, 47(2):289–296, 1956.

[129] Gerald F McCoy, John D McCrea, David E Beverland, W George Kernohan, and RA Mollan. Vibration arthrography as a diagnostic aid in diseases of the knee. a preliminary report. *J. Bone Jt. Surg.*, 69(2):288–293, 1987.

[130] W George Kernohan, David E Beverland, Gerald F McCoy, Alistair Hamilton,

Peter Watson, and RAB Mollan. Vibration arthrometry. *Acta Orthop. Scand.*, 61(1):70–79, 1990.

[131] WG Kernohan, DA Barr, GF McCoy, and RAB Mollan. Vibration arthrometry in assessment of knee disorders: the problem of angular velocity. *J. Biomed. Eng.*, 13(1):35–38, 1991.

[132] Sanjeev Tavathia, Rangaraj Mandayam Rangayyan, Cyril Basil Frank, Gordon Douglas Bell, Katherine O Ladly, and Y-T Zhang. Analysis of knee vibration signals using linear prediction. *IEEE. Trans. Biomed. Eng.*, 39(9):959–970, 1992.

[133] YT Zhang and RM Rangayyan. Adaptive cancellation of muscle contraction interference in vibroarthrographic signals. *IEEE. Trans. Biomed. Eng.*, 41(2):181–191, 1994.

[134] Narender P Reddy, Bruce M Rothschild, Mita Mandal, Vineet Gupta, and Srikanth Suryanarayanan. Noninvasive acceleration measurements to characterize knee arthritis and chondromalacia. *Ann. Biomed. Eng.*, 23(1):78–84, 1995.

[135] Y Shen, RM Rangayyan, GD Bell, CB Frank, YT Zhang, and KO Ladly. Localization of knee joint cartilage pathology by multichannel vibroarthrography. *Med. Eng. Phys.*, 17(8):583–594, 1995.

[136] Zahra MK Maussavi, Rangaraj M Rangayyan, G Douglas Bell, Cyril B Frank, and Katherine O Ladly. Screening of vibroarthrographic signals via adaptive segmentation and linear prediction modeling. *IEEE. Trans. Biomed. Eng.*, 43(1):15, 1996.

[137] Rangaraj M Rangayyan, Sridhar Krishnan, G Douglas Bell, Cyril B Frank, and

Katherine O Ladly. Parametric representation and screening of knee joint vibroarthrographic signals. *IEEE. Trans. Biomed. Eng.*, 44(11):1068–1074, 1997.

[138] Rangaraj M Rangayyan and Yunfeng Wu. Analysis of vibroarthrographic signals with features related to signal variability and radial-basis functions. *Ann. Biomed.Eng.*, 37(1):156–163, 2009.

[139] Yunfeng Wu and Sridhar Krishnan. Combining least-squares support vector machines for classification of biomedical signals: a case study with knee-joint vibroarthrographic signals. *J. Exp. Theor. Artif. Intell.*, 23(1):63–77, 2011.

[140] Noriyuki Tanaka and Minoru Hoshiyama. Vibroarthrography in patients with knee arthropathy. *J. Back Musculoskelet. Rehabil.*, 25(2):117–122, 2012.

[141] Yunfeng Wu, Suxian Cai, Shanshan Yang, Fang Zheng, and Ning Xiang. Classification of knee joint vibration signals using bivariate feature distribution estimation and maximal posterior probability decision criterion. *Entropy*, 15(4):1375–1387, 2013.

[142] Yunfeng Wu, Shanshan Yang, Fang Zheng, Suxian Cai, Meng Lu, and Meihong Wu. Removal of artifacts in knee joint vibroarthrographic signals using ensemble empirical mode decomposition and detrended fluctuation analysis. *Physiol. Meas.*, 35(3):429, 2014.

[143] Rasmus Elbaek Andersen, Lars Arendt-Nielsen, and Pascal Madeleine. A review of engineering aspects of vibroarthography of the knee joint. *Crit. Rev. Phys. Rehabil. Med.*, 28(1-2), 2016.

[144] Mohsen Safaei, Nicholas B Bolus, Alper Erturk, and Omer T Inan. Vibration char-

acterization of the human knee joint in audible frequencies. *Sensors*, 20(15):4138, 2020.

[145] Dagyeong Choi, Soonjae Ahn, Jeseong Ryu, Mitsuo Nagao, and Youngho Kim. Knee acoustic emission characteristics of the healthy and the patients with osteoarthritis using piezoelectric sensor. *Sensor Mater.*, 30(8):1629–1641, 2018.

[146] Hakan Töreyin, Hyeon Ki Jeong, Sinan Hersek, Caitlin N Teague, and Omer T Inan. Quantifying the consistency of wearable knee acoustical emission measurements during complex motions. *IEEE J. Biomed. Health Inform.*, 20(5):1265–1272, 2016.

[147] Dawid Baczkowicz, Edyta Majorczyk, and Krzysztof Krecisz. Age-related impairment of quality of joint motion in vibroarthrographic signal analysis. *BioMed Res. Int.*, 2015, 2015.

[148] Faizan Ali, Waseem Raza, Xilin Li, Hajera Gul, and Ki-Hyun Kim. Piezoelectric energy harvesters for biomedical applications. *Nano Energy*, 57:879–902, 2019.

[149] J Prior, B Mascaro, LK Shark, J Stockdale, J Selfe, R Bury, P Cole, and JA Goodacre. Analysis of high frequency acoustic emission signals as a new approach for assessing knee osteoarthritis. *Ann. Rheum. Dis.*, 69(5):929–930, 2010.

[150] L-K Shark, H Chen, and John Goodacre. Knee acoustic emission: a potential biomarker for quantitative assessment of joint ageing and degeneration. *Med. Eng.Phys.*, 33(5):534–545, 2011.

[151] Manda Paul. *A Novel Wireless Health Orthopedic System Integrating Motion and Acoustic Emission Monitoring*. PhD thesis, UCLA, 2013.

[152] Mohd Noor Anas. Development of a non-invasive bio-acoustics measurement system for assessing articular cartilage knee joint problem. 2014.

[153] Keita Aimoto, Susumu Ota, Kazunori Hase, Takenobu Sakai, Katsuya Kodama, and Hiroaki Nakamura. Development of an impulse response method for assessing knee osteoarthritis at the femorotibial joint: Comparison between healthy young adults and older women with clinical knee osteoarthritis. *J. Med. Biol. Eng.*, 40(1):35–40, 2020.

[154] Caitlin Teague, Sinan Hersek, Hakan Töreyin, Mindy L Millard-Stafford, Michael L Jones, Geza F Kogler, Michael N Sawka, and Omer T Inan. Novel approaches to measure acoustic emissions as biomarkers for joint health assessment. In *2015 IEEE 12th International Conference on Wearable and Implantable Body Sensor Networks (BSN)*, pages 1–6. IEEE, 2015.

[155] Caitlin N Teague, Sinan Hersek, Hakan Töreyin, Mindy L Millard-Stafford, Michael L Jones, Geza F Kogler, Michael N Sawka, and Omer T Inan. Novel methods for sensing acoustical emissions from the knee for wearable joint health assessment. *IEEE. Trans. Biomed. Eng.*, 63(8):1581–1590, 2016.

[156] Caitlin N Teague, Sinan Hersek, Jordan L Conant, Scott M Gilliland, and Omer T Inan. Wearable knee health rehabilitation assessment using acoustical emissions. In *AIP Conference Proceedings*, volume 1806, page 070008. AIP Publishing LLC, 2017.

[157] G Rajalakshmi, C Vinothkumar, A Anne Frank Joe, and T Thaj Mary Delsy. Vibroarthographic signal analysis of bone disorders using arduino and piezoelectric

sensors. In *2019 International Conference on Communication and Signal Processing (ICCSP)*, pages 0082–0086. IEEE, 2019.

[158] Keaton L Scherpereel, Nicholas B Bolus, Hyeon Ki Jeong, Omer T Inan, and Aaron J Young. Estimating knee joint load using acoustic emissions during ambulation. *Ann. Biomed. Eng.*, 49(3):1000–1011, 2021.

[159] Daniel C Whittingslow, Hyeon-Ki Jeong, Venu G Ganti, Nathan J Kirkpatrick, Geza F Kogler, and Omer T Inan. Acoustic emissions as a non-invasive biomarker of the structural health of the knee. *Ann. Biomed. Eng.*, 48(1):225–235, 2020.

[160] Keith Rome and Fiona Cowieson. A reliability study of the universal goniometer, fluid goniometer, and electrogoniometer for the measurement of ankle dorsiflexion. *Foot & ankle international*, 17(1):28–32, 1996.

[161] L Tesio, M Monzani, R Gatti, and F Franchignoni. Flexible electrogoniometers: kinesiological advantages with respect to potentiometric goniometers. *Clinical Biomechanics*, 10(5):275–277, 1995.

[162] Cynthia L Kendell and Edward D Lemaire. Effect of mobility devices on orientation sensors that contain magnetometers. *CMBES Proceedings*, 31, 2008.

[163] Kun Liu, Tao Liu, Kyoko Shibata, Yoshio Inoue, and Rencheng Zheng. Novel approach to ambulatory assessment of human segmental orientation on a wearable sensor system. *Journal of biomechanics*, 42(16):2747–2752, 2009.

[164] Vittorio Passaro, Antonello Cuccovillo, Lorenzo Vaiani, Martino De Carlo, and Carlo Edoardo Campanella. Gyroscope technology and applications: A review in the industrial perspective. *Sensors*, 17(10):2284, 2017.

[165] Nunzio Abbate, Adriano Basile, Carmen Brigante, Alessandro Faulisi, and Fabrizio La Rosa. Modern breakthrough technologies enable new applications based on imu systems. *Journal of Sensors*, 2011, 2011.

[166] José Jair Alves Mendes Jr, Mário Elias Marinho Vieira, Marcelo Bissi Pires, and Sergio Luiz Stevan Jr. Sensor fusion and smart sensor in sports and biomedical applications. *Sensors*, 16(10):1569, 2016.

[167] Andrei M Shkel and Yusheng Wang. Inertial sensors and inertial measurement units. 2021.

[168] James John. *Adaptively controlled MEMS triaxial angular rate sensor*. PhD thesis, RMIT University, 2006.

[169] N Ananthakrishnan and AK Shanthi. Icmr's ethical guidelines for biomedical research on human participants: need for clarification. *Indian J Med Ethics*, 9(3):207–209, 2012.

[170] Andressa Rezende, Camille Alves, Isabela Marques, Marco Aurélio Silva, and Eduardo Naves. Polymer optical fiber goniometer: A new portable, low cost and reliable sensor for joint analysis. *Sensors*, 18(12):4293, 2018.

[171] Mirel Ajdaroski, Ruchika Tadakala, Lorraine Nichols, and Amanda Esquivel. Validation of a device to measure knee joint angles for a dynamic movement. *Sensors*, 20(6):1747, 2020.

[172] Shuozhi Yang and Qingguo Li. Inertial sensor-based methods in walking speed estimation: A systematic review. *Sensors*, 12(5):6102–6116, 2012.

[173] P Chinmilli, Sangram Redkar, Wenlong Zhang, and Tom Sugar. A review on wearable inertial tracking based human gait analysis and control strategies of lower-limb exoskeletons. *Int. Robot. Autom. J*, 3(7):00080, 2017.

[174] Josien C van den Noort, Vanessa A Scholtes, and Jaap Harlaar. Evaluation of clinical spasticity assessment in cerebral palsy using inertial sensors. *Gait & posture*, 30(2):138–143, 2009.

[175] Annemarie Laudanski, Brenda Brouwer, and Qingguo Li. Measurement of lower limb joint kinematics using inertial sensors during stair ascent and descent in healthy older adults and stroke survivors. *Journal of healthcare engineering*, 4(4):555–576, 2013.

[176] Alessio Ghio, Sebastian Escalante, and Jimmy Tarrillo. Analysis of moving average filter for imu measurements on an 8-bit microcontroller. In *2018 IEEE XXV International Conference on Electronics, Electrical Engineering and Computing (INTERCON)*, pages 1–4. IEEE, 2018.

[177] Reham M Abd Elrahim, Eman A Embaby, Mohamed F Ali, and Ragia M Kamel. Inter-rater and intra-rater reliability of kinovea software for measurement of shoulder range of motion. *Bulletin of Faculty of Physical Therapy*, 21(2):80–87, 2016.

[178] Terry K Koo and Mae Y Li. A guideline of selecting and reporting intraclass correlation coefficients for reliability research. *Journal of chiropractic medicine*, 15(2):155–163, 2016.

[179] Davide Giavarina. Understanding bland altman analysis. *Biochemia medica*, 25(2):141–151, 2015.

[180] J Martin Bland and Douglas G Altman. Statistical methods for assessing agreement between two methods of clinical measurement. *International journal of nursing studies*, 47(8):931–936, 2010.

[181] Aakshi Kalra et al. Decoding the bland–altman plot: basic review. *Journal of the Practice of Cardiovascular Sciences*, 3(1):36, 2017.

[182] Talysson MO Santos, Márcio FS Barroso, Rodrigo A Ricco, Erivelton G Nepomuceno, Érika LFC Alvarenga, Álvaro CO Penoni, and Ana F Santos. A low-cost wireless system of inertial sensors to postural analysis during human movement. *Measurement*, 148:106933, 2019.

[183] Melanie Svensson, Veronika Lind, and Marita Löfgren Harringe. Measurement of knee joint range of motion with a digital goniometer: A reliability study. *Physiotherapy Research International*, 24(2):e1765, 2019.

[184] ME Huber, Amee L Seitz, M Leeser, and D Sternad. Validity and reliability of kinect skeleton for measuring shoulder joint angles: a feasibility study. *Physiotherapy*, 101(4):389–393, 2015.

[185] Chee Chin Lim, Marwan Affandi, Shafriza Nisha Basah, and Mohamad Yazid Din. Evaluating lower limb joint flexion by computerized visual tracking system and compared with electrogoniometer and universal goniometer. *Journal of Telecommunication, Electronic and Computer Engineering (JTEC)*, 10(1-4):9–14, 2018.

[186] Reneaud Nicolas, Pierre Emma, Zory Raphael, Chorin Frederic, Thomas Luc, Chavet Pascale, Coyle Thelma, Truchet Eric, Puech Stephane, Ollivier Matthieu, et al. Validity of an instrumented knee brace compared to 3d motion navigation: A cadaveric investigation. *Measurement*, 173:108590, 2021.

[187] CG Song, KS Kim, and JH Seo. Non-invasive monitoring of knee pathology based on automatic knee sound classification. In *Proceedings of the World Congress on Engineering and Computer Science, San Francisco, USA*, 2009.

[188] Yalan Ye, Zhengyi Wan, Benyuan Liu, Hu Xu, Qian Wang, and Tan Ding. Monitoring deterioration of knee osteoarthritis using vibration arthrography in daily activities. *Computer Methods and Programs in Biomedicine*, 213:106519, 2022.

[189] Petros Karvelis, George Georgoulas, Vassilios Kappatos, and Chrysostomos Stylios. Deep machine learning for structural health monitoring on ship hulls using acoustic emission method. *Ships and Offshore structures*, 16(4):440–448, 2021.

[190] B Mascaro, J Prior, L-K Shark, James Selfe, P Cole, and John Goodacre. Exploratory study of a non-invasive method based on acoustic emission for assessing the dynamic integrity of knee joints. *Medical engineering & physics*, 31(8):1013–1022, 2009.

[191] Nazmush Sakib, Tawhidul Islam Khan, Md Mehedi Hassan, and Kurihara Moe. Acoustic emission features in characterizing osteoarthritic knees by applying unsupervised machine learning algorithm.

[192] Liudmila Khokhlova, Dimitrios-Sokratis Komaris, Nikolaos Davarinos, Karuppiah Mahalingam, Brendan O'Flynn, and Salvatore Tedesco. Non-invasive assessment of cartilage damage of the human knee using acoustic emission monitoring: a pilot cadaver study. *IEEE Transactions on Biomedical Engineering*, 2023.

[193] Daniela K Schlüter, Lucy Spain, Wei Quan, Harry Southworth, Nicola Platt, Joe Mercer, Lik-Kwan Shark, John C Waterton, Mike Bowes, Peter J Diggle, et al. Use

of acoustic emission to identify novel candidate biomarkers for knee osteoarthritis (oa). *PLoS One*, 14(10):e0223711, 2019.

[194] Wynand Steenkamp, Pududu Archie Rachuene, Roopam Dey, Nkosiphendule Lindani Mzayiya, and Brian Emmanuel Ramasuvha. The correlation between clinical and radiological severity of osteoarthritis of the knee. *SICOT-J*, 8, 2022.

[195] Wing P Chan, Guo-Shu Huang, Shu-Mei Hsu, Yue-Cune Chang, and Wei-Pin Ho. Radiographic joint space narrowing in osteoarthritis of the knee: relationship to meniscal tears and duration of pain. *Skeletal Radiology*, 37:917–922, 2008.

[196] Dhirendra Kumar Verma, Mirsaidin Hussain, Poonam kumari, and Subramani Kanagaraj. Design, fabrication, and performance validation of a piezoelectric sensor and arduino-based wearable device for knee joint health assessment. In *North-East Research Conclave*, pages 329–339. Springer, 2022.

[197] Mark D Kohn, Adam A Sassoon, and Navin D Fernando. Classifications in brief: Kellgren-lawrence classification of osteoarthritis. *Clinical Orthopaedics and Related Research®*, 474:1886–1893, 2016.

Brief Biodata of the Author

The author, Dhirendra Kumar Verma, was born in the Kanpur city of Uttar Pradesh State. He graduated in Mechanical Engineering in the year 2006 from Shri Ram Murti Smarak College of Engineering & Technology, Bareilly affiliated with Uttar Pradesh Technical University Lucknow, (U.P.). Then, he joined Kamla Nehru Institute of Technology, Sultanpur (U.P.) in the same year to work as a Lecturer in the Department of Mechanical Engineering. He completed his Master's in Mechanical Engineering from Dr. A.P.J. Abdul Kalam Technical University Lucknow, (U.P.) with the specialization in Computer-Aided Design, and further carried his academic career as an Assistant Professor in the Department of Mechanical Engineering in different renowned private engineering colleges in Uttar Pradesh affiliated to the same university. He also served his duties as the Head of the Department of Mechanical Engineering for four years during his academic career and established various labs of Mechanical Engineering during his tenure. In December 2017, he joined the Ph.D. program at IIT Guwahati in the Department of Mechanical Engineering and this research work is carried out during this period.

List of Publications from the Thesis

List of Publications in International Journals

1. **Journal Publications:**

- Verma, D.K., Kumari, P. and Kanagaraj, S., 2022. Engineering Aspects of Incidence, Prevalence, and Management of Osteoarthritis: A Review. Annals of Biomedical Engineering, Springer Nature, pp.1-16. DOI:10.1007/s10439-022-02913-4.
- Verma DK, Hussain M, Kumari P, Kanagaraj S. In-house development of contact microphone-based wearable device for knee joint health assessment using vibroarthrography. Journal of Intelligent Systems with Applications 2022; 5(1): 59-65. DOI: 10.54856/jiswa.202205209.
- Verma DK, Hussain M, Kumari P, Kanagaraj S. Performance evaluation of In-house developed IMU sensor-based wearable digital goniometer for analyzing the knee joint kinematics. Journal of Medical Devices ASME; (Under Review).
- Verma DK, Hussain M, Kumari P, Kanagaraj S. Quantitative and parametric analysis of piezoelectric sensor-based acoustic emission tool as an adaptive biomarker for osteoarthritis detection. Medical Engineering & Physics; (Under Review).
- Verma DK, Boruah L, Kumari P, Kanagaraj S. Detection of Different Stages of Knee Osteoarthritis Using an Acoustic Emission System and Its Validation Through X-Ray Imaging. Annals of Biomedical Engineering; (Under review).

2. **Conferences:**

- Verma DK, Hussain M, Kumari P, Kanagaraj S. Design, Fabrication, and Performance Validation of A Piezoelectric Sensor and Arduino-Based Wearable Device for Knee Joint Health Assessment, at North East Research conclave; Sustainable Science and Technology; IIT Guwahati, May 2022. (National Conference, Received Springer Best Paper Award).
- Verma DK, Hussain M, Kumari P, Kanagaraj S. In-House Development of Contact Microphone-Based Wearable Device for Knee Joint Health Assessment Using Vibroarthrography, at 5th international conference on Medical Devices, ICMD 2022; Gaziantep Turkey, June-2022. (International Conference).
- Verma DK, Patwari S, Kumari P, Kanagaraj S. Detection of osteoarthritis using piezoelectric sensor-based acoustic emission system, at International Conference on Biomaterials, Regenerative Medicine and Devices, Bio-Remedi-2022; IIT Guwahati, December-2022. (International Conference).

3. **Book Chapter:**

- Verma DK, Hussain M, Kumari P, Kanagaraj S. Design, Fabrication, and Performance Validation of A Piezoelectric Sensor and Arduino-Based Wearable Device for Knee Joint Health Assessment, in "Healthcare Research and Related Technologies - Proceedings of NERC 2022" by Springer, DOI: 10.1007/978-981-99-4056-1_22.